

**An Articulated Drill and Hybrid Tracking Navigation System for  
Orthopaedic Surgery**

**Ahmad Nazmi Ahmad Fuad**

**PhD in Biomedical Engineering**

**2019**

**Department of Biomedical Engineering**

**University of Strathclyde**

**Supervisors:**

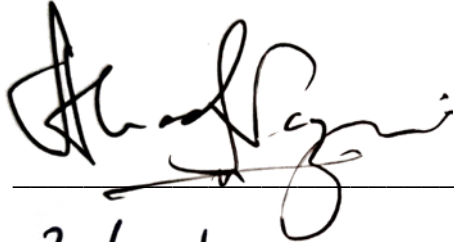
**Dr Wei Yao**

**Professor Philip Rowe**

## I. DECLARATION OF AUTHENTICITY AND AUTHOR'S RIGHTS

This thesis is the result of the author's original research. It has been composed by the author and has not been previously submitted for examination which has led to the award of a degree.

The copyright of this thesis belongs to the author under the terms of the United Kingdom Copyright Acts as qualified by University of Strathclyde Regulation 3.50. Due acknowledgement must always be made of the use of any material contained in, or derived from, this thesis.

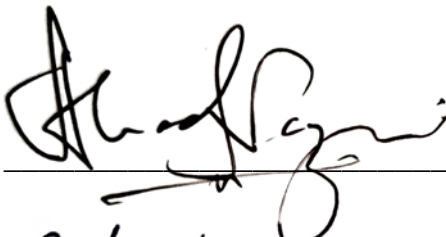
Signed:  Ahmad Nazmi Ahmad Fuad  
Date: 30/09/2019

## II. DECLARATION OF CONTRIBUTION TO PREVIOUSLY PUBLISHED WORK(JOURNAL PUBLICATIONS)

Chapter3, 5, and 6: Portion of these chapters has been published in the International Journal of Medical Robotics and Computer Assisted Surgery (2018) Volume 14, Issue 1. The Author, Ahmad Nazmi Ahmad Fuad, is the first author of this paper. DOI: 10.1002/rcs.1878

Chapter 2, 5, and 6: Portion of these chapters has been published in the Annals of Biomedical Engineering (2018) Volume 46, Issue 3, pp 464-474. The Author, Ahmad Nazmi Ahmad Fuad, is the first author of this paper. DOI: 10.1007/s10439-017-1959-5

Chapter 4, and 6: Portion of these chapters has been published in the Proceedings of the Institution of Mechanical Engineers, Part H: Journal of Engineering in Medicine (2018). The Author, Ahmad Nazmi Ahmad Fuad, is the first author of this paper. DOI: 10.1177/0954411918764508

Signed:  \_\_\_\_\_ Ahmad Nazmi Ahmad Fuad  
Date: 30/09/2019 \_\_\_\_\_

### III. CONTENTS

<b>I.</b>	<b>Declaration of Authenticity and Author’s Rights .....</b>	<b>1</b>
<b>II.</b>	<b>Declaration of Contribution to Previously Published Work(JOURNAL Publications).....</b>	<b>2</b>
<b>III.</b>	<b>Contents .....</b>	<b>3</b>
<b>IV.</b>	<b>Summary of Figures and Tables .....</b>	<b>8</b>
<b>V.</b>	<b>Acknowledgement .....</b>	<b>14</b>
	<b>ABSTRACT .....</b>	<b>16</b>
	<b>CHAPTER 1 - INTRODUCTION AND LITERATURE REVIEW.....</b>	<b>19</b>
1.1	Introduction .....	19
1.1.1	Anatomy of Hip Joint .....	19
1.1.2	Orthopaedic Surgery .....	23
1.2	Total Hip Arthroplasty.....	24
1.3	Computer Assisted Orthopaedic Surgery (CAOS) .....	27
1.3.1	Surgical Navigation System .....	30
1.3.1.1	CT-BasedSurgical Navigation.....	32
1.3.1.2	Fluoroscopy-based Surgical Navigation .....	34
1.3.1.3	Image-free Navigation .....	36
1.3.2	Computer Assisted Orthopaedic Surgery in Total Hip Arthroplasty.....	38
1.3.3	Existing Surgical Navigation System.....	41

---

1.4	Robotics in Orthopaedics .....	46
1.4.1.	Existing Robotic Orthopaedic System .....	47
1.4.2.	Robotics micro-tools.....	51
1.4.3.	Wire Actuators as Tendons.....	57
1.5	Research Question .....	58
1.5.1.	The Need for Articulated Drill Sheath with capability to mill under different configuration .....	58
1.5.2.	The Need for Hybrid Tracking System to track articulated drill sheath when milling inside the bone .....	59
1.5.3.	The Need for Navigation Software for articulated drill sheath to Visualize the Tracking.....	60
1.5.4.	The Need to Measure Reaction Force when Milling in Different Configurations, and Confirm the Capability of Articulated Drill System to Sustain Bending.....	61
1.5.5.	The Need to Analyze the 3D Geometry of Curved Tunnel from Milling Guided by the Navigation System .....	62
1.5.6.	The Need to Test the Accuracy of the Navigation System in Milling the Femoral Stem Shape Inside Femur Sawbone.....	62
1.6	Research Objectives .....	63
1.7	Thesis Outline .....	64
1.8	Conclusion .....	64
CHAPTER 2 - CONCEPT OF ARTICULATED DRILL AND ITS NAVIGATION SYSTEM .....		67
2.1.	Introduction .....	67
2.2.	Concept Design.....	68

---

2.3.	Kinematics and coordination transformation .....	71
2.4.	Design of The Articulated Drill System .....	78
2.4.1	Design of a Novel Articulated Drill Mechanism .....	78
2.4.2	Servo Arm and Wire Driven System.....	79
2.4.3	Electronics and Microcontrollers .....	82
2.4.4	Limitation to the Design.....	84
2.4.5	Hardware Design and Manufacture .....	85
2.5.	A Hybrid Tracking System.....	93
2.6.	Conclusion .....	96
CHAPTER 3 - NAVIGATION SOFTWARE OF THE STREERABLE DRILL NAVIGATION SYSTEM .....		99
3.1.	Introduction .....	99
3.2.	General Overview of Navigation Software .....	100
3.2.1	Virtual Fixtures .....	102
3.2.2	3D Collision Detection.....	106
3.3.	Concept and Logic/Steps of Navigation System .....	108
3.3.1.	Programming the Software .....	108
3.3.2.	Importing the Femur 3D Model .....	115
3.3.3.	Establishing Safe Surgical Boundary .....	117
3.3.4.	Importing the Surgical Tool 3D Model.....	119
3.3.5.	Registration of Both 3D Models to the Tracking System .....	119
3.3.6.	Collision of Surgical Tool with Safe Surgical Boundary.....	122

---

3.3.7. Summary of the Concept .....	124
3.4. Conclusion .....	126
CHAPTER 4 -FORCE MEASUREMENT EXPERIMENT .....	128
4.1. Introduction .....	128
4.2. Cutting Tool – Orthogonal Cutting.....	128
4.2.1 Force model of bone cutting by spherical rotating tool.....	129
4.3. Experiment on Measurement of Reaction Force .....	130
4.3.1 Action-Reaction Force.....	130
4.3.2 Vertical Configuration.....	131
4.3.3 Lateral Configuration.....	138
4.3.4 Assembly of the test rig.....	144
4.3.5 Data Acquisition .....	145
4.3.6 Data Analysis .....	146
4.3.7 Limitation of Experiment.....	147
4.3.8 Results .....	147
4.4. Conclusion .....	157
CHAPTER 5 - SYSTEM INTEGRATION AND EXPERIMENTS.....	159
5.1. Introduction .....	159
5.2. System integration .....	159
5.3. Potentiometer tracking calibration .....	160

---

5.4.	Experiment in sawbones - (A) 3D geometric analysis of the shape of the cut area (B) Accuracy Analysis/Symmetry Analysis .....	169
5.4.1	Materials and Methods.....	170
5.4.2	Results - (A) 3D geometric analysis of the shape of the cut area.....	177
5.4.3	Results - (B) Accuracy Analysis/Symmetry Analysis.....	190
5.5.	Conclusion .....	194
CHAPTER 6 - DISCUSSION.....		196
6.1.	Static Performance of Articulated Drill System Under Different Configurations.....	196
6.2.	3D Geometric Analysis of The Shape of The Cut Area .....	206
6.3.	Accuracy Analysis/Symmetry Analysis.....	208
6.4.	Limitation of the Research.....	212
a.	Limitation of the Hardware .....	212
b.	Limitation of the Software.....	213
c.	Limitation of the Experiments/Testing .....	213
6.5.	Conclusion .....	214
CHAPTER 7: FUTURE RESEARCH.....		218
7.1.	Hardware.....	218
7.2.	Software .....	218
7.3.	Experimentation .....	219
REFERENCES.....		220



---

#### IV. SUMMARY OF FIGURES AND TABLES

Figure 1.1: Lateral View of Hip Bone taken from Netter's Atlas of Human Anatomy (Netter, 2014).....	20
Figure 1.2: Fibrous capsule of hip joint and the ligaments that form it. Taken from Netter's Atlas of Human Anatomy (Netter, 2014).....	22
Figure 1.3: Skin incisions for direct anterior (light blue), mini-posterior (dark blue), and conventional posterior (red extensions to dark blue) approaches to the hip(Derek F Amanatullah et al., 2014). ....	25
Figure 1.4: System setup for a CT-based navigation system, including the basic components and their associated local coordinate system (COS) by (Nolte and Beutler, 2004).....	33
Figure 1.5: System setup for 2D fluoroscopy-based navigation system, including the basic components and their associated local coordinate system (COS) by (Nolte and Beutler, 2004).....	35
Figure 1.6: System setup for an image-free navigation system, including the basic components and their associated local coordinate systems (COS) by (Nolte and Beutler, 2004).....	37
Table 1.1: Existing Surgical Navigation System available in clinical setting and their features. ....	46
Table 1.2: Existing Robotic Orthopaedic System, and Flexible Robotic System in Surgery. ....	55
Figure 2.1:A prototype of the articulated drill mechanism .....	69
Figure 2.2: Kinematic sketch of the articulated drill. The point T is not a prismatic joint. The box symbol represents the motor box of the articulated drill sheath. ....	72
Figure 2.3: Kinematics in 2D (planar space). The body frame of each $A_i$ , for $1 < i < m$ , is based on the joints that connect $A_i$ to $A_{i-1}$ and $A_{i-2}$ . ....	74
Figure 2.4: Kinematics of a PRR manipulator for the articulated drill, and transformation of its local coordinate system into the global coordinate	

---

system. The point m is not a prismatic joint. The box symbol represents the motor box of the articulated drill sheath. ....	76
Figure 2.5: CAD of the articulated drill .....	80
Figure 2.6: Wire driven system inside of articulated drill sheath. ....	81
Figure 2.7: Electronic diagram of main and accessory microcontrollers along with components attached to them. ....	83
Figure 2.8: A prototype of the articulated drill .....	85
Figure 2.9: Base part dimensions .....	87
Figure 2.10: Base part outline .....	87
Figure 2.11: Middle part dimensions .....	88
Figure 2.12: Middle part outline .....	89
Figure 2.13: Drill end part dimensions .....	90
Figure 2.14: Drill end part outline .....	90
Figure 2.15: Chuck part dimension .....	91
Figure 2.16: Chuck part outline .....	91
Figure 2.17: Assembly of Articulated Drill Sheath .....	92
Figure 2.18: Motor box outline .....	93
Figure 2.19: The Optical Tracking system .....	94
Figure 3.1: Components that are integrated in the navigation software enabling real-time visualization of articulated drill even when the tip is inside the bone.....	102
Table 3.1: Additional libraries imported apart from standard JAVA Processing libraries. ....	114
Figure 3.2: 3D model of femur in navigation 3D virtual space.....	116
Figure 3.3: Setting up the boundary of the safe surgical volume (a) The femur and implant 3D models; (b) Position the femoral stem inside the 3D bone model; (c) Safety area is defined as the deeper green area; (d) The milling is guided by the safety boundary.....	118
Figure 3.4: 3D model of both femur and articulated drill in navigation 3D virtual space.....	120

---

Figure 3.5: Manipulation and guiding the drilling process inside the bone within the safe surgical area defined by the femoral stem implant CAD model .....	122
Figure 3.6: Error warning from navigation system whenever the mill tip made contact with the safe surgical boundary followed by the stopping of drill motor.....	124
Figure 3.7: Concept of the navigation software in reference to basic concept of CAOS that divides the system into surgical object (SO), virtual object (VO), Navigation (NAV), and end effector (EE). .....	125
Figure 4.1:Simulation of a spherical tool with 6 cutting edges; (a) tool, bone, coordinates, feed direction, and the resulting chip, (b) simulation results for two voxel sizes (Moghaddam et al., 2008).....	130
Figure 4.2: (A) Test rig setup for 0 degree in forward configuration; (B) Close up view of the burr tip position relative to bone sample surface. Red arrow in both pictures indicates direction of milling / linear stage during testing.....	134
Figure 4.3: (A) Test rig setup for 10 degree in forward configuration; (B) Close up view of the burr tip position relative to bone sample surface. Red arrow in both pictures indicates direction of milling / linear stage during testing. ....	135
Figure 4.4: (A) Test rig setup for 20 degree in forward configuration; (B) Close up view of the burr tip position relative to bone sample surface. Red arrow in both pictures indicates direction of milling / linear stage during testing. ....	136
Figure 4.5: (A) Test rig setup for 30 degree in forward configuration; (B) Close up view of the burr tip position relative to bone sample surface. Red arrow in both pictures indicates direction of milling / linear stage during testing. ....	137
Figure 4.6: (A) Test rig setup for 0 degree in lateral configuration; (B) Close up view of the burr tip position relative to bone sample surface. Red arrow in both pictures indicates direction of milling / linear stage during testing.....	140

---

Figure 4.7: (A) Test rig setup for 10 degree in lateral configuration; (B) Close up view of the burr tip position relative to bone sample surface. Red arrow in both pictures indicates direction of milling / linear stage during testing.....	141
Figure 4.8: (A) Test rig setup for 20 degree in lateral configuration; (B) Close up view of the burr tip position relative to bone sample surface. Red arrow in both pictures indicates direction of milling / linear stage during testing.....	142
Figure 4.9: (A) Test rig setup for 30 degree in lateral configuration; (B) Close up view of the burr tip position relative to bone sample surface. Red arrow in both pictures indicates direction of milling / linear stage during testing.....	143
Figure 4.10: Force-Time Curve of 0 Degree Bending in Forward Configuration. ....	147
Figure 4.11: Force-Time Curve of 10 Degree Bending in Forward Configuration. ....	148
Figure 4.12: Force-Time Curve of 20 Degree Bending in Forward Configuration. ....	149
Figure 4.13: Force-Time Curve of 30 Degree Bending in Forward Configuration. ....	150
Figure 4.14: Force-Time Curve of Comparison of Bending Degree in Forward Configuration. ....	151
Figure 4.15: Force-Time Curve of 0 Degree Bending in Lateral Configuration. ....	152
Figure 4.16: Force-Time Curve of 10 Degree Bending in Lateral Configuration. ....	153
Figure 4.17: Force-Time Curve of 20 Degree Bending in Lateral Configuration. ....	154
Figure 4.18: Force-Time Curve of 30 Degree Bending in Lateral Configuration. ....	155
Figure 4.19: Force-Time Curve of Comparison of Bending Degree in Lateral Configuration. ....	156
Figure 5.1: System integration for the articulated and steerable drill .....	160

Figure 5.2: Joint 1 Calibrated Angle vs. Goniometer (A)Positive (B) Negative .....	162
Figure 5.3: Joint 2 Calibrated Angle vs Goniometer (A) Positive (B) Negative .....	164
Figure 5.4: Joint 1 Absolute Error (A) Positive (B) Negative .....	166
Figure 5.5: Joint 2 Absolute Error (A) Positive (B) Negative .....	168
Figure 5.6: System setting for the articulated drill and its navigation system in a sawbone test rig.....	170
Figure 5.7: Manipulation using the articulated and steerable drill .....	172
Figure 5.8: Registration of articulated drill to the optical tracking system. ..	173
Figure 5.9:A graphical user interface (GUI) of a navigation system.....	174
Figure 5.10: Completion of milling and fitting of implant.....	176
Figure 5.11: Bone milling completed and ready to be sent for CT imaging.	177
Table 5.1:Summary of deviation analysis; dmax(+), maximum positive deviation; dmax(-), maximum negative deviation; davg(+), mean positive deviation; davg(-), mean negative deviation; RMSD, root mean square of deviation. ....	178
Table 5.2: Deviation distribution between femoral stem implant and cut area of femur sawbones. ....	181
Figure 5.12: Isometric view of all three-cut area of femur sawbones and deviation colour map (DCM) (mm).....	183
Figure 5.13: Deviation colour map (DCM) of cut area 1 of femur sawbones in four views.....	188
Figure 5.14: Deviation colour map (DCM) of cut area 2 of femur sawbones in four views.....	188
Figure 5.15: Deviation colour map (DCM) of cut area 3 of femur sawbones in four views.....	189
Figure 5.16: The chromatogram used for an analysis of the milling procedure. ....	190

---

Figure 5.17: Percentage deviation distribution of point cloud data of cut area of femur sawbone. ....	193
Figure 5.18: Standard deviation of point cloud data of cut area of femur sawbone. ....	193

## v. ACKNOWLEDGEMENT

Firstly, I would like to express my deep gratitude to both of my supervisors, Dr Wei Yao and Prof. Philip Rowe for the continuous support, guidance, teaching, and frequent positive encouragements throughout my PhD study. Their guidance helped me greatly in all the time of completing my research and writing this thesis. They are both an excellent advisor and mentor for me.

Secondly, I would also like to thank Prof. Mary Grant for guidance in postgraduate study and provide me an opportunity to have access to the bovine tissue laboratory. I would also like to thank Dr Philip Riches for educating me in engineering principle in detail and provide me access to the force testing laboratory.

I thank my good friend and research group member, Hariprashanth Elangovan for inspiring advices, stimulating discussions and debates, guidance in mechanics and electronics, and for all the fun we had together. Not to forget, University of Strathclyde for giving me opportunity to pursue my postgraduate study in a conducive and interesting manner.

Besides that, I would also like to thank the government of Malaysia, particularly the Ministry of Science, Technology, and Innovation for awarding me scholarship to fund my tuition fees, and my living cost here in United Kingdom.

Last but not least, I would like to thank my family; my parents, my wife, and my siblings for supporting me spiritually, morally, and stress reliever throughout live in general and writing this thesis.



## ***ABSTRACT***

The need for an articulated drill is driven by the increasing clinical requirement for improving the surgical outcomes and decreasing the complications of the THA procedure. Besides that, after the total hip arthroplasty (THA) procedure, there is also probability of the patient end up with unequal leg lengths, which are referred to as a leg-length discrepancy (LLD). One way to reduce the risk in THA procedure is improving accurate placement and alignment of implants using robotic technology. In Total Hip Arthroplasty (THA), the usage of robotic orthopaedic surgery per se is applied in the acetabular cup positioning and orientation, and femoral stem positioning. However, in robotic orthopaedic surgery with tracking and navigation system, the femoral stem insertion depends on hand-rasping method and confirmation of position by placing tracking marker at the neck shaft of femoral stem after insertion. Besides that, femoral milling with navigation for anatomic femoral stem insertion was not feasible due to its slightly curved profile. This is because current tools are not able to track milling that follows the curve profile of anatomic femoral stem. The emergence of robotic micro-tools give opportunity for developing an articulated drill system that has the ability to mill inside femoral canal when it is combined with CAOS and is trackable under minimally invasive approach. This research has the objectives of design and development of articulated drill sheath with motor control from straight shaft to bendable shaft, design and development of hybrid tracking system, combination between optical tracking system and potentiometer

tracking system in order to track surgical tool inside the bone, design and development of navigation software for articulated drill sheath, to measure reaction force when milling in different bending configuration and rake angles, and understanding the static performance of articulated drill system under different configurations, and confirm the capability of the articulated drill system to sustain bending when milling under different configuration, to analyse the 3d geometry of curved tunnel from milling guided by the navigation system, and test the accuracy of the navigation system in milling the femoral stem shape inside femur sawbone.

Articulated drill tip sheath with motor control from straight shaft to bendable shaft was designed and developed. Besides that, hybrid tracking system, combination between optical tracking system and potentiometer tracking system in order to track surgical tool inside the bone was also designed and developed. Streams of input from both optical tracking system and potentiometer tracking system are integrated in the navigation software of articulated drill navigation system. The navigation system for articulated drill sheath was designed and developed. The navigation system is a multi-modality computer-aided integration system. The navigation software is able to integrate optical tracking system and potentiometer tracking system.

Experiment on measurement of reaction force has been done. The reaction force when milling in different bending configuration and rake angles has been measured, and the static performance of articulated drill system

under different configurations has been understood. The articulated drill system is able to sustain bending in different configuration while milling the bone sample. The articulated drill system was integrated and was used for evaluation experiments in sawbones. 3D geometric analysis of the shape of the cut area experiment was done. The analysis of results confirmed that the tracking system is able to guide the articulated drill inside femur, in which a deviation between cut area and outline of femoral stem from navigation software was in range from -0.759 mm to 1.151 mm. Accuracy Analysis/Symmetry Analysis experiment was done. The accuracy of the navigation system is within 1.728 mm.

**Keywords - Robotics; Articulated; Tracking; Navigation; Hybrid Navigation; Orthopaedics; Total Hip arthroplasty (THA);**

## **CHAPTER 1 - INTRODUCTION AND LITERATURE REVIEW**

### **1.1 Introduction**

This chapter will explain the literature review on computer assisted orthopaedic surgery (CAOS), its application in hip arthroplasty, limitation of femoral stem implantation using current CAOS technology, utilization of robotic micro tools in surgery, and potential advantages of articulated drill system.

#### **1.1.1 Anatomy of Hip Joint**

Hip joint is ball and socket synovial joint. It is articulation between femur bone and the hip bone that is made up by ilium, ischium and pubis (Figure 1.1).

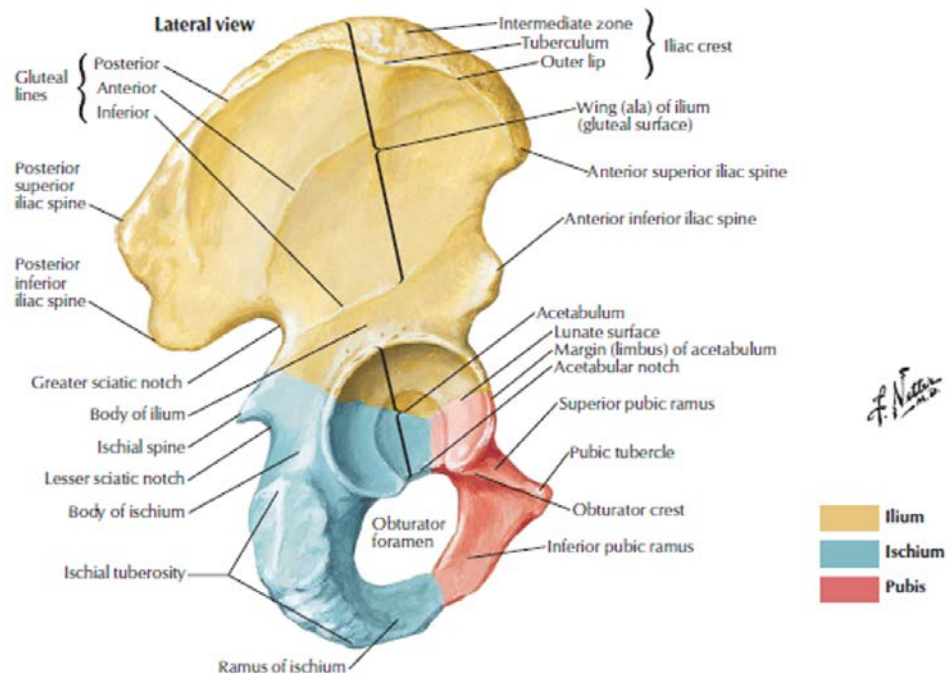


Figure 1.1: Lateral View of Hip Bone taken from Netter's Atlas of Human Anatomy (Netter, 2014)

Femur, also known as thigh bone, is the longest bone in human body. The proximal end articulate with the hip bone and the distal end articulate with patellar and tibia to form the knee joint (Moore et al., 2013). The proximal end of femur consists of the head of femur, neck of femur, greater trochanter, and lesser trochanter. The head of femur is orientated superomedially, and slightly anteriorly when articulate with acetabulum to form the hip joint (Moore et al., 2013). Hip bone is one half of pelvic bone that consists of two sets of ilium, ischium, and pubis joint together. The ilium is the largest bone and located superiorly in the hip bone. It makes up for superior part of acetabulum (Moore et al., 2013). The ischium is the bone that makes the inferior part of hip bone. Ischium form

the acetabulum at its superior part by fusing with ilium and pubis (Moore et al., 2013). The pubis is the bone that makes up the anteromedial part of hip bone and makes up the anterior part of acetabulum (Moore et al., 2013). Acetabulum is part of hip bone that is formed by articulation of ilium, ischium, and pubis. It is cup shape socket that articulates with head of femur forming the ball and socket joint (Moore et al., 2013). Acetabulum is layered with additional fibrocartilagenous called acetabular labrum and its purpose is to deepen the acetabulum to hold more surface of head of femur securely (Moore et al., 2013). The articular surface of head of femur to acetabulum is lunate. In order to stabilize the hip joint, it contains a strong fibrous capsule and transverse acetabular ligament that covers the articulation surface. The fibrous capsule cover the articulation surface proximally to the acetabulum and transverse acetabular ligament, and distally to the greater trochanter at the anterior of femur and intertrochanteric crest at the posterior femur (Moore et al., 2013). Additionally, some fibres go around the neck, holding the femoral neck in the acetabulum. The fibrous capsule consists of iliofemoral ligament, ischiofemoral ligament, and pubofemoral ligament as shown in Figure 1.2 below.

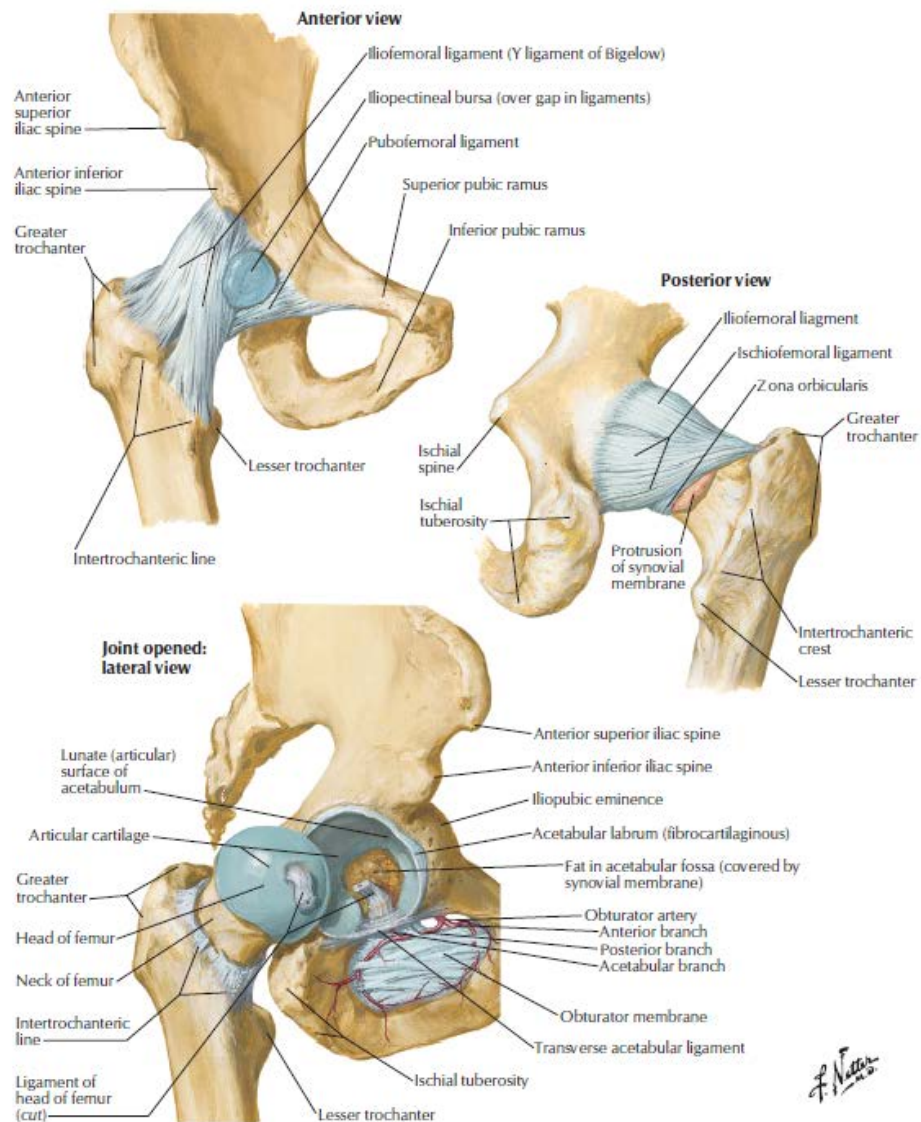


Figure 1.2: Fibrous capsule of hip joint and the ligaments that form it. Taken from Netter's Atlas of Human Anatomy (Netter, 2014).

Iliofemoral ligament holds the femoral head in acetabulum during standing, thus prevent hyperextension of hip joint. Ischiofemoral ligament stabilize the posterior aspect of hip joint and similar to iliofemoral ligament, it holds the femoral head in acetabulum to prevent

hyperextension of hip joint. Pubofemoral ligament stabilize the anterior and inferior aspect of hip joint, thus preventing over-abduction of the hip joint (Moore et al., 2013). Covering the fibrous capsule is the synovial membrane, and it also covers the neck of femur between the attachment of the fibrous capsule and the edge of articular cartilage of the head of femur and non-articular area of the acetabulum (Moore et al., 2013). Area that is not filled by the head of femur is filled by a fat pad in the acetabular fossa (Moore et al., 2013).

### **1.1.2 Orthopaedic Surgery**

Orthopaedics is medical specialty that concerned with the musculoskeletal system diseases of the human body and the musculoskeletal system comprises of the bones, joints, muscles, tendons, nerves (Solomon et al., 2010). Orthopaedic surgery is one of treatment options for orthopaedic diseases. Common procedures in orthopaedic surgery includes arthroscopy, fusion, internal fixation, arthroplasty, osteotomy, and soft tissue repair(Solomon et al., 2010).



## **1.2 Total Hip Arthroplasty**

Total hip arthroplasty (THA) is a surgery to replace the hip joint with artificial prosthesis that consists of acetabular cup and femoral stem. The procedure involve removal of head and proximal neck of femur by excision, and removal of acetabular cartilage and subchondral bone(Siopack and Jergesen, 1995). Besides that, an artificial canal is created in proximal medullary region of femur for insertion of femoral stem prosthesis. Second component, the acetabular component is inserted at the acetabular space to replace the acetabular cartilage and subchondral bone. THA is one of the procedures that widely performed due to proven to be successful in elimination pain and restoring the function of the hip that damaged from osteoarthritis. In United States, total hip arthroplasty is performed about 170 000 times every year and about 300 000 times worldwide (Siopack and Jergesen, 1995). THA is indicated for patients that have severe pain and impaired daily activities due to presence of osteoarthritis. Other disease that indicated for THA are developmental dysplasia of the hip, Paget's disease, trauma, and osteonecrosis of the femoral head (Siopack and Jergesen, 1995, Solomon et al., 2010).

Total Hip Arthroplasty(THA) initially was performed by transtrochanteric approach but later, alternative approaches such as conventional posterior and lateral approaches replacing transtrochanteric approach(Jolles and Bogoch, 2006). This is because transtrochanteric approach results in disturbance to osseous and soft tissue anatomy causing

unnecessary complications such as trochanteric non-union(Bergström et al., 1973, Amstutz and Maki, 1978). However, the conventional posterior and lateral approach were reported to have association with nerve injury(Abitbol et al., 1990). Following that, these conventional approaches were modified with objective of limiting the amount of soft tissue dissection and minimize damage to surrounding tissue, hence minimally invasive THA were discovered and new alternative to conventional approaches.

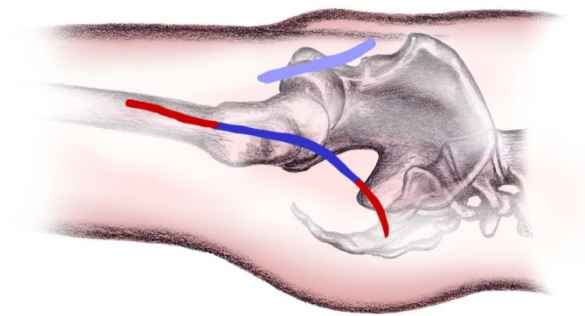


Figure 1.3: Skin incisions for direct anterior (light blue), mini-posterior (dark blue), and conventional posterior (red extensions to dark blue) approaches to the hip(Derek F Amanatullah et al., 2014).

Conventional posterior incision is usually 10-25 cm long (red extensions). Single MIS incisions are usually less than 10 cm long (blue). In the 2-incision approach, both are usually less than 5 cm long. Courtesy of(Derek F Amanatullah et al., 2014).

Based on Figure 1, minimally invasive THA can be approached either by single incision or two-incision approach. The approaches are direct anterior approach, anterolateral approach, direct lateral approach, posterior approach, and two-incision approach that is combination of anterior approach to acetabulum and posterior approach to the proximal femoral shaft (Berry et al., 2003). Minimally invasive THA has problem of more limited visualization of surgical area, but this limitation can be reduced by incorporating computer-assisted navigation that improve visualization to correctly position the components (Ybinger and Kumpan, 2007).

---

### **1.3 Computer Assisted Orthopaedic Surgery (CAOS)**

Surgical robotic technology has been developing for decades to the extent that many surgical practices now benefit from the deployment of surgical robotic platforms. These benefits include improved implant positioning accuracy and homogenisation of positioning results(Nawabi et al., 2013, Tarwala and Dorr, 2011, Joskowicz and Hazan, 2016, Jerabek et al., 2014), reduction of intra-operative blood loss in surgery(Bukowski et al., 2016) and improving patient outcomes in long-term (Joskowicz and Hazan, 2016, Banchetti et al., 2018). In orthopaedic surgery, computer aided orthopaedic surgery (CAOS) has been advancing by using robotic surgical devices and navigation systems, resulting in a great improvement of surgical field visibility and the enhancement of surgical accuracy (Nolte and Beutler, 2004).In particular, the use of robotic surgical devices for orthopaedic surgery has become more widely accepted for its greater precision and accuracy in implant positioning and orientation particularly in computer-assisted total knee replacement surgery that is successful and widespread application with nearly 500,000 surgeries documented around the world(Lonner, 2009, Joskowicz and Hazan, 2016).There are three types of surgical robotic systems that have been developed for orthopaedics surgery, which are passive, semi-active and active systems. Passive systems control surgical tools by moving a cutting guide block or a drilling guide sleeve while a surgeon handles the tool with his free hands (Jaramaz and Nikou, 2012, Smith et al., 2014). Semi-active system limits the movement of surgical tools

---

within a pre-operative planned surgical area by means of a robot arm(Sugano, 2003), examples including MAKO (Sugano, 2003, Buechel and Conditt, 2016, Jacofsky and Allen, 2016) and ACROBOT(Jakopec et al., 2001). Active systems such as ROBODOC (Bargar et al., 1998) and CASPAR (Sikorski and Chauhan, 2003)can execute surgical planning automatically independent of surgeon's hands.

In robotic orthopaedic surgery, the surgeon needs to perform procedures precisely and safely within a limited space; and this requires effective surgical guidance by means of a surgical navigation. Surgical navigation in orthopaedic surgery works by optically tracks objects via camera and visualize the virtual models of the surgical tools and the anatomy is operated on in real-time, acting as a guide for the surgeon during surgical procedures. Advancement in radiographic imaging enables the reconstruction of imaging data into three dimensional (3D) images, which can be used in surgical pre-operative planning to various surgical procedures(Brown, 1979).The digital radiographic images serve as a navigation map for the procedures, where the surgical tools' CAD models are incorporated into the map for the purpose of visualizing its position, orientation and its movement to an accuracy of one millimetre or one degree (Sikorski and Chauhan, 2003).This method improves the accuracy and precision of the surgery and gives surgeon a better and wider view of the surgical field(Joskowicz and Hazan, 2016, Banchetti et al., 2018).

In orthopaedic surgery, implantation requires accurate operation and positioning in order to get the best outcome and best functional results(Qiao et al., 2015). For example, an accurate reduction of fractures will result in restoration of the anatomy of the limb such as better bone union and prevent limb malformation(Tosounidis et al., 2015), and restoration of physiology of the limb such as improving the limb's functional biomechanical(Qiao et al., 2015). In joint replacement surgery, well-aligned and accurate positioning of hip or knee prosthesis is less likely to lead to complication of dislocation or abnormal gait pattern (Sikorski and Chauhan, 2003). Besides that, faster operating time has lesser priority than better technical outcome because patient will less likely to suffer complications when the surgeon takes extra time during operation to ensure better surgical outcome (Sikorski and Chauhan, 2003). Currently, there are vast number of tools and aids in orthopaedic surgery ranging from simple ones such as broaching reamer, drills, hammers, and retractors to more advanced tools such as endoscopic procedures, intra-operative fluoroscopy, and mechanical alignment jigs and cutting blocks. Now, computer-assisted orthopaedic surgery (CAOS) has been introduced to improve accuracy in surgery. It has the potential to give positive impact in surgery with precise intra-operative navigation to ensure high standards of accuracy in surgery. There are documented study and report of utilization of CAOS in total hip arthroplasty (DiGioia et al., 1998a, Clavé et al., 2015, Kagiya et al., 2016, Han et al., 2019, Chang et al., 2017, Zheng, 2018, Banchetti et al., 2018), total knee arthroplasty (Hafez et

---

al., 2006, Martelli et al., 2000, Banks, 2009, Roche et al., 2009, Haas et al., 2005, Dai et al., 2017, Dai et al., 2018, Buechel and Conditt, 2016, Joskowicz and Hazan, 2016), pelvic osteotomy (Langlotz et al., 1998, Pflugi et al., 2017, Alexander et al., 2018, Armand et al., 2018, Archer et al., 2015), and in spine screw insertion in spinal surgery (Arand et al., 2001, Tian et al., 2017, Fan et al., 2018, Qiang Yuan et al., 2018). These methods give surgeons better visualization of complete constructs/attachments between implants and bone.

### **1.3.1 Surgical Navigation System**

According to Nolte and Beutler's research(2004), there are three major components of surgical navigation. Surgical object (SO) means the anatomical location of surgical action. Virtual object (VO) includes a virtual representation of a surgical object that allows surgeon to plan the surgical procedure before the actual surgery and execute it intra-operatively. Navigator (NAV) is a device that establishes the coordinate systems (COS) of the surgical field targets and the location and orientation of utilized end effectors (EE).In order to fully utilize the surgical navigation system, certain processes can be optionally setup into the system. Those are calibration of end-effectors, registration, and dynamic referencing. Calibration for end effector is required to describe its geometry in the coordinate of the navigator. To calibrate the end effector, a rigid attachment of optical markers is introduced in the optical tracking system. Registration is a process that a surgical navigation

system links the SO and VO and allows them to be displayed on the monitor in real-time/online or offline mode. It is realized by surgeons' identifying key anatomical landmarks resulting in better accuracy of the alignment. Dynamic referencing is one of important requirement for a surgical navigation system. It is necessary for positioning control compensation of a possible motion of the navigator and/or surgical objects during the surgical procedures. This is established by attaching dynamic referencing bases (DRBs), which consist of three or more reflective markers or light emitting diodes (LEDs) arranged in a pattern at the surgical device so that it acts as the base of reference to other surgical objects in tracking. The DRBs can either be fixed to the patient representing fixed anatomy or it can be mobile when attached to surgical tools.

Surgical navigation system has three categories, which are volumetric surgical navigation, non-volumetric surgical navigation and image-free surgical navigation. Volumetric surgical navigation employs 3D radiographic images such as reconstructed 3D CT-Scan and 3D fluoroscopy. Non-volumetric surgical navigation uses 2D radiographic images such as fluoroscopy guided navigation system. Image-free surgical navigation does not use any radiographic imaging but uses the tracking system to define various anatomical landmarks intra-operatively.



### **1.3.1.1 CT-Based Surgical Navigation**

Currently, one of the most widely use radiographic imaging for volumetric surgical navigation in orthopaedic is CT-Scan. Despite the inconvenience to the patient taking CT-Scan and its cost(Sikorski and Chauhan, 2003), CT-Scan is the best when visualizing bone tissue and can be reconstructed into 3D model. CT-Scan image acquired is used for pre-operative planning of the surgical action and then transferred into the OR for execution of the surgery. Registration is done by linking the CT coordinate system and the surgical object system via coordinate transformation  $T_{SO-VO}$ , thus enabling visualization of surgical device in action over the visualization of bone anatomical model (Nolte and Beutler, 2004). According to Lavallee (1996), the two most common type of registration technique are paired points technique and surface registration technique. Surface registration technique can be further divided into two, which are anatomical landmark technique and fiducial-based technique. Both of these techniques require defining of the anatomical landmark and image segmentation in the pre-operative planning.

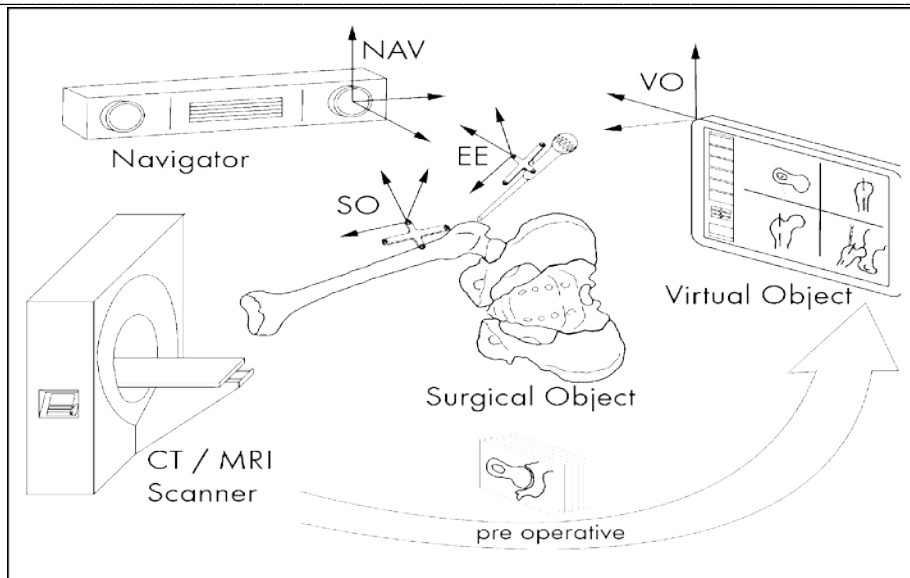


Figure 1.4: System setup for a CT-based navigation system, including the basic components and their associated local coordinate system (COS) by (Nolte and Beutler, 2004).

CT-based surgical navigation is first applied in spine surgery. It is used as support system for insertion of pedicle screws in the spine (Lavallée et al., 1995, Amiot et al., 1995, Glossop et al., 1996, Laine et al., 2000, Tian et al., 2017, Fan et al., 2018, Qiang Yuan et al., 2018). Following this, CT-based surgical navigation is applied to other area of orthopaedic surgery such as hip arthroplasty(THA) and it is used to get more precision and better positioning of implants (DiGioia et al., 1998b, Tsutsui et al., 2016, Fujii et al., 2017, Imai et al., 2018).

### 1.3.1.2 Fluoroscopy-based Surgical Navigation

As an alternative to CT-based navigation technology, fluoroscopy-based surgical navigation emerge from research on co registration of pre-operative 3D images with intra-operative images obtained from state of the art intra-operative fluoroscopy (Nolte and Beutler, 2004). It works by taking the fluoroscopic image coordinate system and transforms it into surgical object system via  $T_{SO-VO}$ . This enables control of the end effectors on monitor as virtual object. In contrast with Ct-based surgical navigation, fluoroscopy-based surgical navigation's coordinate transformation  $T_{SO-VO}$ , is further divided into  $T_{SO-CA} \cdot T_{CA-VO}$ .  $T_{SO-CA}$  is obtained from the optical camera tracking both the surgical object and the image intensifier of the fluoroscopy image scanned. On the other hand,  $T_{CA-VO}$  is obtained from fluoroscopy C-arm's cone beam x-ray projection that acts as optical camera for the coordinate system. It has couple of known shortcomings which is image distortions originates from image intensification process and deformation of C-arm shaped frame requiring further calibration of the C-arm (Nolte and Beutler, 2004).

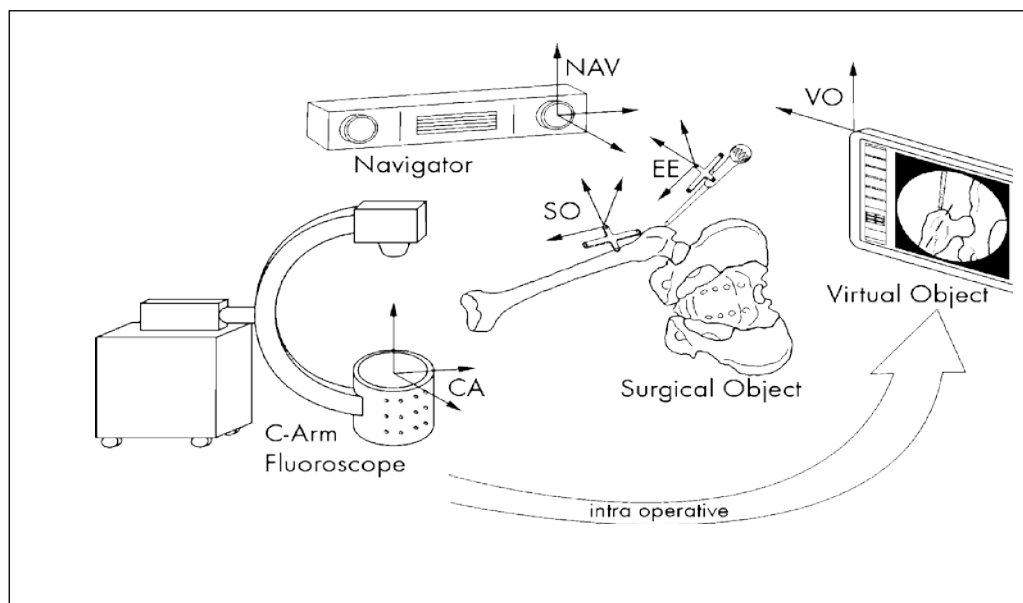


Figure 1.5: System setup for 2D fluoroscopy-based navigation system, including the basic components and their associated local coordinate system (COS) by (Nolte and Beutler, 2004).

Fluoroscopy-based surgical navigation works by acquisition of several fluoroscopy images and transfer it into navigation computer which then undistorted. This will provide real-time projection of all tracked end-effectors in the fluoroscopy view range. Fluoroscopy-based surgical navigation has been developed into 3D fluoroscopy that is associated with lower radiation dose and lower rate of malpositioning when compared with 2D fluoroscopy-based navigation (Thakkar et al., 2017, Lang et al., 2016, Zhou et al., 2016).

### **1.3.1.3 Image-free Navigation**

Image-free Navigation by its name means that the system doesn't use any pre-operative or intra-operative radiological images. It works by surgeons defining various anatomical and reference landmarks to construct the virtual image of the surgical object. Defining anatomical and reference landmarks requires tracked end-effectors that has pointed tip or specialized instrument such as palpation hooks in order to directly digitized the landmarks intra-operatively (Nolte and Beutler, 2004). Besides the advantages of absence of radiological imaging, it has another feature called pivoting procedures. This feature enables determination of specific kinematic joint characteristics such as hip centre of rotation, and knee and ankle joint in total knee arthroplasty.

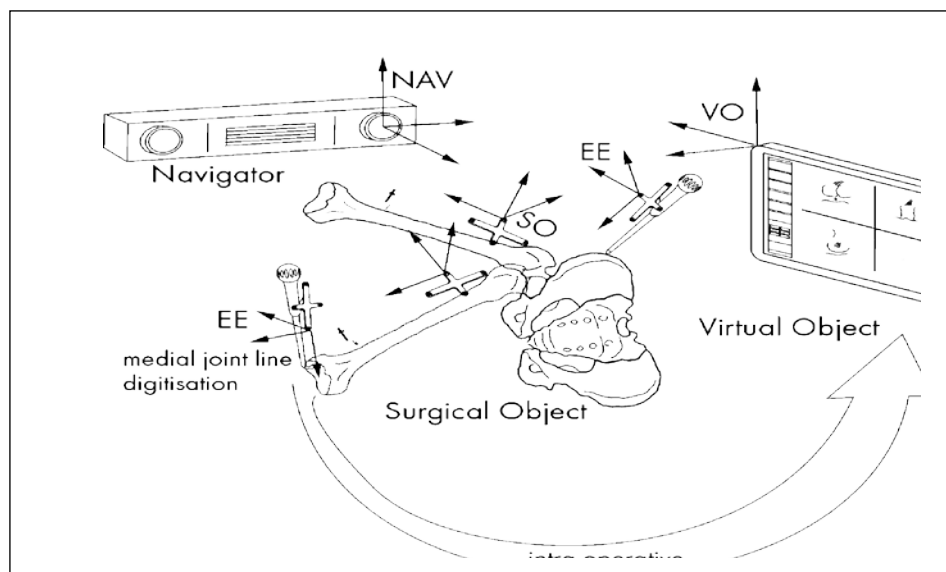


Figure 1.6: System setup for an image-free navigation system, including the basic components and their associated local coordinate systems (COS) by (Nolte and Beutler, 2004).

A more advanced image-free navigation system incorporate the use of statistical models of the addressed bony anatomy to construct virtual image of the bone (Stindel et al., 2002). This technology is called bone morphing technologies. This technology is based on sufficient number of high-resolution volumetric image datasets or on 3D surface scan of cadaveric bone samples and sufficient in the definition means it depends on the required accuracy, complexity and the morphological variability of the bone structure (Stindel et al., 2002).

Initially, image-free navigation is suited for anterior cruciate ligament (ACL) reconstruction and TKA due to its simplicity and superior workflow of the surgical modules (Nolte and Beutler, 2004,

Brisson et al., 2004, Lee et al., 2016). Image-free navigation has also been applied to other surgical procedures such as high tibial osteotomies(Kim et al., 2016), total knee arthroplasty (Reuven et al., 2017) and THA(Paprosky et al., 2019, Christ et al., 2018, Deep, 2018). However, there are challenges of accurately acquirement of all the necessary anatomical landmarks such as pubicum tuberculae in computation of anterior pelvic plane in THA and percutaneous digitization of landmarks in determination of leg mechanical axis in high tibial osteotomies; due to minimally invasive nature of the procedure (Nolte and Beutler, 2004). Besides that, the anatomical structure of virtual objects constructed are not as detailed as the image-based navigation system and the flaw is more prominent if there is major deformities involve in the surgical procedure (Sikorski and Chauhan, 2003).

### **1.3.2 Computer Assisted Orthopaedic Surgery in Total Hip Arthroplasty**

In Total Hip Arthroplasty (THA), CAOS is being practiced on both acetabular cup positioning and orientation, and femoral stem positioning. However, the implantation of femoral stem still uses the hand-rasping method instead of femoral milling, as the current rigid tools are not trackable inside femoral canal during milling or not able to mill the canal for anatomic femoral stem type implantation. Review done by

Hamlin et al (2005) showed that several studies focused only on the acetabular cup positioning due to inability of optical tracking system to track inside the bone during femoral milling for femoral stem implantation. Hence, the positioning of femoral stem is based on the hand-rasping method followed by the placement of tracker at femoral stem's neck shaft after insertion(Hamlin et al., 2005).In reducing the trauma, minimally invasive procedures are increasingly demanded for the THA surgery. There are several advantages using the femoral milling in a minimally invasive procedure compared to using the hand-rasping method, such as preventing intra-operative fractures and providing better fit with less trauma (Nishihara et al., 2006). Since the Minimally Invasive Surgery (MIS) has a better outcome and less complication, it is more widely practiced compared to the conventional approach. The femoral milling in MIS is not commonly practiced or developed due to the inability to track mill tip inside the bone to determine how deep the milling has been done, and space-constraint. This minimally invasive procedure needs a more dexterous manipulator for femoral milling. The implant malposition is a known potential cause for post-operative complication, be it acetabular cup malposition or femoral stem malposition. Malposition of the femoral stem due to various placements has been associated with poor outcomes such as cement mantle fracture, component loosening and subsidence (Min et al., 2008), and it is one of the factor in failure of the femoral component(Munuera and Garcia-Cimbrello, 1992). In addition,



the varus placement is also associated with the instability (Vresilovic et al., 1994). This error in technique can be minimized with the advent of CAOS, through which accurate and precise positioning of femoral stem is possible (Dorr, 2009).

An advantage in using the navigation system is that it may improve visualization and accuracy, and also control in MIS which is known to have limited exposure and direct visualization (Sikorski and Chauhan, 2003, Kanlić et al., 2006). Aside from that, surgeons will get better control, feedback, ability to correct errors and excellent documentation (Sikorski and Chauhan, 2003). A CT-based navigation technique has the ability to allow surgeons to precisely plan the alignment of the acetabular cup and femoral stem before the procedure and execute it according to the plan. Moreover, the exact real-time measurements and tracking enable surgeons to make better judgement in final positioning of the cup relative to the pelvis and femoral stem (Hafez et al., 2006). Additionally, a navigation system can improve accuracy in surgery by allowing its simulation and optimize planning via pre-planning feature of CAOS, and it has the potential to reduce invasiveness (Sugano, 2003, Viceconti et al., 2003). Moreover, the navigation enables development of minimally invasive surgical technique in Total Hip Arthroplasty because it permits the accurate orientation and fixation of the implant while looking only at the monitor (DiGioia et al., 1998b, DiGioia et al., 1998a). Multiple studies had concluded that a navigation system in the Total Hip Arthroplasty is

very accurate and reproducible, and more precise than the conventional technique(Jolles et al., 2001, Zheng, 2018, Banchetti et al., 2018, Chang et al., 2017, Zheng and Nolte, 2018, Perets et al., 2018a, Perets et al., 2018b).

### **1.3.3 Existing Surgical Navigation System**

The development of surgical navigation system in the past decades has given rise to a number of surgical navigation system made available at the clinical setting. Existing surgical navigation system includes OrthoPilot by Aesculap (Germany) (Chen et al., 2019), BrainLAB Navigation System by BrainLAB (Germany) (Fomekong et al., 2017), Surgetics Station by Praxim (France) (Robinson and Colombet, 2017), Stryker Navigation System by Stryker Orthopaedics (Molli et al., 2011), StealthStation by Medtronic Navigation (Takeba et al., 2018), and ORTHOsoft by Zimmer Biomet (Siddiqi et al., 2017).

One of the available surgical navigation systems is the OrthoPilot - an image-free, wireless navigation system used in the orthopaedic surgery. It builds the model of patient's anatomy intra-operatively via fixture of reflective markers fixed to the bone. These markers are tracked via optical tracking system. It registers the anatomical landmark to build the virtual model of patient's anatomy(Yamamoto and Ishibashi, 2016). The benefit of OrthoPilot is significant improvement in the patient function but it has longer operative time (Chen et al., 2019). The accuracy study on

OrthoPilot showed a satisfactory result in imageless navigation THA with less than 10 degrees of average discrepancies between the intra- and the post-operative measurements in all prosthetic alignment parameters, and less than 5 mm in leg length discrepancies (Takeda et al., 2017). This system showed that it could track the bone and implant positioning; it does not document whether this system could track surgical tools either outside the bone or inside the femoral canal (Takeda et al., 2017).

Another surgical navigation system is the BrainLAB Navigation System - an image-guided navigation system with optical tracking system that tracks passive markers fixed at the bone (Renkawitz et al., 2011, Fomekong et al., 2017). It is used in the orthopaedic surgery and neurosurgery, and it can navigate tools without pre-operative images by utilizing its bone morphing software. It has been documented that BrainLAB Navigation System improves the accuracy and safety of pedicle screw placement in spinal surgery (Rahmathulla et al., 2014), improves the accuracy of implantation of component in total knee arthroplasty (Cheng et al., 2012), and it is capable of laser surface scanning without rigid fixation in endonasal transphenoidal surgery that reduced the operation time (Duque et al., 2014). Although this system can track rigid surgical tools beyond the skull in neurosurgery, this system lacks the capability to track the flexible surgical tool inside the bone.

The Surgetics Station is another available navigation system that is a passive optical, open-platform, imageless system with the ability to measure knee alignment and kinematics in addition to guiding tunnel position in anterior cruciate ligament (ACL) reconstruction surgery (Robinson and Colombet, 2017). It has been documented that the usage of SurgeticsStation in ACL reconstruction surgery results in accurate positioning of graft in anatomic area, and prevention of femoral notch impingement (Plaweski et al., 2011). This navigation system demonstrates tracking rigid tools inside the knee joint but lacks the capability to track flexible tools inside the body, and it is not documented that this navigation system can incorporate hybrid tracking system in its navigation.

Other surgical navigation system accessible in the clinical setting is the Stryker Navigation System. It is an imageless system, which utilises the optical tracking system that tracks tracker pins placed at the bone shaft. It registers the anatomical landmarks to produce a virtual image in the navigation system (Molli et al., 2011). It has been documented that the total knee arthroplasty accompanied by this navigation system proves to be an effective tool in restoring the deformities of femur and tibia (Klein et al., 2006). It has also shown to improve the accuracy of the acetabular cup placement for total hip arthroplasty (Lin et al., 2011). However, it has the disadvantages of tracking only the rigid tools and not the flexible tools, as it only tracks via optical tracking system.

Another surgical navigation system applied in clinical setting is the StealthStation Navigation System. It is an image-guided navigation system with the capabilities of using and integrating multiple sources of radiographic images; it uses optical tracking system or electromagnetic tracking system (Sidhu et al., 2012). This navigation system proved in increasing the accuracy of pedicle screw placement in the orthopaedic surgery (Van de Kelft et al., 2012, Takeba et al., 2018, Molloy et al., 2014). Although the system has the capability of integrating with robotics, flexible catheters, and microscope integration, the system lacks navigation from the hybrid tracking system and the integration of flexible manipulator with milling capabilities.

ORHTOsoft is also another surgical navigation system that is imageless, has discs reflective markers instead of spherical reflective markers in its optical tracking system, and has bone morphing using navigation pointer. It was documented that this navigation system improves the accuracy of acetabular cup orientation in THA (Liu et al., 2015), and significant increase in accuracy of femoral hip resurfacing surgery component orientation regardless of surgeon's level of experience (Stiehler et al., 2015). Since this navigation system only uses optical tracking system to track its markers, it lacks the capability to track using hybrid tracking system that could potentially track flexible manipulator that can mill inside the femoral canal.

Table 1.1 below shows the existing surgical navigation systems along with its features. A navigation system that can track using hybrid navigation system is not available. A hybrid navigation system combines the optical tracking system with another tracking system such as electromagnetic tracking system, ultrasound tracking system, or potentiometer tracking system. This hybrid tracking system has the advantages to expand tracking ability by compensating flaw of one tracking system with the advantages of another tracking system such as to track flexible manipulator milling inside the femoral canal.

Navigation System	Features
The OrthoPilot® by Aesculap (Tuttlingen, Germany)(Jenny et al., 2009, Yamamoto and Ishibashi, 2016, Chen et al., 2019, Takeda et al., 2017)	<ul style="list-style-type: none"> <li>- Implanted wires and sensors allow the computer to track the position with infra-red technology.</li> <li>- Bony anatomy is marked with another infra-red sensors attached to a probe.</li> </ul>
BrainLAB (Heimstetten, Germany)(Renkawitz et al., 2011, Pitto et al., 2009, Fomekong et al., 2017, Rahmathulla et al., 2014, Duque et al., 2014)	<ul style="list-style-type: none"> <li>- Pre-operative CT Scan or intra-operative Bone Morphing® software and infrared navigation to guide the reamer accurately.</li> <li>- Reference pins inserted to bony anatomy and dynamic reference base is attached to it.</li> </ul>

<p>Surgetics® Station by Praxim (La Tronche/France)(Stindel et al., 2005, Stindel et al., 2008, Robinson and Colombet, 2017)</p>	<ul style="list-style-type: none"> <li>- Uses two infra-red light emitting cameras, which receive its signals back by the reflective markers.</li> <li>- Passive system and markers are mounted in specific configuration for each item being tracked.</li> <li>- Micro-millimetre positioning navigation aid and visualization can be based on anatomic data from radiological imaging sources.</li> </ul>
<p>Bone Morphing® (Parratte et al., 2007, Stindel et al., 2004, Stindel et al., 2002, Bae and Song, 2011)</p>	<ul style="list-style-type: none"> <li>- Allows building of 3D models of patient bones directly during surgery by taking a large set of exposed bone surface points with a pointing tool.</li> </ul>
<p>Stryker Navigation System (Stryker Orthopaedics) (Molli et al., 2011, Lin et al., 2011)</p>	<ul style="list-style-type: none"> <li>- Imageless navigation system.</li> <li>- Uses infrared cameras and light-emitting diodes to track tracker pins placed in shaft of the bones.</li> <li>-Registration by identification of anatomical landmarks.</li> <li>- Has "reactive workflow" software and has algorithm to calculate the centre of the ankle joint.</li> </ul>
<p>StealthStation (Medtronic Navigation) (Molloy et al., 2014, Takeba et al., 2018, Van de Kelft et al., 2012)</p>	<ul style="list-style-type: none"> <li>- An image-guided navigation system that can merge images from CT, MRI, CTA, MRA, or 2D/3D fluoroscopic.</li> <li>- Automatic registration system and automatic detection of fiducials.</li> <li>- Optical or electromagnetic tracking capabilities.</li> </ul>
<p>ORTHOsoft (Zimmer Biomet) (Siddiqi et al., 2017, Stiehler et al., 2015, Liu et al., 2015)</p>	<ul style="list-style-type: none"> <li>- Imageless navigation system</li> <li>- Reflective marker discs used instead of spherical reflective markers that offer better range of visibility to the camera.</li> <li>- Bone morphing via navigation pointer.</li> </ul>

Table 1.1: Existing Surgical Navigation System available in clinical setting and their features.

#### 1.4 Robotics in Orthopaedics

Robotic surgery has been applied in various specialties that includes urology (Rassweiler et al., 2006), gynaecology (Advincula and Song, 2007), and general surgery (Marecik et al., 2007). The advantages of robotic surgery over traditional open approach are reduction in hospital stays,

reduction in complication rates, and surgeons are able to perform fine movement task better. However, the disadvantages of robotics surgery are it increases the operation time, big financial cost, and the need for specific training to use the robotic equipment and techniques. (Hussain et al., 2014). In orthopaedics, robotic surgery can be classified in three categories, which are autonomous robotic surgery (Schulz et al., 2007), haptic robotic surgery (Banks, 2009), and passive robotic surgery (Roche, 2014). Its usage has been increased due to positive short-term radiological outcome, increased accuracy of the component's alignment, and better consistency in ligament balance (Lang et al., 2011). The advent of computer-aided surgery (CAS) and surgical robotics has given a lot of improvement to minimal invasive surgery (MIS). It enhances three advantages of MIS over conventional surgery, which are free manoeuvrability for the instrument, sensory feedback and three-dimensional imaging (Plinkert and Löwenheim, 2009).

#### **1.4.1. Existing Robotic Orthopaedic System**

In the past decades, the robotic orthopaedic system has been developed and documented in numerous studies, which gave rise to a number of commercially available robotic orthopaedic systems that has been applied in clinical setting.

Earliest documented robotic orthopaedic system is ROBODOC that is still being improved based on the research data over past



decades (now renamed into THINK Surgical TSolution-One). It is an active-autonomous, image-based, robotic milling system with navigation system that applies in the hip arthroplasty, knee arthroplasty, and ankle arthroplasty (Liow et al., 2017). It is documented that ROBODOC system have high degree of accuracy with results showed the difference between pre-operative plan and post-operative CT were less than 5% in terms of canal fill, less than 1 mm in gap, and less than 1 degree in mediolateral and anteroposterior alignment (Nishihara et al., 2004). However, there are several disadvantages of this system to be noted, such as the longer operation time, the robot manipulator arm was rigid, has higher learning curve, operation done with straight femoral stem, and requires normal open incision approach rather than Minimally Invasive Surgery (MIS) approach (Netravali et al., 2016).

Some other early robotic orthopaedic system is CASPAR - an image-guided, active robotic milling system used for THA and TKA (Allen et al., 2018). It has been shown to have increase accuracy in femoral preparation and position on the femoral side (Wu et al., 2004). Even so, CASPAR has shown low accuracy of post-operative anteversion angles of the femoral stem compared with the pre-operative plan (Mazoochian et al., 2004). On top of that, CASPAR needs longer operation time, increases intra-operative blood loss, significant lower hip abductor function, rigid manipulator, requires normal open incision approach, and higher overall complication rate (Siebel and Käfer, 2005).

Active constraint robot (ACROBOT) is another robotic orthopaedic system. It is a semi-active robot with active constraint robotic milling system, image-based, and surgical navigation system that was used in total knee arthroplasty (Jakopec et al., 2001). Its drawbacks are the rigid manipulator, and the absence of virtual navigation tracking system (Jakopec et al., 2003).

The BRIGIT system is also a robotic orthopaedic system; it is a semi-active robot, acts as positioner of tool-guides for sawing or drilling, imageless, and not guided by navigation system for used in total knee arthroplasty or osteotomy (Maillet et al., 2005). It has high precision of trajectory positioning and has ability of motion control (Kuang et al., 2018). But its flaws are the use of rigid manipulator, and not tracked and guided by a navigation system.

Another developed robotic orthopaedic system is Mako RIO. It is a semi-active robot, image-based robotic milling system with the ability of real-time tracking and positioning via the navigation system, and has the capability known as the Tactile Guidance System (TGS), which provides tactile feedback to the surgeon during operation (Kuang et al., 2018, Jacofsky and Allen, 2016). It has been documented to be used in the Minimally Invasive Surgery (MIS) of unicompartmental knee arthroplasty with improved accuracy of component positioning, improved precision, and has good post-operative outcome (Buechel and Conditt,

2016, Bell et al., 2016, Millar et al., 2018, Lonner and Klement, 2019). Other than that, Mako RIO is also used in MIS of Total Hip Arthroplasty (THA) with better precision and accuracy in component positioning, and better post-operative outcome (Banchetti et al., 2018, Qin et al., 2018). It is a system with good potential in the future, but it lacks the capability to track the end effector inside the bone during milling because it is tracked via optical tracking system and uses rigid manipulator in milling the bone.

A small size, lightweight, and portable device called the Navio Precision Freehand Sculpting (PFS), is a freehand intelligent micro tool that gives control in the hand rather than a robotic arm (Smith et al., 2014, Brisson et al., 2004, Lonner, 2016). It provides good accuracy in the bone cutting, guided by the image free navigation system (Lonner et al., 2015, Leelasestaporn, 2018). This is done by controlling the contact of rotary cutting tool to only cut the bone based on the pre-planning. The PFS system has the ability to give surgeons real-time feedback on the bone kinematics, range of motion, and implant placement. The system tracks in real-time and displays both the tool and the bone surface on the monitor. The PFS tracks by detecting the presence of tracking array attached at the tool via optical tracking. The pre-planning feature enables display of target area to be cut (Brisson et al., 2004, Lonner, 2016, Shaner et al., 2016). Other advantages of PFS system are the ability to cut complex shapes, reduces incision size by reducing direct

visualization of the bone, and control of the cut (Levison et al., 2000, DiGioia III et al., 2003, DiGioia et al., 1998a, Shaner et al., 2016, Lonner, 2016). This is done by means of stopping the motor, or retracting behind a guard (Brisson et al., 2004). There is one clear disadvantages of PFS system, which is lack of comparison between pre-operative planning and post-operative cut of the bone due to it being image-free navigation system (Brisson et al., 2004, Smith et al., 2014). It can only give virtual representation of the bone surface traced during registration stage. Also, it may increases the surgery time due to the planning stage is done intra-operatively (Smith et al., 2014, Nolte and Beutler, 2004). Another disadvantages of this system are it uses rigid milling tool, and the end-effector cannot be tracked inside the bone because it uses optical tracking system (Leelasestaporn, 2018, Lonner, 2016, Shaner et al., 2016).

#### **1.4.2. Robotics micro-tools**

In the early 2000s, the advantages of free manoeuvrability for the instrument are still not fully developed since some areas in surgical operations are still not accessible via rigid surgical tools, or the current surgical tools are not accurate enough for MIS (Dario et al., 2000). Therefore, following that, free manoeuvrability tools, or flexible surgical tools have been investigated. Through the use of these flexible tools, surgeons can access problematic zones such as sinuses in endonasal sinus surgery, visualization of hidden tissue structures in arthroscopy

(Dario et al., 1997, Payne et al., 2015, Roche and Calder, 2015), to avoid lateral collateral ligament (LCL) injury in anterior cruciate ligament (ACL) reconstruction surgery (Watanabe et al., 2011), and a curved-drilling approach in core decompression of the femoral head osteonecrosis (Alambeigi et al., 2017). Besides that, the development gave rise to emergence of laparoendoscopic single-site surgery (LESS) procedure (Wang et al., 2018) with developed system such as da Vinci Single-Site system for urologic surgery (Kaouk et al., 2014), SPRINT surgical robot system used in laparoscopic surgery (Quaglia et al., 2014), and i-Snake surgical robot that is capable to multitask with two flexible arms and articulated head (Shang et al., 2012). These flexible robots have high degree of freedom to provide dextrous movement inside body cavity, and have intuitive manoeuvrability (Wang et al., 2018). Some flexible tools have also demonstrated to be able to control a needle puncture and penetrate tissues from any point within the body such as in tissue biopsies (Brett, 2007); reduce insertion forces and prevent buckling by using robot-assisted and steerable electrode prototypes in cochlear implant surgery (Zhang et al., 2010); and carry out vascular catheterization to treat cardiac and vasculature disease (Beasley, 2012). However, the flexible tools available are not able to provide bone milling in orthopaedic surgery due not being stiff enough for milling and the buckling effect (Hu et al., 2018, Li et al., 2017, Wang et al., 2018).

The emergence of robotic micro-tools gives the opportunity for developing an articulated drill tip, which can be integrated into computer-aided surgical system. The benefits include the utilization of femoral milling in MIS total hip arthroplasty, tunnel drilling in ACL reconstruction, milling in revision of arthroplasty, and drilling in head and neck surgery. Due to the fact that articulated drill tip is not trackable via optical tracking system, this project focus on developing hybrid navigation system for tracking articulated drill tip by using both optical and potentiometer tracking system. Optical tracking system tracks the surgical tools outside the drill hole while potentiometer tracking system is used to track the end of articulated drill tip. The articulated drill tip system is then experimented on CAOS total hip arthroplasty followed by evaluation of the positioning and orientation of femoral stem placement by femoral milling. Table 1.1 below highlights the features of robotic surgical system mentioned above and also the proposed new system by the research in filling the research gap.

Robotic/steerable drill	Manipulator	Tracking	Navigation	Control
<b>Blue Belt</b> (Smith et al., 2014, Lonner, 2016, Leelasestaporn, 2018, Shaner et al., 2016)	Rigid	Optical Tracking	Virtual model	Free-hand
<b>MAKO</b> (Sugano, 2003, Kuang et al., 2018, Jacofsky and Allen, 2016)	Rigid with haptics	Optical Tracking	Virtual model	Semi-active
<b>OMNIBotics iBlock</b> (Siddiqi et al., 2017, Koenig and Plaskos, 2019, Figueroa et al., 2019)	Rigid	Optical Tracking	Virtual model	Semi-active
<b>Mazor X</b> (Bozzio et al., 2019, Fiani et al., 2018)	Rigid with haptics	Optical Tracking and Fluoroscopy	Virtual model	Semi active
<b>Rosa Knee System</b> (Klein et al., 2019, Parratte et al., 2019)	Rigid with haptics	Optical Tracking	Virtual model	Semi-active
<b>ACROBOT</b> (Jakopec et al., 2001, Jakopec et al., 2003)	Rigid	Mechanical Tracking	Over-constrain	Semi-active
<b>ROBODOC</b> (Bargar et al., 1998, Liow et al., 2017, Netravali et al., 2016)	Rigid	Mechanical Tracking	No	Active

<b>BRIGIT</b> (Maillet et al., 2005)	Rigid		Mechanical Tracking	No		Semi-active
<b>CASPAR</b> (Siebert et al., 2002)	Rigid		Mechanical Tracking	No		Active
<b>Continuum Manipulator</b> (Alambeigi et al., 2017)	Flexible		X-ray	X-ray		Passive
<b>da Vinci Single-Site system</b> (Kaouk et al., 2014)	Flexible		Visual Camera	Direct Navigation	Visual	Semi-active
<b>SPRINTSurgicalSystem</b> (Quaglia et al., 2014)	Flexible		Optical Tracking	Direct Navigation	Visual	Semi-active
<b>i-SnakeSurgicalSystem</b> (Shang et al., 2012)	Flexible		Visual Camera	Direct Navigation	Visual	Semi-active
<b>Our Articulated Drill</b>	Flexible with milling capability		Optical Tracking Potentiometer Tracking	+ Virtual model		Free-hand

Table 1.2: Existing Robotic Orthopaedic System, and Flexible Robotic System in Surgery.



Since the femoral stem is slightly curved to follow the anatomical shape of femur, current robotic surgical tools may not be sufficient to mill the femoral canal under minimally invasive hip arthroplasty.

The concept of articulated drill system by three bar kinematic chain is possible to solve this problem. This is because the tools need to fit within the small incision and inside femoral canal, able to bend to enable milling the curve shape of femoral stem, and the tool is rigid enough to make femoral canal drilling possible without buckling effect at the base. Flexible manipulators for surgery have been developed for arthroscopy (Dario et al., 2000, Dario et al., 1997, Payne et al., 2015, Roche and Calder, 2015), ACL reconstruction surgery (Watanabe et al., 2011), vascular catheterization (Reddy et al., 2007), laparo-endoscopic single site surgery (LESS) (Wang et al., 2018), urology (Kaouk et al., 2014), laparoscopy (Quaglia et al., 2014, Shang et al., 2012), and catheter ablation (Schmidt et al., 2008) but these flexible manipulators are not capable of milling the bone, particularly the femoral canal on top of being a dextrous manipulator.

### **1.4.3. Wire Actuators as Tendons**

The articulated drill system proposed by the researcher has wire-driven steering capability for bending of the joints. There are studies done on the concepts of wire-driven steerable manipulator for minimally invasive surgery (Cha et al., 2010)(Haraguchi et al., 2015, Ji et al., 2019, Chen et al., 2016, Li et al., 2016), wire-driven manipulator for laparoscopic surgery (Hu et al., 2018, Ibrahim et al., 2015, Shang et al., 2012, Quaglia et al., 2014), wire-driven flexible manipulator with electromagnetic positioning (Song et al., 2015, Song et al., 2018), wire-driven manipulator for bronchoscopic intervention (Liu et al., 2016), tendon-sheath driven manipulator for endoscopic surgery (Lau et al., 2015), 3PUU parallel manipulator that has capability of drilling but lacks the capability of moving inside small space due to its large size (Fernandes and Selvakumar, 2018), and minimal invasive tendril robot for in-space inspection (Mehling et al., 2006) has been developed. However, these studies of tendon-driven continuum manipulators, tendon-driven serpentine manipulators, and concentric tube manipulators lacks the study on the capability of manipulators to mill bone on top of able to articulate into small space (Li et al., 2017). The benefit of wire driven manipulators include the fact that there is no large space requires for actuation, and an ability to actuate the tools into a curved configuration(Ji et al., 2019).

## **1.5 Research Question**

### **1.5.1. The Need for Articulated Drill Sheath with capability to mill under different configuration**

The need for an articulated drill is driven by the increasing clinical requirement for improving the surgical outcomes and decreasing the complications of the THA procedure. Besides that, after the total hip arthroplasty (THA) procedure, there is also probability of the patient end up with unequal leg lengths, which are referred to as a leg-length discrepancy (LLD). One way to reduce the risk in THA procedure is by improving the accurate placement and alignment of implants using robotic technology. In Total Hip Arthroplasty (THA), the usage of robotic orthopaedic surgery per se is applied in the acetabular cup positioning and orientation, and femoral stem positioning. However, in robotic orthopaedic surgery with tracking and navigation system, the femoral stem insertion depends on hand-rasping method and confirmation of position by placing tracking marker at the neck shaft of femoral stem after insertion. Besides that, femoral milling with navigation for anatomic femoral stem insertion was not feasible due to its slightly curved profile. This is because current tools are not able to track milling that follows the curve profile of anatomic femoral stem.

It is this researcher's hypothesis that a minimally invasive hip arthroplasty procedure would benefit from a flexible manipulator. Conventional drills can only make a straight pilot tunnel from the entrance

point of the femur. Since the femoral stem is slightly curved to follow the anatomical shape of femur, current surgical tools are not sufficient to remove femoral cortex during minimally invasive revision hip arthroplasty. Moreover, the studies done on full utilization of robotic surgical system for both acetabular cup and femoral stem milling and implantation is limited to normal incision approach rather than minimal invasive surgery (MIS) approach (Schulz et al., 2007). This minimally invasive procedure needs an articulated manipulator for femoral milling. Existing flexible manipulators have high dexterity but lacks the capability of milling on top of being flexible. The flexible tools available are not able to provide bone milling in orthopaedic surgery due not being stiff enough for milling and the buckling effect (Hu et al., 2018, Li et al., 2017, Wang et al., 2018).

### **1.5.2. The Need for Hybrid Tracking System to track articulated drill sheath when milling inside the bone**

Optical tracking system can only track objects within the line of sight of the camera. However, when milling inside the bone, the optical tracking system unable to track due to obstruction of line of sight. Some CAOS system such as MAKO Surgical Robot (Jacofsky and Allen, 2016) and Navio Precision Sculpture System(Lonner, 2016) able to track end effector when milling the bone up to certain depth due to kinematics of the rigid manipulator used. The proposed articulated drill sheath by the researcher has some degree of flexibility and need additional tracking

system to track the end effector of articulated drill sheath deep inside femoral canal. The researcher's proposal of incorporating potentiometer tracking system with optical tracking system is to track the articulated drill system when milling inside femoral canal. The potentiometer will track the changes in joint angle of each joint of articulated drill sheath. As the optical tracking system only can track the open part of the articulated drill mechanism, when the tip of the articulated drill tunnels and bends inside the bone, a potentiometer tracking system is developed to provide the position information for the articulated manipulator.

### **1.5.3. The Need for Navigation Software for articulated drill sheath to Visualize the Tracking**

Review of existing navigation system showed that most of navigation system navigates the surgery by optical tracking system, electromagnetic tracking system, or ultrasound. Navigation system with feature of integration optical tracking system with another tracking system such as potentiometer tracking system (hybrid tracking system) is not documented. Besides that, it is not documented that a navigation system with capability to navigate articulated manipulator that can also mill inside the bone. The researcher proposes to develop a navigation system that can visualize input from hybrid tracking system to track articulated drill sheath.

#### **1.5.4. The Need to Measure Reaction Force when Milling in Different Configurations, and Confirm the Capability of Articulated Drill System to Sustain Bending**

The articulated drill system has milling capability on top of having capability to articulate. The capability of milling under different configurations of bending are to be tested to determine whether the cutting force is sufficient enough to cut bone, and to confirm the capability of articulated drill system to sustain bending while milling the bone. This experiment will determine the static profile of articulated drill system in milling bone. This experiment will be done because the researcher needs to determine which configuration has the best bone cutting capability so that the data could be used in future research on optimizing the articulated drill system. The effects of buckling is also to be observed because it is documented that flexible manipulators have characteristic of buckling under high opposing force due to lack of stiffness (Hu et al., 2018, Wang et al., 2018).

### **1.5.5. The Need to Analyze the 3D Geometry of Curved Tunnel from Milling Guided by the Navigation System**

Experimentation on 3D geometric analysis of the shape of the cut area in comparison to femoral stem outline in pre-plan of navigation software will be done to determine accuracy and repeatability of articulated drill system in milling the shape of femoral stem inside the bone. This experiment will be done to measure the deviation of the cut area from the femoral stem outline in the pre-plan. This experiment is limited to cutting the curved shape of femoral stem inside femur only.

### **1.5.6. The Need to Test the Accuracy of the Navigation System in Milling the Femoral Stem Shape Inside Femur Sawbone.**

The experiment accuracy analysis/ symmetry analysis will be done to measure the accuracy of articulated drill system in cutting the shape of femoral stem inside the femur sawbone. This experiment will determine whether the articulated drill system have sufficient accuracy in milling the femoral stem shape in order for femoral stem implantation. ROBODOC have been documented to achieve accuracy of 1 mm gap (Nishihara et al., 2004). Thus, this experiment will be done to determine whether the articulated drill system have accuracy not far from ROBODOC accuracy.

## **1.6 Research Objectives**

The objectives of this research are:

- Design and development of articulated drill sheath with motor control from straight shaft to bendable shaft
- Design and development of hybrid tracking system, combination between optical tracking system and potentiometer tracking system in order to track surgical tool inside the bone.
- Design and development of navigation software for articulated drill sheath.
- To measure reaction force when milling in different bending configuration and rake angles, and understanding the static performance of articulated drill system under different configurations, and confirm the capability of the articulated drill system to sustain bending when milling under different configuration.
- To analyse the 3D geometry of curved tunnel from milling guided by the navigation system.
- To test the accuracy of the navigation system in milling the femoral stem shape inside femur sawbone.



## **1.7 Thesis Outline**

This thesis is divided into seven chapters. Chapter one will discuss on the literature review, research gap, objectives of this research, and the research methodology. Chapter two will discuss on concept and hardware of articulated drill system and its hybrid navigation system. Chapter three will discuss on the navigation software of the articulated drill system. Chapter four will discuss on force measurement experiment, and to confirm the capability of articulated drill system to sustain bending when milling under different configuration. Chapter five will discuss the experiment on 3D geometric analysis of the shape of the cut area, and accuracy analysis/symmetry analysis. Chapter six will be the discussion section of the thesis, and discuss on the limitation of the research, Chapter seven will describe the potential future research following this research.

## **1.8 Conclusion**

Total hip arthroplasty (THA) is one of common procedure done due to its proven success rate. THA has evolved from conventional approach to minimally invasive approach. Minimally invasive approach has benefits of minimizing soft tissue damage, faster post-operative recovery, and better outcome. However, minimally invasive approach has disadvantages of limited visualization of surgical area. Computer assisted orthopaedic surgery (CAOS) technology is applied to overcome the challenges of limited

---

visualization of surgical area. CAOS has further developed to incorporate robotic surgical devices resulting in additional advantages of enhancing accuracy and precision aside from visualization of surgical area. Application of CAOS with robotic surgical device in THA is currently practiced only on acetabular cup milling, positioning, and orientation, while femoral stem positioning is still using hand-rasping method followed by insertion of trial with tracker instead of femoral milling. The main reason behind it is because currently there are yet any method to track milling procedure inside femoral canal due to limitation of optical tracking system that requires clear line of sight between camera and object tracked. Besides that, minimally invasive approach limits the use of standard rigid surgical mill due to small surgical window. The emergence of robotic micro-tools give opportunity for development of articulated drill system that is when combined with CAOS has the ability to mill inside femoral canal and is trackable under minimally invasive approach. Articulated drill system is developed to minimize complications in THA such as prevention of intra-operative fractures, dislocations and leg length discrepancy by a new level of precision. This research has the objectives of design and development of articulated drill tip sheath with motor control from straight shaft to bendable shaft, design and development of hybrid tracking system, combination between optical tracking system and potentiometer tracking system in order to track surgical tool inside the bone, design and development of navigation system for articulated drill sheath, to measure reaction force when milling in different bending

---

configuration and rake angles, and understanding the static performance of articulated drill system under different configurations, and confirm the capability of the articulated drill system to sustain bending when milling under different configuration to analyse the 3D geometry of curved tunnel from milling guided by the navigation system, and to test the accuracy of the navigation system in milling the femoral stem shape inside femur sawbone.

---

## **CHAPTER 2 - CONCEPT OF ARTICULATED DRILL AND ITS NAVIGATION SYSTEM**

### **2.1. Introduction**

This chapter will explain on the concept of articulated drill system for total hip arthroplasty as a whole. It covers concept design that highlighted the development of articulated drill tip integrated into CAOS robotic surgical system derived from the emergence of robotic micro-tools. A three-bar kinematic chain is therefore used for the concept of the articulated and steerable drill.

The design of the articulated and steerable drill system consists of the three multiple rigid segments that act as a sheath to a flexible shaft connected with a drill/bur attaching at the end to the control box before the actuation of the flexible drill took place. The hardware for articulated drill system is therefore comprised of three main components which is the articulated drill sheath, the motor box and the flexible drill shaft that fits inside the articulated drill sheath.

The second part is the design is the development of a hybrid tracking system for the articulated drill tip that consists of an optical tracking system and a potentiometer tracking system. The optical tracking system will track the base of articulated drill sheath and the potentiometer tracking system is linked to track the articulated drill sheath inside the bone. Therefore, the

potentiometer system will act as the extension for the optical tracking system. Tracking is made possible with the kinematics of articulated drill and data obtained from potentiometer tracking system. Optical tracking system and potentiometer tracking system are integrated in the navigation software of articulated drill navigation system.

## **2.2. Concept Design**

The research is driven by the clinical requirements in improving the accuracy and reducing the trauma in orthopaedic surgery. Despite the precision of robotics in surgery, the current system only focuses on the locational accuracy of the end point and entrance point of femoral tunnels respectively. In the case of Minimally Invasive Surgery (MIS) Total Hip Arthroplasty (THA), the current robotic surgical system does not focus on the shape of the pathway in femur and can only make a straight tunnel from the entrance point of the femur. Since the femoral stem is slightly curved to follow the anatomical shape of femur, a new articulated surgical drill is required to mill a curved femoral canal under the guidance of its navigation system for THA. The emergence of robotic micro-tools give opportunity for development of articulated drill tip integrated into CAOS robotic surgical system. The articulated drill can benefit patients by adopting a minimal invasive approach due to its variable bending configuration. The benefit includes utilization of femoral milling in MIS total hip arthroplasty, tunnel

drilling in ACL reconstruction, milling in revision of arthroplasty, and drilling in head and neck surgery.

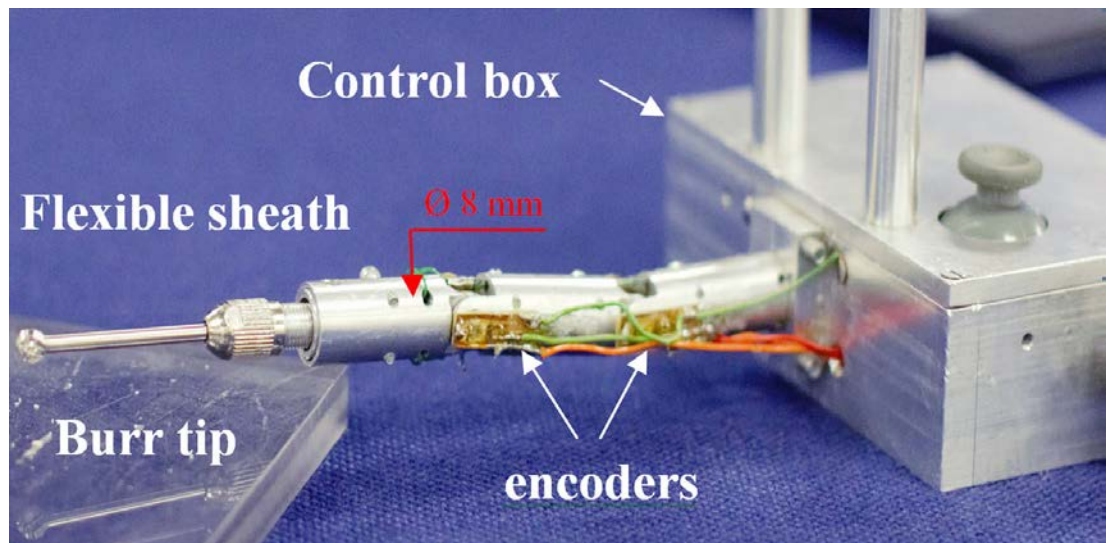


Figure 2.1:A prototype of the articulated drill mechanism

As the current robotic systems are not able to perform femoral milling for MIS THA, the researcher's proposed system consists of a full actuated and dexterous articulated manipulator which allows accurate and precise position and orientation control; a multimodality tracking and navigation system provide a breakthrough technology to enhance the capability of the surgical robotic tools; and a cutting edge technology of mapping and pre-operative surgical planning. This system demonstrates an innovative robotic platform to allow surgeons to achieve a new level of precision and flexibility.

The concept design of the system shown in Figure 2.1 consists of a novel articulated drill to enable intra-operative tunnelling, and a navigation system for tracking and navigating for the end-effector (EE) inside the bone. Due to the fact that the articulated drill tip is not trackable via current optical tracking system, this research focus on developing hybrid tracking system for the articulated drill by integrating optical tracking devices and position sensors in the articulated tips. The optical tracking system tracks the surgical tools outside the drilling canal, while potentiometers are used to track the end of the articulated drill tip. A navigation system of the new robotic system guides the procedure by providing a real-time virtual model of the articulated drill and its association with a CAD bone model from a CT scan. The articulated drill system is then experimented in sawbones, followed by an evaluation of the positioning of femoral stem placement by femoral milling. This system demonstrates an innovative robotic platform designed to allow surgeons to achieve a degree of precision and flexibility in milling inside bone. The manipulator is required to fit within a small incision inside the femoral canal, to be able to bend for the milling of the curved shape in the femur, and to be rigid enough to make femoral canal possible without any buckling at the base.

---

### 2.3. Kinematics and coordination transformation

A serial manipulator that consists of three rigid segment is designed as the articulated drill mechanism from the kinematic sketch of the mechanism in Figure 2.2. This is because simulates the structure of human finger that can be inserted into small canal and is capable of bending. The drill mechanism is designed as a kinematic chain with three bar in serial attached by two revolute joints, allowing one link to rotate with respect to the other links. As illustrated in the following figure 2.2, the geometric model for each link is specified as  $A_i$  in a single rigid body; the origin of the body frame determines the axis of rotation. The rotation in the chain occurs about a revolute joint, therefore the origin of the body is the joint between  $A_i$  and  $A_{i-1}$  for each  $i > 1$ . The  $x_i$  -axis for the body frame of  $A_i$  is defined as the line through the two points where the joints are in  $A_i$  as shown in Figure 2.3. The kinematics of the manipulator is calculated using Denavit–Hartenberg (D–H) parameters (Denavit and Hartenberg, 1955).



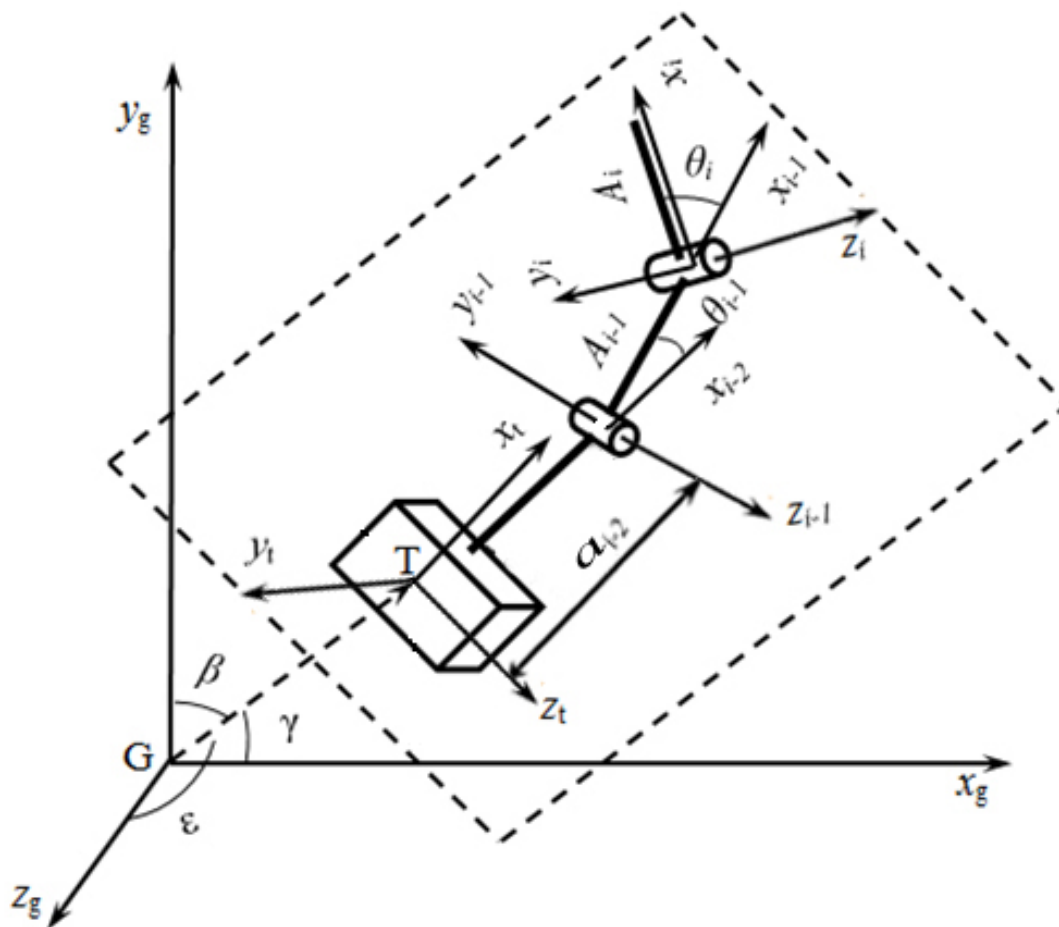


Figure 2.2: Kinematic sketch of the articulated drill. The point T is not a prismatic joint. The box symbol represents the motor box of the articulated drill sheath.

To determine the location of each link in a plane, the homogenous transformation matrix is applied to the point  $(x_t, y_t)$  at the base of the link as,

$$T_1 = \begin{pmatrix} \cos \theta_1 & -\sin \theta_1 & x_t \\ \sin \theta_1 & \cos \theta_1 & y_t \\ 0 & 0 & 1 \end{pmatrix} \quad (1)$$

Based on Figure 2.3,  $a_{i-1}$  is the distance between the joints in  $A_{i-1}$ . The angle between  $A_i$  and  $A_{i-1}$  is denoted by  $\theta_i$ . Therefore, the homogenous transformation matrix  $T_i$  for link  $A_i$  for  $1 < i \leq m$  is as shown below,

$$T_i = \begin{pmatrix} \cos \theta_i & -\sin \theta_i & a_{i-1} \\ \sin \theta_i & \cos \theta_i & 0 \\ 0 & 0 & 1 \end{pmatrix} \quad (2)$$

The equation above describes the difference between the body frame  $A_i$  and the body frame  $A_{i-1}$ . The equation shows the transformation of the links by rotating it counter-clockwise by  $\theta_i$  and then translating it along x-axis by  $a_{i-1}$ . It is expressed by moving  $A_i$  from its body frame into the body frame of  $A_{i-1}$ . By applying again the same transformation matrix  $T_{i-1}T_i$ , we can move both  $A_i$  and  $A_{i-1}$  to the body frame of  $A_{i-2}$ . We can follow the same procedure until  $A_m$  by multiplying the transformation matrices.

$${}^m_3T = {}^m_1T {}^1_2T {}^2_3T \quad (3)$$

In a planar space  $y_m-x_m$ , the articulated drill sheath is a Planar Three-Link Manipulator. Therefore,  $A_i$  is  $1 \leq i \leq m$  with  $m$  is replaced by three. The transformation starts with body frame  $A_3$  as shown in Figure 2.3, by which  $T_3$  is applied to it to rotate by  $\theta_3$  and then translated by  $a_2$ . Following that, body frame  $A_2$  will take place at the initial configuration  $A_3$  and will be attached to  $A_3$ . To complete the transformation,  $T_2$  is applied to the previous results and it

will rotate both  $A_2$  and  $A_3$  by  $\theta_2$  and then translated them by  $a_1$ . This will put  $A_2$  and  $A_3$  in their proper configuration and  $A_1$  can be placed in the initial configuration. In the kinematics of the articulated drill manipulator, each  $T_i$  is defined by two parameters,  $a_{i-1}$  and  $\theta_i$ .

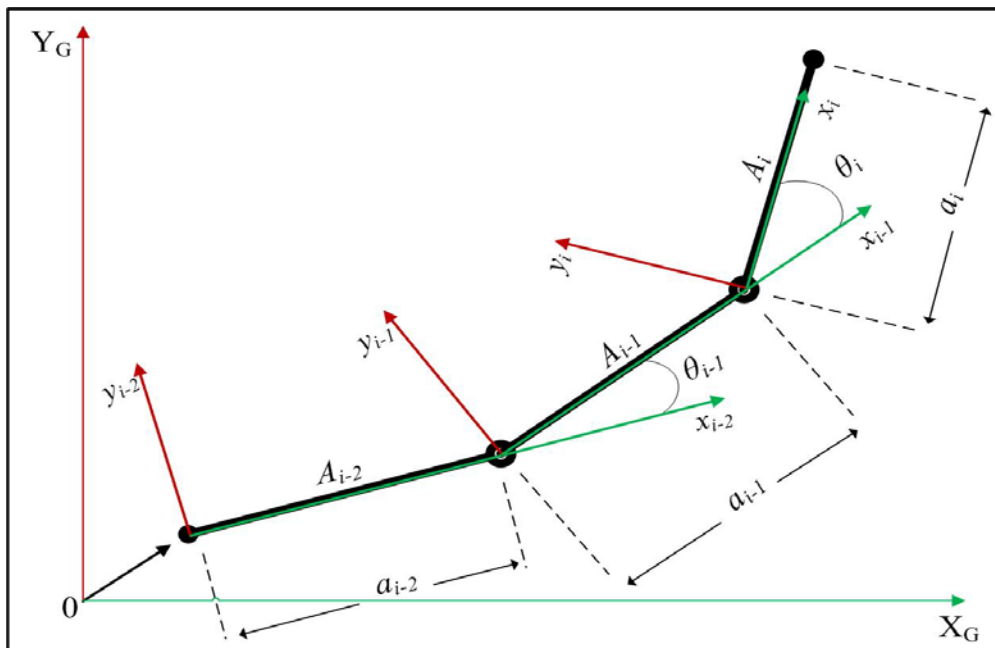


Figure 2.3: Kinematics in 2D (planar space). The body frame of each  $A_i$ , for  $1 < i < m$ , is based on the joints that connect  $A_i$  to  $A_{i-1}$  and  $A_{i-2}$ .

$$T_i = \begin{pmatrix} \cos \theta_i & -\sin \theta_i & 0 & a_{i-1} \\ \sin \theta_i \cos \alpha_{i-1} & \cos \theta_i \cos \alpha_{i-1} & -\sin \alpha_{i-1} & -\sin \alpha_{i-1} d_i \\ \sin \theta_i \sin \alpha_{i-1} & \cos \theta_i \sin \alpha_{i-1} & \cos \alpha_{i-1} & \cos \alpha_{i-1} d_i \\ 0 & 0 & 0 & 1 \end{pmatrix} \quad (4)$$

As in the planar kinematics, the first matrix for 3D transformation,  $T_1$ , is special. It is a representation of any position and orientation of  $A_m$ , it could

be defined as a general rigid-body homogeneous transformation matrix. This results in the rigid-body homogeneous transformation matrix  $T_m$ , being applied after the homogeneous transformation matrix, that for each  $i$  the value is  $2 \leq i \leq 4$ . Thus, only  $T_1$  will be defined as general rigid-body homogeneous transformation matrix and this represents the base six degree of freedom movement that is tracked by the optical tracking device. The 3D transformation will be defined as  $T_i$  from equation 4 for each of the link in the articulated drill sheath. The general rigid-body homogeneous transformation ( $T_1$ ) is a 4 x 4 matrix that performs the rotation given by  $R(\beta, \gamma, \epsilon)$ , followed by a translation given by  $x_t, y_t, z_t$ . The result is transformation of the kinematics into global coordinate system as in equation 5 below.

$$\begin{aligned}
 & {}^g_m T \\
 &= \begin{pmatrix} \cos \beta \cos \gamma & \cos \beta \sin \gamma \sin \epsilon - \sin \beta \cos \epsilon & \cos \beta \sin \gamma \cos \epsilon + \sin \beta \sin \epsilon & x_t \\ \sin \beta \cos \gamma & \sin \beta \sin \gamma \sin \epsilon + \cos \beta \cos \epsilon & \sin \beta \sin \gamma \cos \epsilon - \cos \beta \sin \epsilon & y_t \\ -\sin \gamma & \cos \gamma \sin \epsilon & \cos \gamma \cos \epsilon & z_t \\ 0 & 0 & 0 & 1 \end{pmatrix}
 \end{aligned}
 \tag{5}$$

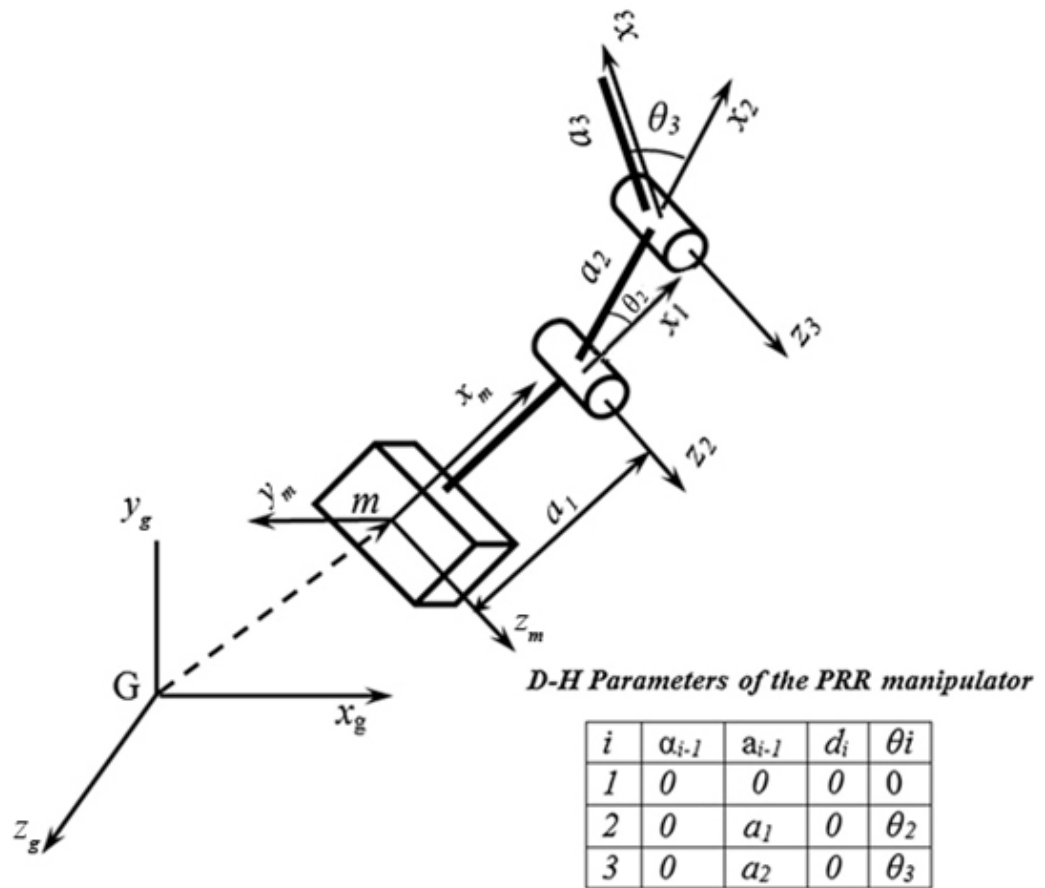


Figure 2.4: Kinematics of a PRR manipulator for the articulated drill, and transformation of its local coordinate system into the global coordinate system. The point  $m$  is not a prismatic joint. The box symbol represents the motor box of the articulated drill sheath.

Based on Figure 2.4, the spatial kinematics of articulated drill sheath is slightly different variable in compare to Equation 4. In articulated drill sheath, two of the DH parameters are assumed to be constant at zero. Those two parameters are  $d_i$ , the distance along  $z_i$ -axes at each revolute joint, and  $\alpha_{i-1}$ , which is the angle between the  $z_i$ -axes and  $z_{i-1}$ -axes. This is because of structure of the articulated drill is such that the two parameters mentioned are to be constant at zero. The resulting equation is as below.

$$T_i = \begin{pmatrix} \cos \theta_i & -\sin \theta_i & 0 & a_{i-1} \\ \sin \theta_i & \cos \theta_i & 0 & 0 \\ 0 & 0 & 1 & 0 \\ 0 & 0 & 0 & 1 \end{pmatrix} \quad (6)$$

Equation 6 interprets as two operations are performed in succession, which are translation by counter-clockwise rotation by  $\theta_i$  about the  $z$ -axis, and translation by  $a_{i-1}$  along the  $x_{i-1}$ -axis. This homogeneous transformation matrix  $T_i$ , is applied for each  $i$  such the value is  $2 \leq i \leq 4$ . This is because  $T_1$  is defined as a general rigid-body homogenous transformation matrix to denote the six degree of freedom of the free handle that is tracked by the optical tracking device. Since the articulated drill sheath is a three-bar linkage, the  $m$  value in  $A_m$  is 3 with  $T_2 - T_4$  denotes the transformation from the base of articulated drill sheath towards the tip of the articulated drill sheath. Therefore, the end-effector F in the body frame of the last link  $A_3$  (Figure2.2), appears in the coordination of G as

$${}^gT_3 = {}^gT_i {}^mT_3 \quad (7)$$

where, G denotes the global coordinate system of the navigation system.

Although the articulated sheath is three links, it provides one more DOF as it is actuated by one tendon mechanism for bending the flexible shaft with a drill/ burr tip attached. The maximal bending angle is limited by  $90^\circ$

---

between the tip and the base of the articulated sheath. As the maximal bending angle is  $90^\circ$  the workspace is a half-circle when the handle is fixed. The 3-link PRR manipulator is based on a 6 DOFs “freehand” handle; in minimally invasive Total Hip Arthroplasty, as the entry space is very limited, handle motion might only be allowed to push along and rotate the axis of the fix part of the flexible shaft. In addition, with the extra bending of the articulated sheath, the workspace would be a double half sphere described in the Figure 2.2. This workspace also shows the flexibility of the manipulator. Thus, it can tunnel a curved canal inside the femur which makes the implantation more precise.

## **2.4. Design of The Articulated Drill System**

### **2.4.1 Design of a Novel Articulated Drill Mechanism**

The articulated drill manipulator consists of three multiple rigid segments that act as a sheath to an articulated shaft with a drill/bur attaching at the end, as illustrated in Figure 2.5. The proximal end segment is connected to the motor box shown in Figure 2.5. The motor box controls the action of the articulated drill. It contains a servo motor, thumb stick to control servo motor's movement, and a microcontroller board. The potentiometers are located at the revolution joint that connects each two segments and linked by two rivets that allow free rotation of the joint. Inside the sheath, two ball bearings are installed to

link each segment of the sheath to the flexible shaft that drives the drilling, which allows a free rotation and force transmission. This mechanism allows a maximal speed of 30000 rpm, with free rotation and force transmission. The 3mm flexible shaft runs through a 5mm hole at the base. The hole is made wider than the shaft's diameter to enable some clearance and prevent backlash when the shaft is rotating at high speed.

#### **2.4.2 Servo Arm and Wire Driven System**

The articulated drill system has a wire-driven steering capability for rotating the joints. There are several studies done proving wire-driven manipulator as stated in Chapter 1. The benefit of wire driven manipulators include the fact that there is no large space requires for actuation, and an ability to actuate the tools into a curved configuration (Ji et al., 2019). There are two 2mm holes on the wall of the sheath segments running above and beneath the flexible shaft hole. These two channels are designed for wires that connect the drill end part to the servo motor with the torque value of 11.3kg/cm at 6.0V, enabling bending of the joints in both clockwise and counter-clockwise directions. The middle part is split into two to enable assembly of the flexible shaft and the ball bearings. These split parts are combined together by four screws. The third connected hole would be 9mm in diameter by which



the distal end of the chuck part is placed. The chuck part will be held to the drill end part by 2 ball bearings. At distal end of drill end part would be a hole that is perpendicular to the three connected holes with diameter of 3mm. This hole functions to tighten the drill bit to the chuck by inserting a metal rod through it.

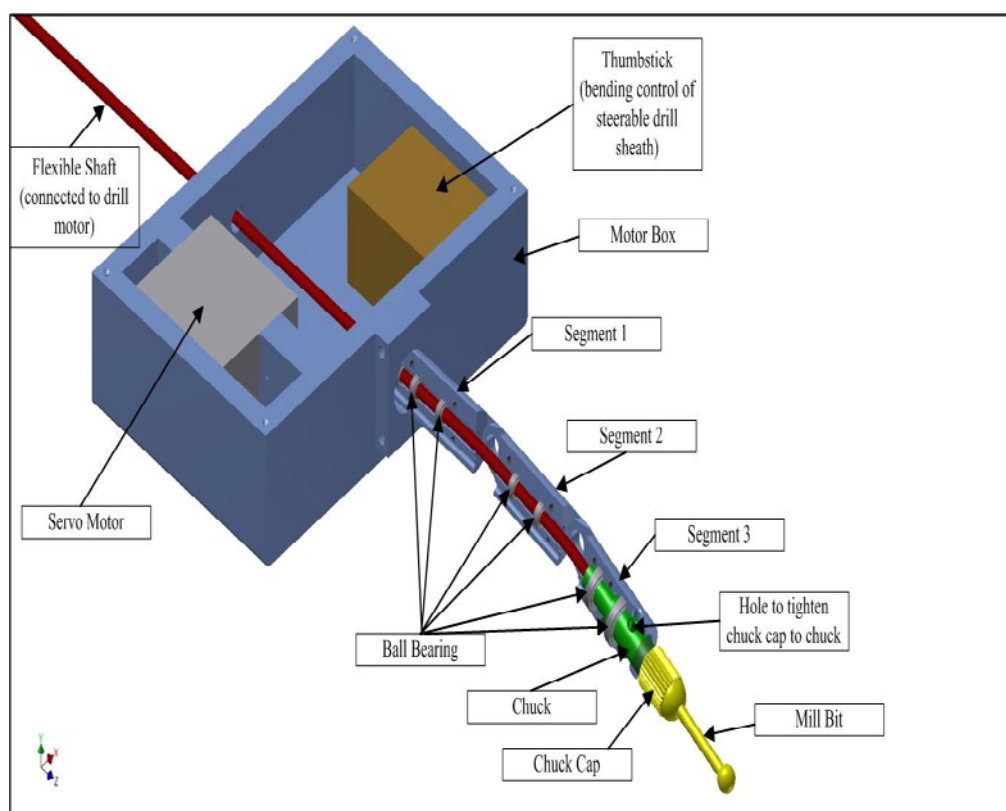


Figure 2.5: CAD of the articulated drill

The bending of the articulated drill sheath is controlled by the wires running inside the articulated drill sheath. The wires are braided steel wires that have tensile limit of 50 pounds of force. The wires act like tendons, providing opposing tension when bending the articulated drill

sheath. The wires are anchored at the drill's end part to provide active bending at joint 1 while joint 2 will bend passively following the bending of joint 1. The wire is tied to the servo arm of high torque servo motor that is located inside the motor box at the base of articulated drill sheath. The high torque servo motor is used so that the bending can be sustained during milling of the femoral canal. The servo arm used was circular servo arm and the two wires are attached at two opposite ends of the servo arm as shown in Figure 2.6. When the servo arm rotates, tension will increase in one wire while the other wire will reduce in tension. The wires act like tendons, providing opposing tension when bending the articulated drill sheath. The bending will provide one more degree of freedom to the articulated drill sheath on top of the degree of freedom provided by free hand at the base of articulated drill sheath. This enables it to navigate through the small incision and inside the femoral canal and cut a curved path. The twist or rotational motion of the articulated drill can be performed manually.

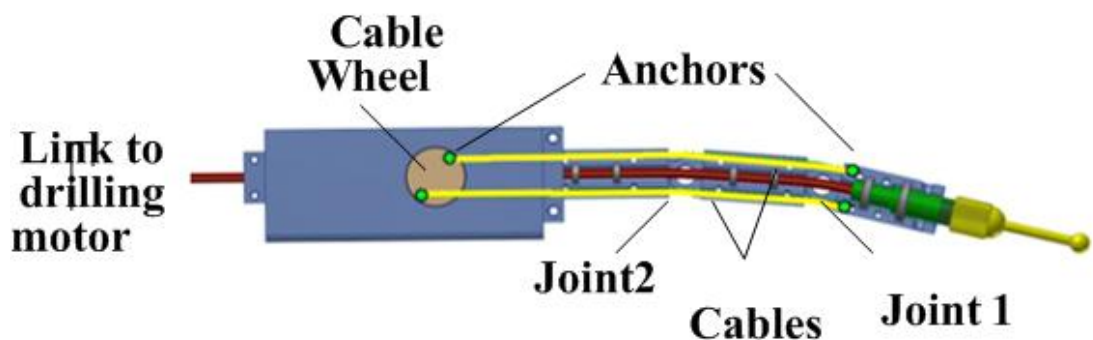


Figure 2.6: Wire driven system inside of articulated drill sheath.

### **2.4.3 Electronics and Microcontrollers**

There are two microcontrollers installed in the articulated drill system. The main microcontroller, Arduino Mega 2560 R3 functions to collect analogue signal from two potentiometer at two joints of articulated drill sheath, supplying 5V power to the potentiometers, collect digital signal from optical tracking system, supply 5V power to the accessory microcontroller inside motor box, and transmit serial data of both tracking system to PC via USB. The main microcontroller gets its power from the power adaptor port of the microcontroller. The accessory microcontroller, Arduino Nano functions to collect analogue signal from the thumb stick and process it to control the servo arm inside motor box, provides 3.3V power to the thumb stick, and collect signal from servo motor and process its response to the signal from thumb stick. The servo motor's power is provided by external voltage regulator because it requires 6V power to operate optimally. The wire connections between the main microcontroller, accessory microcontroller, servo motor, and two potentiometers are connected via RS-232 port at the side of motor box. The electronic diagram of the microcontrollers is shown in Figure 2.7.

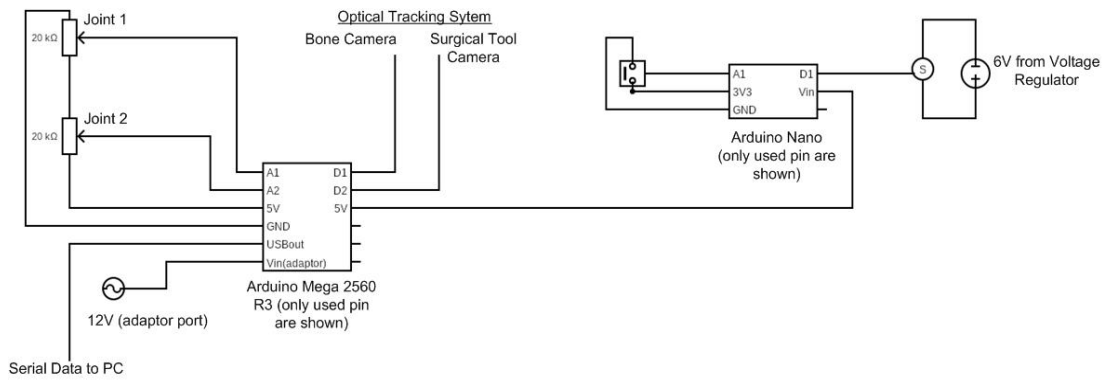


Figure 2.7: Electronic diagram of main and accessory microcontrollers along with components attached to them.

#### **2.4.4 Limitation to the Design**

The stiffness test was not directly done but from the force measurement experiment, the results showed that the articulated drill system is able to sustain bending and stiffness to mill on the surface of bovine bone sample. Further research can be done to directly measure the stiffness of articulated drill system at variable bending degree in both forward and horizontal configuration.

The placement accuracy of the tip at this moment is depends on the kinematic algorithm in the software and tracking data from both tracking systems. Direct test of placement accuracy and improvements to it will be included in further research.

Synchronization of data is done at software level at this moment due to financial constraint to obtain synchronization board to synchronize all input data. Further researches on hardware synchronization and optimizing data synchronization are recommended.

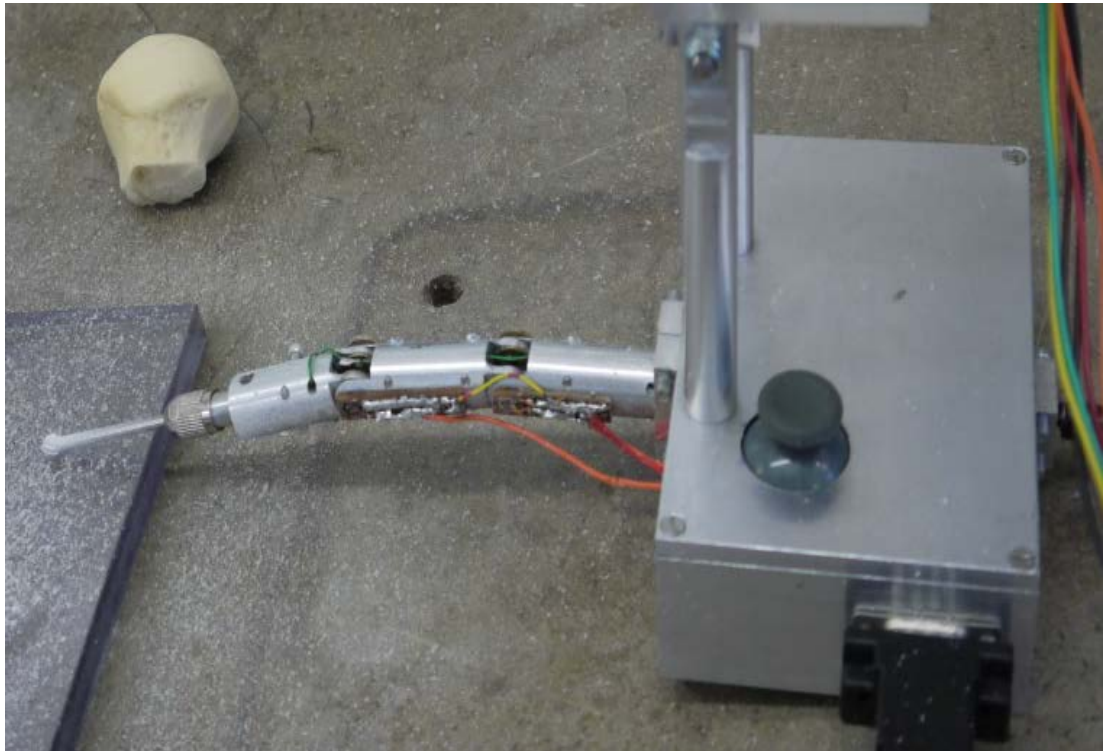


Figure 2.8: A prototype of the articulated drill

#### 2.4.5 Hardware Design and Manufacture

The hardware for articulated drill system is comprised of three main components which is the articulated drill sheath, the motor box and the flexible drill shaft that fits inside the articulated drill sheath as shown in Figure 2.6.

The articulated drill sheath is designed using Autodesk Inventor 2013 CAD application. It is designed to fit in the femoral canal with external diameter of less than 15mm. This enables it to navigate inside the femoral canal via minimal invasive surgery's incision while milling the area. The sheath is made up from aluminium since aluminium is lighter, easier to machine when compare with medical grade stainless steel. The

articulated drill sheath consists of 4 parts which are the base part, middle part, drill end part and the chuck part.

The base part measures 52.5mm in length, 14.42mm in diameter with a wider proximal end of 20mm diameter as shown in Figure 2.9. The proximal end is connected to the motor box. The joint connecting the base part and the middle part consisted of two rivets that allow free rotation of the joint. Inside the sheath, two ball bearings are installed to link each half of the sheath to the flexible shaft that drives the drilling with the maximal speed of 30,000 rpm. This design allows the drill mechanism to have a free rotation and strong force transmission. The base part is split into two to enable assembly of the flexible shaft and the ball bearings as shown in Figure 2.10. These split parts are combined together by four screws. Inside of the base part is a 5mm hole by which a 3mm diameter flexible shaft will run through. The hole is made wider than the shaft's diameter to enable some clearance when the shaft is rotating at high speed. Besides that, there will be two holes of 2mm diameter running top and below the flexible shaft hole. These two holes is for wires that connect the drill end part to the motor, enabling bending of the joints in clockwise and counter-clockwise direction

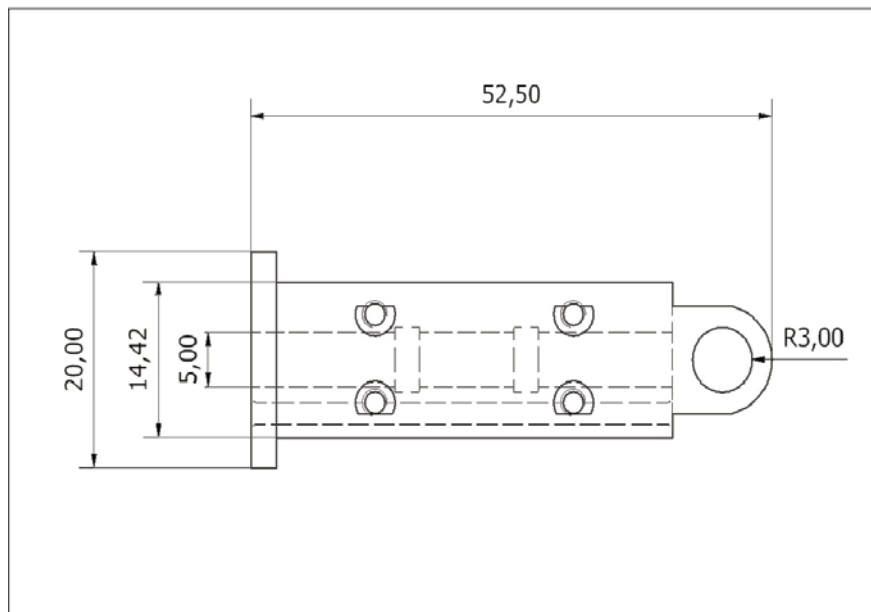


Figure 2.9: Base part dimensions

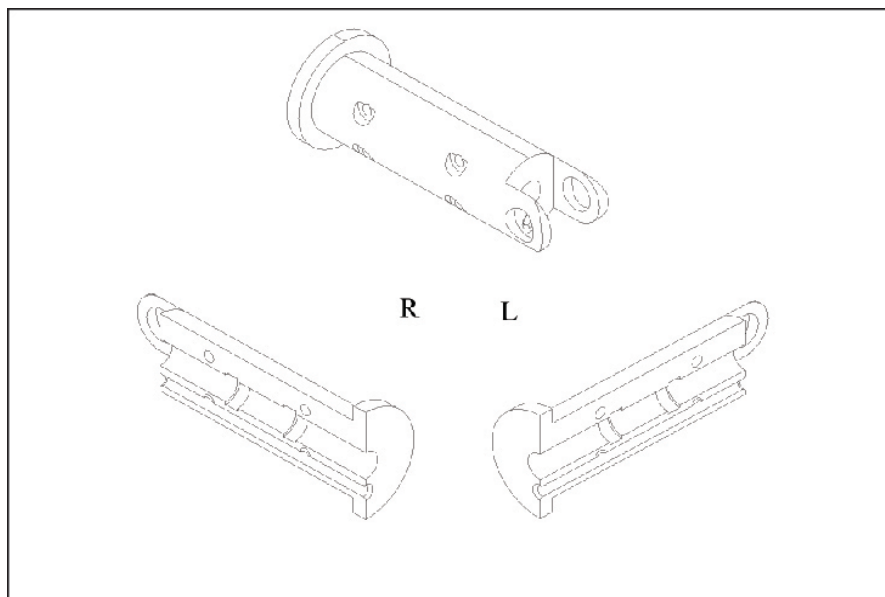


Figure 2.10: Base part outline

The middle part measures 50mm in length and 14.42mm in diameter as shown in Figure 2.11. It has two joints that link the middle part to both base part and drill end part. Each joint has two rivets connecting the



middle part to others. Inside the sheath, two ball bearings are installed to link each half of the sheath to the flexible shaft. The middle part is split into two to enable assembly of the flexible shaft and the ball bearings as shown in Figure 2.12. These split parts are combined together by four screws. Inside of the base part is a 5mm hole by which a 3mm diameter flexible shaft will run through. The hole is made wider than the shaft's diameter to enable some clearance when the shaft is rotating at high speed. Besides that, there will be two holes of 2mm diameter running top and below the flexible shaft hole. These two holes are for wires that connect the drill end part to the motor.

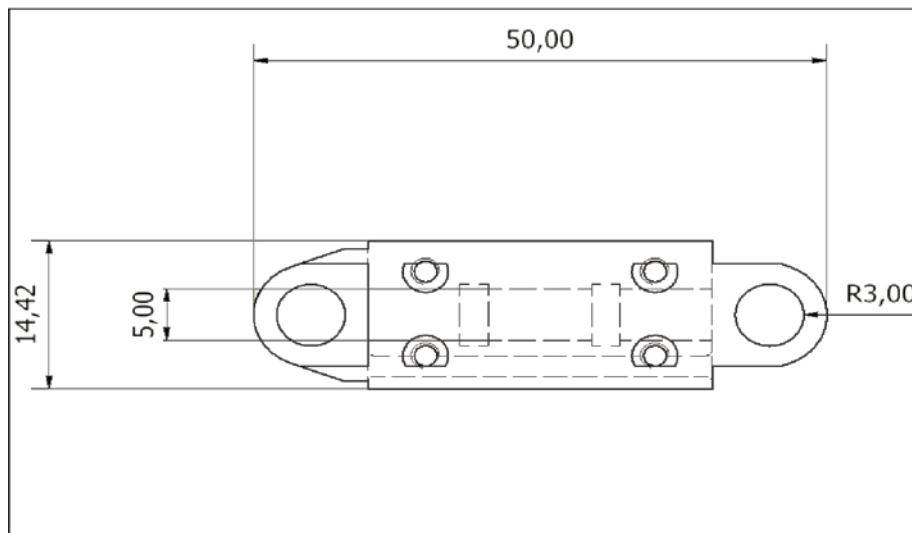


Figure 2.11: Middle part dimensions

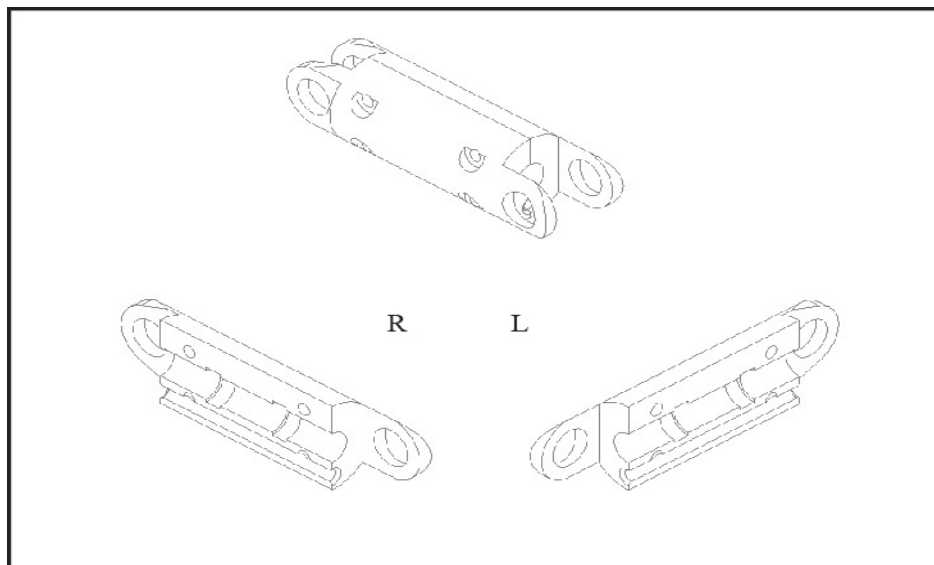


Figure 2.12: Middle part outline

The drill end part measures 40mm in length and 14.42mm in diameter as shown in Figure 2.13. It is connected to the middle part proximally via the same joint with rivets. Inside of it contains three different diameter holes that connected with each other. The proximal hole has 5 mm in diameter for the flexible shaft. Then, it is connected to a 7mm hole by which the proximal end of the chuck part fits in. The third connected hole would be 9mm in diameter by which the distal end of the chuck part is placed. The chuck part will be held to the drill end part by 2 ball bearings. At distal end of drill end part would be a hole that is perpendicular to the three connected holes with diameter of 3mm. This hole functions to tighten the drill bit to the chuck by inserting a metal rod through it. The drill end part is also split into two to enable assembly of the shaft and the ball bearings as shown in Figure 2.14. These split parts are combined together by four screws. There will be two holes

measuring 2mm in diameter and 5mm in length running above and below the three connected holes. These holes act as endpoint anchoring the wires from the motor.

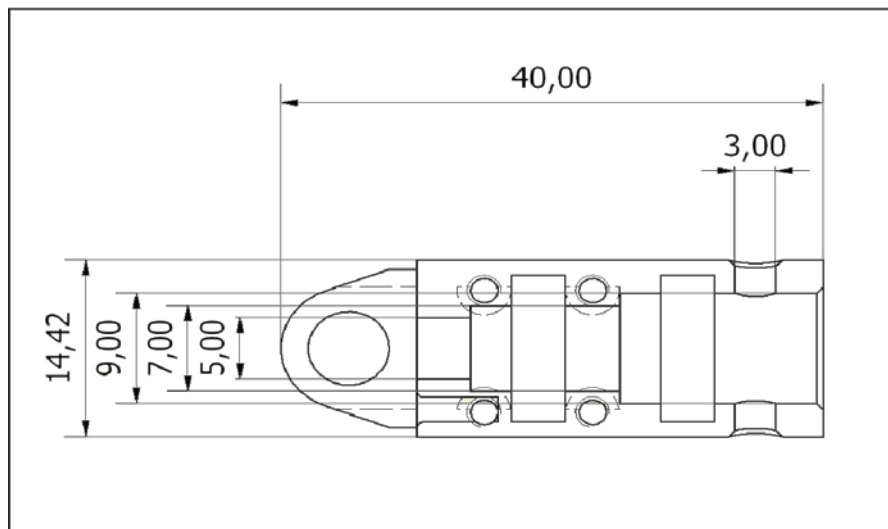


Figure 2.13: Drill end part dimensions

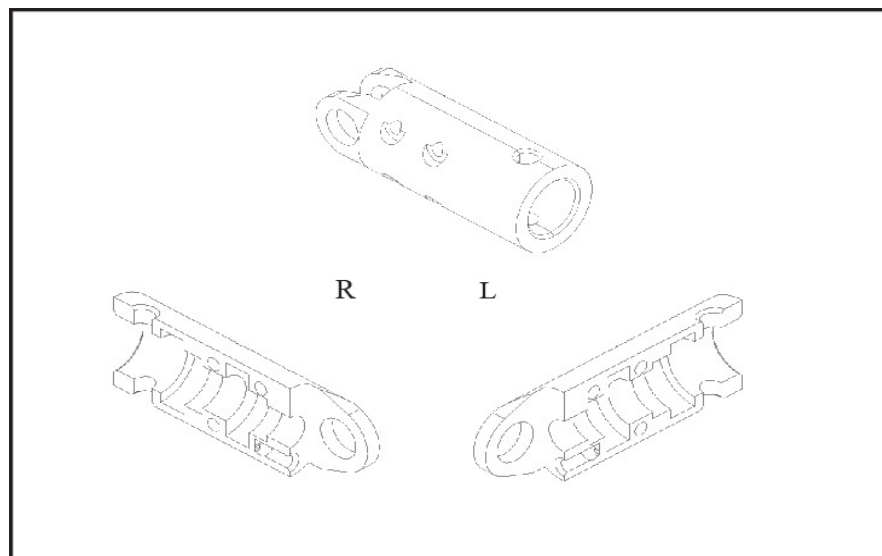


Figure 2.14: Drill end part outline

The chuck part measures 41mm in length with proximal outer diameter of 6mm and distal outer diameter of 8mm as shown in Figure

2.15. It has proximal inner diameter hole of 3mm for the flexible shaft to be fit and distal inner diameter hole of 5mm for the insertion of burr tip. There is a 3mm diameter hole at the middle of the chuck as shown in Figure 2.16. The purpose of this hole is to fix the chuck part rotation when tightening the collet. It is done by inserting a 3mm metal rod to prevent the chuck part from rotating.

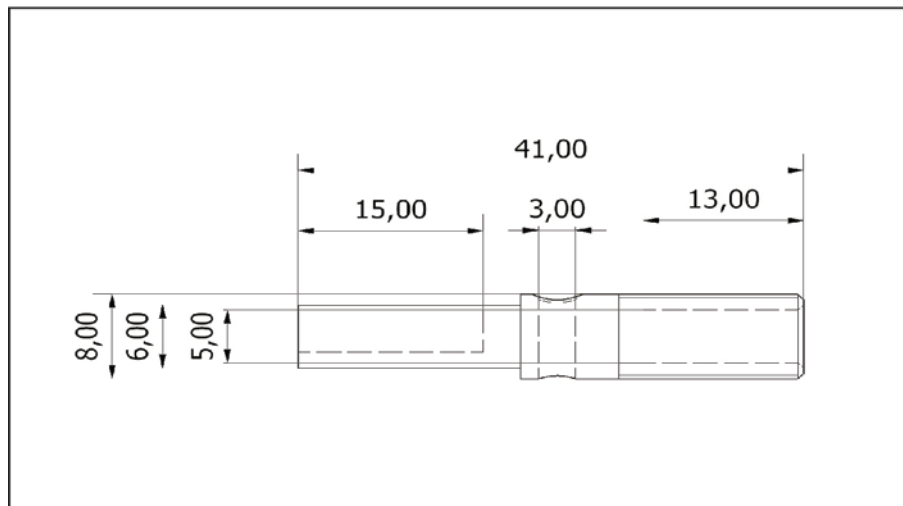


Figure 2.15: Chuck part dimension

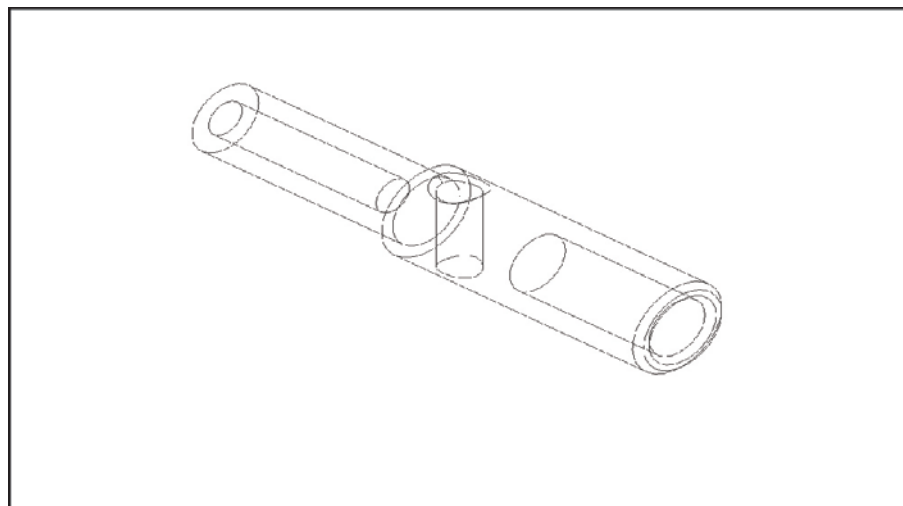


Figure 2.16: Chuck part outline

The motor box is connected to proximal end of base part and it is where the actuation of the articulated drill took place (Figure 2.17). The motor box is designed to be a handle with a servo motor and a microcontroller board fitted in as shown in Figure 2.18. The microcontroller controls the servo and streams data from the potentiometer. Besides that, the bending control of the articulated drill sheath will be done from the motor box.

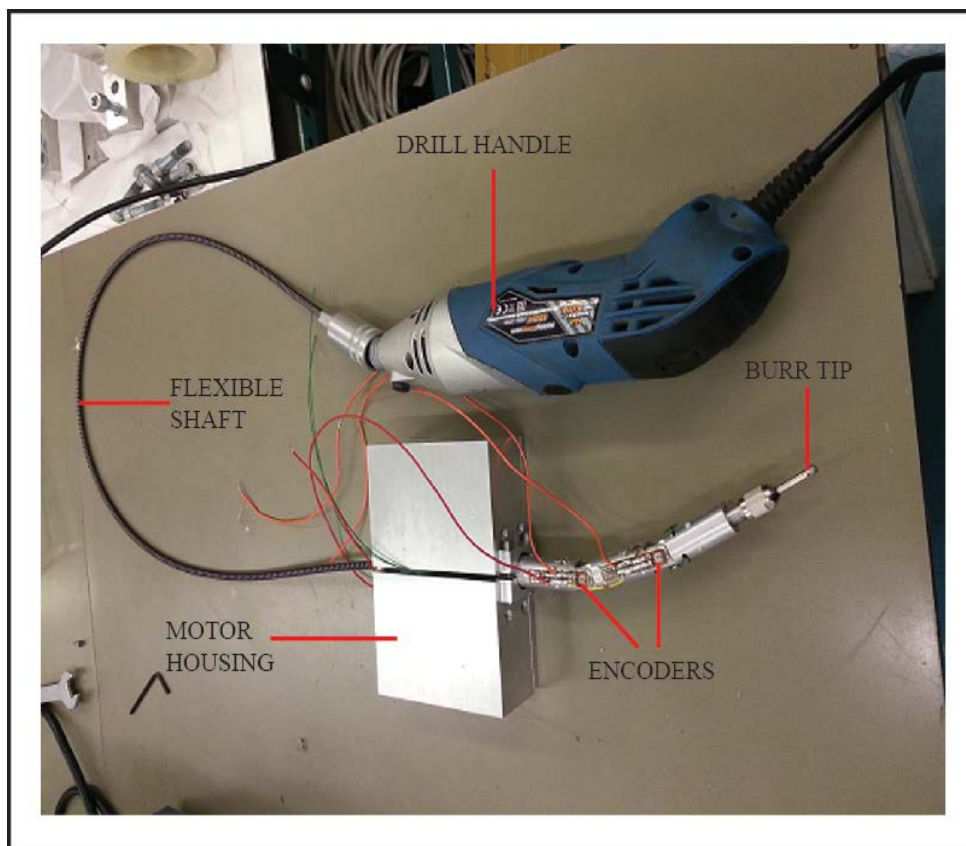


Figure 2.17: Assembly of Articulated Drill Sheath

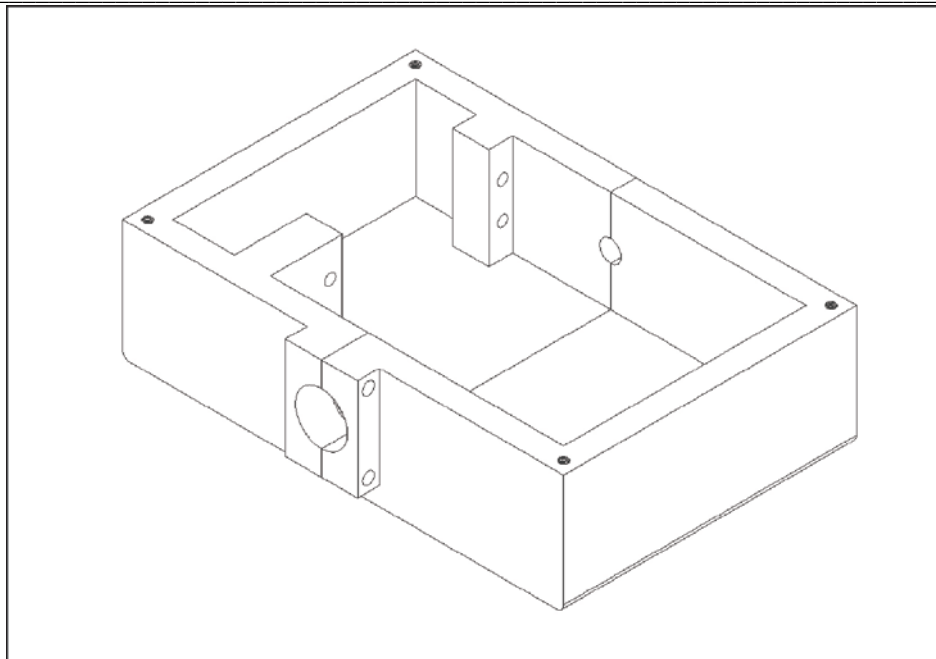


Figure 2.18: Motor box outline

## 2.5. A Hybrid Tracking System

This tracking system has the ability to track articulated manipulator inside the bone. This is approached by combining the optical tracking system and position tracking as shown in Figure 2.19. Optical systems are used to track the surgical objects and tools outside the drill hole, while potentiometers placed at each joint of the sheath are used to track the bending angle of an articulated drill. Combined with the kinematics of the drill, the tip position of the articulated drill can be tracked in this system. The reason for hybrid tracking system is that optical tracking system has disadvantages which are unable to track objects without clear line of sight between tracker and the camera (Watzinger et al., 1999, Xia et al., 2018). In order to track the articulated drill sheath inside the bone, the potentiometer tracking system will

act as the extension for the optical tracking system. The optical tracking system will track the base of articulated drill sheath and the femur bone. The potentiometer system tracking is linked to track the base of the articulated drill sheath.



Figure 2.19: The Optical Tracking system

As the optical tracking system only can track the open part of the articulated drill mechanism, when the tip of the articulated drill tunnels inside the bone, a potentiometer tracking system is developed to provide the position information for the articulated manipulator. The optical tracking system consists of beacons of infrared LED trackers which are stationary, and a small infrared camera attach to each surgical object. The beacon containing infrared LED arranged in a specific pattern and acts as a stationary reference plane. Micro infrared cameras interpolated to give 1024 x 768 pixels doing a frame rate of up to 100 frames per second act as mobile/

independent trackers, attach to each surgical object. The surgical objects with the camera track their distance and coordinate from the LED beacons.

The articulated drill sheath tracking inside bone is done with potentiometers attached at each joint of the sheath. The encoders track the bending angle of each of the joint and determine the position of the burr tip with reference to the base of the manipulator calculated by its forward kinematics. Hence, it acts as an extension of the optical tracking system. The encoder is constructed from 20k $\Omega$  button potentiometer. When potentiometer shaft rotates, the resulting voltage varies, following Ohm's Law. The bending angle of each joint of the articulated drill sheath is equal to rotational angle of potentiometer shaft. Hence, the voltage output of the potentiometer at each degree of rotation is taken and mapped as bending angle of the joints. Analogue data from the potentiometers are connected to a microcontroller board for conversion to digital data. The data are then read by the navigation system as the rotation angle for joint 1 and joint 2. The angle data, combined with the length of each segment, are then used to map the location of the articulated sheath location and synchronized it with its virtual object. This tracking system tracks and updates the virtual object when the surgery has been done. Once the milling process has been completed, the tracking system creates a virtual milling pattern on the CAD image.



## 2.6. Conclusion

Improvement of the surgical outcome and decreasing complications of THA procedure drives the need for an articulated drill. One of the troublesome complications of THA is limb length discrepancy. The best way to reduce the risk of that complication is to improve accurate placement and alignment of implants using CAOS and robotic technology. At the moment, usage of robotic surgical device in THA is limited to acetabular cup positioning. This is because under minimally invasive surgery, femoral milling is a challenge since rigid surgical mill cannot properly mill the femoral canal and the tip of the surgical mill is not trackable inside the bone. The emergence of robotic micro-tools gives opportunity to develop articulated drill integrated into CAOS robotic surgical system. The articulated drill will be tracked by hybrid tracking system, a combination of optical tracking system and potentiometer tracking system. Kinematics of articulated drill consists of homogenous transformation matrix that denotes the six degree of freedom at the base of articulated drill ( $T_1$ ), and transformation matrix of planar three link manipulator of articulated drill sheath ( $T_2 - T_4$ ). The articulated drill itself consists of three multiple rigid segment that envelop a flexible shaft with a burr tip at distal end. Proximal end of the articulated drill is the motor box that contains the motor, and microcontroller board. The bending of articulated drill is controlled by wires running inside the articulated drill sheath that act like tendons and it is directly connected to the motor. Articulated drill system will use hybrid tracking system to track its tip outside and inside the bone. Hybrid

tracking system is a combination of optical tracking system to track the base of articulated drill outside the bone, and potentiometer tracking system to track the tip inside the bone. Tracking the tip inside the bone is made possible with the kinematics of articulated drill and the bending angle data obtained from potentiometer tracking system. Streams of input from both optical tracking system and potentiometer tracking system are integrated in the navigation software of articulated drill navigation system. The navigation software also has input of 3D model of femur, and femoral stem. 3D model of femur is obtained from reconstructed 3D image of CT scan, while the femoral stem 3D model is obtained from the CAD model of the femoral stem. The articulated drill is visualized from its CAD model. Each of the 3D model has vertices of 3D coordinate outlining its shape to enable the use of collision algorithm that give rise to safe surgical boundary that make up the safe surgical volume. Safe surgical volume is the volume that is permissible to be milled by the navigation software. Should the articulated burr tip touches the safe surgical boundary, an error message will pop-up that state to stop the milling. The potentiometer used is a button analogue potentiometer that is calibrated with digital goniometer for each degree of rotation. Calibrated encoders of both joint 1 and joint 2 have a precision of about 1 degree in measuring the angle.

Articulated drill tip sheath with motor control from straight shaft to bendable shaft was designed and developed. Besides that, hybrid tracking system, combination between optical tracking system and encoder tracking

system in order to track surgical tool inside the bone was also designed and developed.

---

## **CHAPTER 3 - NAVIGATION SOFTWARE OF THE STREERABLE DRILL NAVIGATION SYSTEM**

### **3.1. Introduction**

This chapter will explain on the navigation software part of the articulated drill navigation system. The navigation system is a multi-modality computer-aided integration system. It starts by first developing the mapping system of the articulated drill tip, acquiring the 3D images of a femur and a femoral stem implant. The mapping enables the 3D model of the bone and the 3D model of femoral stem; both are linked together and can be viewed virtually, enabling virtual interaction between the models. The boundary of safe surgical volume is then being setup in order to enable precise milling that follow the shape of the implant. The process is followed by the pre-operative planning of computer assisted orthopaedic surgery (CAOS). Digital image of the bone and surgical tools is obtained, and this will then be mapped into the navigation system. The navigation system provides real time guidance for a surgeon specifically during the procedure of total hip arthroplasty.

The navigation software is part of the component of the navigation system that integrates the tracking system and guides the articulated drill virtually. As compared to the current navigation software, this new navigation software combines the optical sensors and encoder sensors. Thus, it has the additional ability to track articulated drill inside the bone. With this navigation

software, the articulated drill in the navigation system is therefore defined as a type of hybrid navigation system that combines optical tracking system and potentiometer tracking system. The system now capable to define collision whenever the minimum distance between the surface of 3D bone model and articulated drill model reaches zero and overcome the limitation movement of 3D model of articulated drill sheath when drilling inside the bone.

### **3.2. General Overview of Navigation Software**

Hybrid navigation systems are being develop since early 2000s to allow surgeons to fully utilize CAOS advantages in total hip arthroplasty (Nolte and Beutler, 2004). Hybrid navigation system combines optical tracking system with other tracking system such as electromagnetic tracking system, ultrasound tracking system, and potentiometer tracking system. Articulated drill navigation system is a type of hybrid navigation system that combines optical tracking system and potentiometer tracking system. The navigation software is the component that integrates the tracking system and guides the articulated drill virtually.

This navigation software has additional ability to track articulated drill inside the bone compared to current navigation software. This is approached by combining optical sensors and encoder sensors. Based on Figure 3.1, streaming data from optical sensors act as input for location tracking of surgical object such as the bone, and location tracking of end effector, which

---

is the base of articulated drill. The optical sensors enable this navigation software to track the location of objects outside the bone. On top of that, since the articulated drill is a three-bar linkage structure, potentiometers are placed at each revolute joint of articulated drill inputting streams of bending angle values of each joint into the navigation software. Hence, aside from location tracking of the articulated drill, this navigation software is capable to track bending angle of each joint in the articulated drill. This combination of tracking system or hybrid tracking system enables extended virtual visualization of articulated drill beyond the limitation of optical tracking system. In a tight and obscured line of sight of optical tracking cameras, rotary tracking system further navigates and shows the exact location of the tip of articulated drill. These two inputs are then integrated into the software's kinematic algorithm resulting in visualization of virtual articulated drill that moves in every motion the actual articulated drill does even when the articulated sheath and the tip is within enclosed space out of the optical tracking camera's line of sight.

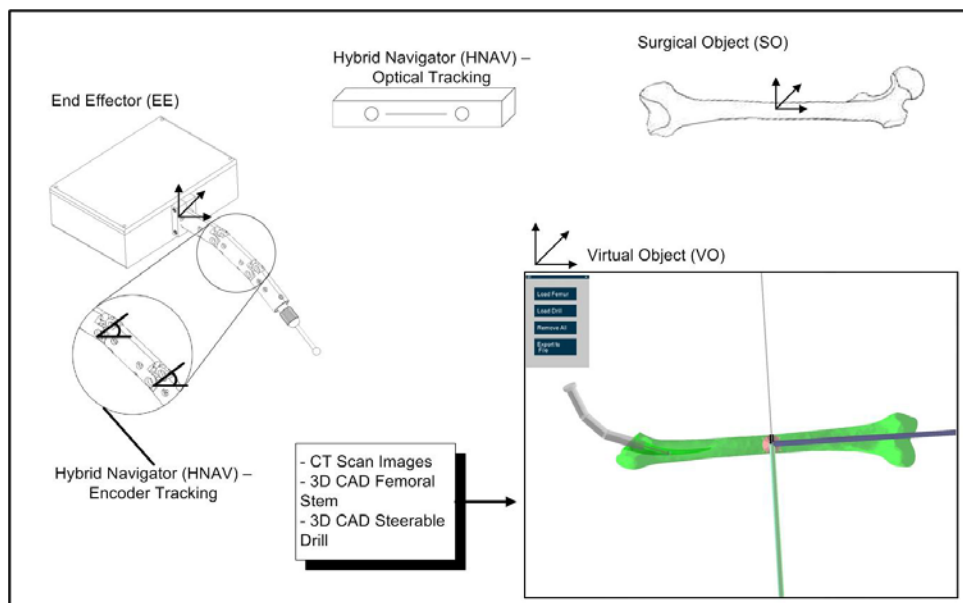


Figure 3.1: Components that are integrated in the navigation software enabling real-time visualization of articulated drill even when the tip is inside the bone.

### 3.2.1 Virtual Fixtures

In the navigation system, the virtual fixtures are represented by safe surgical boundary that limits the movement of 3D model of articulated drill sheath when drilling inside the bone. The limitation by virtual fixtures enables the articulated drill system to drill only in area within the safe surgical boundary. Any movement beyond the safe surgical boundary will trigger a response to stop to drill's motor.

According to Rosenberg and Louis B (1993), virtual fixtures are abstract perceptual information added to virtual simulation platform that assist users by giving them partial sense of reality in virtual space when doing specific task, or also known as addition of sensory information to

the workspace for improved telepresence in telemanipulation. Bowyer et al. (2014) summarize that virtual fixtures are software generated constraints which restrict the motion of a robotic manipulator into predefined regions or constrain it to move along a pre-planned path, and high-level control algorithms that can assist human in collaborative manipulation tasks between man and machine, thus reducing mental workload, task time, and errors (Bowyer et al., 2014). Moreover, Bettini et al. (2004) stated that virtual fixture is a guidance of user motions in virtual space towards preferred direction or area and avoids unwanted directions or area. A study done by Li et. al. (2007) describes a fast potential-collision-constraint-detection method based on a 3-D surface model and covariance tree data structure. The 3D surface model used in the study was a 3d model of human skull. The 3D surface of the skull acts as the boundary constraints to determine the "no fly zones". They use the boundary constraints to limit task behaviour and movement of the surgical robot in endoscopic sinus surgery. Another study stated the use of extrapolated datasets of magnetic resonance to create a 3D dynamic virtual fixtures to act as boundary constraints for minimally invasive cardiac surgery (Ren et al., 2008). In 2012, Yamamoto et al. developed a method for creating a forbidden-region virtual fixture based on a static point cloud data. It is done pre-operatively. by selecting a region and convert it into a boundary constraint (Yamamoto et al., 2012). Nakazawa et al. (2016) developed a cone shaped virtual fixture without



preoperative computed tomography images or magnetic resonance. They generated the boundary constraint by marking the edges of the top and bottom plane of a workspace. In 2014, Tang et al. proposed another method to generate virtual fixtures without preoperative radiological images by marking areas near the surfaces of organ (Tang et al., 2014). In 2018, an innovative robot safety control method of surgical instruments dynamic tracking endoscope was developed that is based on spatial dynamics flexible virtual fixtures. Serial spatial points and hyperboloid parameters are used to generate dual-layer hyperboloid model (Zheng et al., 2018). Studies above shown that 3D models from pre-operative radiological images, 3D CAD models, point cloud 3D images, and non-radiological images 3D models surfaces can be used to generate boundary constraints. Thus, combination of virtual fixtures and kinematic constraint enables this navigation system to have a safe surgical boundary. Usage of virtual constraint guidance (VCG) or kinematic constraint enables the CAD model to behave similar to physical tool by applying local constraints at the point of assembly and limits its movement along pre-defined paths (Tching et al., 2010, Gonzalez et al., 2012). Besides that, kinematic constraints that is applied to the 3D model, and the physics engine can help deal with imperfections in the VF (David et al., 2014).

The local collision detection depends on the physical tool with built-in sensors, thus limiting the CAD model movements in navigation system to

the movements of physical tool. This navigation system's VCG is based on physical articulated drill sheath's kinematics that limits the movement of 3D model of articulated drill sheath according to the physical tool. This includes the mechanical joints kinematics created by linking the segment bodies of the articulated drill sheath.

In Haptic VF, there is addition of force exerted back to the human user, and this improves safety, precision, or speed of manipulation (Abbott et al., 2007). There are two types of Haptic VF, which are guidance VF (GVF) and forbidden-region VF (FRVF). GVF simply guides the instrument along a path determined by the VF and kinematic constraints. FRVF limits the movement of certain 3D models away from pre-determined forbidden region (Park et al., 2011), hence the safe surgical area. FRVF or safe surgical boundary is needed so that the articulated drill will move along the desired path. The FRVF defined the maximum allowed position error and it also works as a threshold. It gives the benefit of simplify the task (Rosenberg, 1993, Payandeh and Stanistic, 2002), and reduction of damage done by tools to the forbidden region (Li et al., 2005). In addition to that, FRVF is describe as free of movement within the virtual space until it reaches the forbidden region boundary (David et al., 2014). It is then prohibiting any further movement beyond the boundary by the means of haptic feedback, stopping the drill motor, or impedance of movement as it moves closer to the boundary.

VF has been applied in education such as character writing virtual tutor system (Solis et al., 2002), rehabilitation assist system (Ueki et al., 2012, Adamovich et al., 2005, Veras et al., 2008), surgical robots for minimally invasive surgery (Li et al., 2007, Li and Okamura, 2003, Bettini et al., 2004), interactive simulation of CAD models assemblies (Tching et al., 2010), robotic cardiac catheter navigation (Park et al., 2011), teleoperated environment peg-in-a-hole task (Rosenberg, 1993), guidance for user along pre-determined path (Bettini et al., 2004), prevention of operation of tools in forbidden region (Abbott et al., 2007), impedance-controlled devices (Payandeh and Stanisic, 2002), and admittance-controlled devices (Taylor et al., 1999). In this navigation system, the FRVF is the area by which the bone should not be drilled; a bone with outlined femoral stem model inside it.

### **3.2.2 3D Collision Detection**

According to Pozo et al. (2012), There are four types of collision in 3D simulation system, which are point-point collisions, edge-edge collisions, edge-face collisions, and face-face collisions. In full haptic simulation, there are two types of the collision detection process. The first method is based on bounding volumes of the 3D models and the second method is based on local minimum distance between 3D models (Jiménez et al., 2001, Park et al., 2011). This navigation system uses the second method

by defining collision whenever the minimum distance between the surface of 3D bone model and articulated drill model reaches zero. Since the drill tip is spherical, the distance is calculated by using the sphere's centre and radius. Therefore, when the distance between the safe surgical boundary and the sphere's centre is more than the sphere's radius, the drill tip is considered to be in safe area. But, if the distance between the safe surgical boundary and the sphere's centre is less than the sphere's radius, the drill tip is considered to be in the FR. Whenever the distance between the safe surgical boundary and the sphere's centre is less or/and equal to the sphere radius, the warning system will activate and the drill's motor will be stopped. Collision detection system consist of two parts, which are collision detection, and collision response (Basdogan and Srinivasan, 2002). Collision detection is detecting collision in virtual space by determining the position and orientation of the end-effector. When collision occurs, the collision response react by sending virtual feedback to the user through the interface indicating collision has occurred(Sofronia et al., 2012).

### **3.3. Concept and Logic/Steps of Navigation System**

#### **3.3.1. Programming the Software**

The navigation software has been developed in JAVA Processing language (<https://processing.org/>). It is developed along with standard JAVA Processing libraries with additional libraries as shown in Table 1. JAVA Processing language is chosen because it is an open source programming language and environment for people who want to create images, animations, and interactions. It also has several programming libraries to accommodate various 2D, 3D and interactive software development. The navigation software has the following features:

- Can accommodate numerous virtual objects at one time
- The virtual objects can be added and removed
- Has a 3D space with grid and axis, which the virtual objects can be moved, rotated and overlapped with other objects.
- Has safe surgical boundaries to limit the area to be milled.
- Registration of optical tracking and encoder tracking data with integration of both data to track object movement outside and inside the bone.
- Collision detection algorithm and warning algorithm whenever safe surgical boundary is in contact with surgical tool 3D model.

JAVA Processing Libraries	Description
Arduino	This library allows you to control an Arduino board from Processing without writing code for the Arduino. Instead, you upload a standard firmware (program) to the board and communicate with it using the library. The firmware is called Firmata and is included in the Arduino software. This library was written by Arduino <a href="https://playground.arduino.cc/Interfacing/Processing/">https://playground.arduino.cc/Interfacing/Processing/</a>
bRigid	bRigid provides classes for an easier handling of jBullet in Processing. bRigid is thought as a kind of Processing port for the bullet physics simulation library written in C++. This library allows the interaction of rigid bodies in 3D. Geometry/ Shapes are built with Processing PShape Class, for convenient display and export(dx). Jbullet is a Java port of Bullet (c) 2008 Martin Dvorak <a href="http://jbullet.advel.cz/">http://jbullet.advel.cz/</a> Bullet Continuous Collision Detection and Physics Library (c) 2003-2013. This library was written by Daniel Koehler - 2013 <a href="http://www.lab-eds.org">www.lab-eds.org</a>
ControlP5	<p>A GUI (graphical user interface) library for processing. Its features are:</p> <p>Automatic controller-event detection</p> <p>ControlP5 offers a range of controllers that allow you to easily change and adjust values while your sketch is running. Each controller is identified by a unique name assigned when creating a controller. ControlP5 locates variables and functions inside your sketch and will link controllers to matching variables or functions automatically</p> <p>ControlP5toggle. Controller changes can easily be captured within your sketch by implementing the controlEvent function</p> <p>ControlP5controlEvent.</p> <p>Show, hide, load, save</p> <p>Controllers that have been added to your sketch can be arranged in tabs and groups to keep your controller sets organized. All controllers are drawn on top of a processing sketch by default. Several key combinations allow you to show and hide the user interface, and to saved and loaded ControlP5 properties, ControlP5properties. The position of a controller can be adjusted during runtime by moving a controller while the ALT-key is pressed.</p> <p>Key-commands</p> <p>ALT-mouseMove move controllers</p> <p>ALT-h show and hide controllers</p> <p>ALT-shift-s save controller setup in an properties-</p>

	<p>document  ALT-shift-I load a controller setup from a properties-document  Custom Fonts  By default controlP5 uses a bitFont to render text. To display text in PFont-format, controlP5 uses a wrapper called ControlFont ControlP5controlFont.  Custom Buttons  Create controllers which use image-based states instead of the default controlP5-look ControlP5button.  This library was written by Andreas Schlegel  <a href="http://www.sojamo.de/libraries/controlP5/">http://www.sojamo.de/libraries/controlP5/</a> .</p>
GLgraphics	<p>GLGraphics is a library intended to extend the capabilities of the OpenGL renderer in Processing. It includes classes to handle opengl textures, image post-processing filters, 3D Models, and shaders in GLSL, Cg and CgFX. It also includes an off-screen rendering surface with antialias support.  This library was written by AndresColubri for the programming environment processing.  <a href="http://glgraphics.sourceforge.net/">http://glgraphics.sourceforge.net/</a></p>
Javacpp	<p>JavaCPP provides efficient access to native C++ inside Java, not unlike the way some C/C++ compilers interact with assembly language. No need to invent new languages such as with SWIG, SIP, C++/CLI, Cython, or RPython. Instead, similar to what cppy strives to do for Python, it exploits the syntactic and semantic similarities between Java and C++. Under the hood, it uses JNI, so it works with all implementations of Java SE, in addition to Android, Avian, and RoboVM.  This library was written by Bytedeco<a href="http://bytedeco.org/">http://bytedeco.org/</a></p>
Matrix	<p>This library is an extension of Processing language that enables use of matrices in mathematical calculation inside Processing.</p>
Mesh	<p>Mesh is a library for creating Voronoi, Delaunay and Convex Hull diagrams in Processing.  This library was written by Lee Byron.  <a href="http://leebyron.com/mesh/">http://leebyron.com/mesh/</a></p>
Processing serial	<p>This library is an extension of Processing language that reads and writes data to and from external devices one byte at a time. It allows two computers to send and receive data. This library has the flexibility to communicate with custom microcontroller devices and to use them as the input or output to Processing programs.</p>
Processing openGL	<p>Processing openGL (Open Graphics Library) is a cross-platform graphics interface for 3D and 2D graphics. This library allows Processing programs to utilize the speed of an OpenGL accelerated graphics card. This expands the potential for drawing more to the screen and creating</p>

<p>Proscene</p>	<p>larger windows.</p> <p>ProScene (pronounced similar as the Czech word "prosím" which means "please") is a free-software java library which provides classes to ease the creation of interactive 2D/3D scenes in Processing.</p> <p>ProScene extensively uses interactive frames, i.e., coordinate systems that can be controlled with any HID, allowing to easily setup an interactive 2D or 3D scene.</p> <p>ProScene provides seamless integration with Processing: its API has been designed to fit that of Processing and its implementation has been optimized to work alongside with it. It supports all major Processing flavours: Desktop, JS, and Android. The key features include:</p> <p>Generic support to Human Interface Devices (HIDs), including not only the mouse and the keyboard, but advanced HID's such as a touch screen, a space navigator or a kinect.</p> <p>Keyboard shortcuts and HID bindings customization.</p> <p>Hierarchical coordinate systems (frames), with functions to convert between them.</p> <p>Interactive frames (including the camera) which may be manipulated by any HID.</p> <p>Arcball, walkthrough and third person camera modes.</p> <p>Default interactivity to your Processing scenes through the mouse (or touch screen) and keyboard that simply does what you expect.</p> <p>Visibility culling: Back-face and view-frustum culling.</p> <p>Keyframes.</p> <p>Animation framework.</p> <p>Object picking.</p> <p>Screen drawing, i.e., drawing of 2d primitives on top of another (2d or 3d) scene.</p> <p>Off-screen rendering mode support.</p> <p>Save and load configurations.</p> <p>2D and 3D Interactive mini-maps.</p> <p>This library was written by Jean Pierre Charalambos, National University of Colombia.  <a href="http://nakednous.github.io/">http://nakednous.github.io/</a></p>
<p>Quickhull3d</p>	<p>This library is extension of Mesh library. Its contains the algorithms for creating diagrams in Mesh library are based on. It contains the algorithm <math>O(n \log(n))</math> complexity, works with double precision numbers, is fairly robust with respect to degenerate situations, and allows the merging of co-planar faces.</p> <p>This library was written by Lee Byron.  <a href="http://leebyron.com/mesh/">http://leebyron.com/mesh/</a></p>



Toxiclibs_p5	<p>toxiclibs is an independent, open source library collection for computational design tasks with Java &amp; Processing developed by Karsten "toxi" Schmidt. The classes are purposefully kept fairly generic in order to maximize re-use in different contexts ranging from generative design, animation, interaction/interface design, data visualization to architecture and digital fabrication, use as teaching tool and more.</p> <p>This library collection consists of:                  270+ classes                  18 packages bundled into 7 libraries                  altogether &gt;25k lines of code</p> <p>This library was written by Karsten "toxi" Schmidt.  <a href="http://toxiclibs.org/about/">http://toxiclibs.org/about/</a></p>
Toxiclibscore	<p>This packages/module of toxiclibs library feature:</p> <ul style="list-style-type: none"> <li>toxi.geom</li> <li>2d/3d vector maths</li> <li>AABB, sphere, plane, triangle, ray</li> <li>octree</li> <li>splines</li> <li>4x4 matrix</li> <li>intersection tests</li> <li>Mesh container</li> <li>OBJ and STL exporters (able to support massive files, with optional STL color support)</li> <li>toxi.math</li> <li>common interpolation methods (demo included in download)</li> <li>unit translators (between dpi, points, mm, pixels, useful for PDF generation)</li> <li>some (collected) faster &amp; convenient implementations of assorted common math functions (similar to processing, only without dependency on PApplet)</li> <li>sin/cos lookup tables</li> <li>Perlin &amp; Simplex noise</li> <li>wave generators</li> <li>toxi.image.util</li> <li>grayscale image filters</li> </ul>
Toxi.Colorutils	<p>This package/module of toxiclibs library features:</p> <ul style="list-style-type: none"> <li>toxi.color</li> <li>float based color type with RGB, HSV, CMYK accessors &amp; operators</li> <li>named colors &amp; hues</li> <li>color lists, ranges, themes</li> <li>color theory strategies</li> </ul>

	super flexible color sorting with many presets
Toxi.Datautils	This package/module of toxiclibs library features: toxi.util.datatypes TypedProperties class for dealing with Java property files ArrayUtil Float/Integer ranges (with/without bias) Singleton registry
Toxi.Verletphysics	This package/module of toxiclibs library features: toxi.physics basic 2d & 3D particle physics engine with Verlet integration

ToxiVolumeutils	<p>This package/module of toxiclibs library features:</p> <p>toxi.volume          Mesh generation from point cloud 3d points          volume generation from created mesh          extension of toxi.geom package./module.</p>
-----------------	--

Table 3.1: Additional libraries imported apart from standard JAVA Processing libraries.

The navigation software has a refresh rate of 60 frames per second and 9600 baud data transfer from the hybrid tracking system. The refresh rate and data transfer rate are set at software programming level. The data transfer from hardware to software has total latency of 25ms (20ms from main microcontroller board and 5ms from accessory microcontroller board) as stated in the specification of the microcontroller board. The tracking system data is collected via two microcontrollers, a main microcontroller, Arduino Mega 2560 R3 that is plugged in directly to computer, and Arduino Nano inside motor box that connects the potentiometer to the main microcontroller. Experimentation to quantify the refresh rate and latency was not done. This are to be included in future research on improvements and optimization of the navigation software.

Besides that, synchronization was absent due to no synchronization board included in the electronics of the hybrid tracking system. However, the navigation software paired the latest data signal from optical tracking system with the latest data signal from the

potentiometer tracking system at software level. Integration of synchronization board and experimentation are to be included in future research.

### **3.3.2. Importing the Femur 3D Model**

As shown in Figure 3.2, Femur 3D model is obtained by scanning a femur sawbone in a CT scanner. This model is then imported to create a 3D mesh model. The scanned data in the form of 'xyz-cood' file format is then imported to MESHLAB version 1.3.2 to create a 3D mesh via Alpha complex /shaping method. MESHLAB is an open source package that allow user to import and export mesh files in various file formats including OBJ, XYZ and STL file formats. The 3d model is then imported into the navigation software and its local coordinate is established. The steps of using reconstructed 3D CT images in CAOS have been stated in study by Nolte and Beutler(2004). Advantages of using 3D reconstructed CT images is that it can model the patient's anatomy particularly bone and grossly altered anatomy but it comes with disadvantages of introducing ionizing radiation to the body, and cost and time consuming pre-operative planning (Hamlin et al., 2005). However, despite that disadvantages, the benefit of using 3D reconstructed CT images weighs more and it is acceptable in various orthopaedic surgery such as pedicle screw placement (Glossop et al., 1996, Laine et al.,

2000), total hip arthroplasty (Tching et al., 2010, Rosenberg, 1993), and total knee arthroplasty (Jiménez et al., 2001, Park et al., 2011). Once imported, the virtual objects can be moved, rotated and overlapped with other objects. This mapping software will then be integrated with the tracking system by which, the function to translate, roll, yaw and pitch will be set to move with the respective tracked surgical objects. The mapping enables a surgeon to virtually view both 3D model of a bone and 3D model of a femoral stem, thus enabling surgeon to plan the position of femoral stem inside bone model. Also, the coordinates of both the femur and femoral stem models can be linked together to enable virtual interaction between the models.

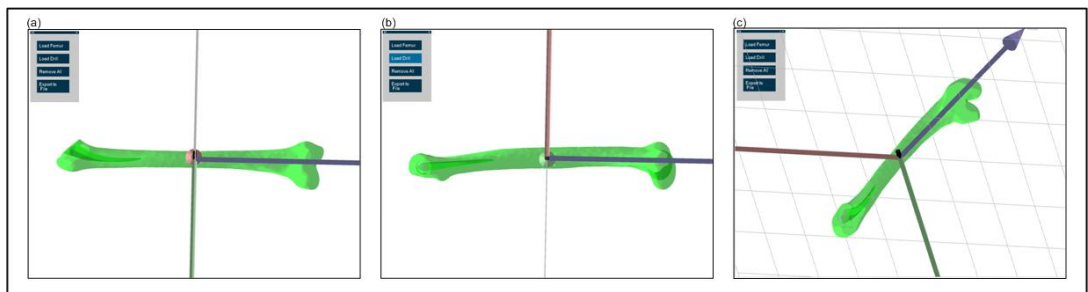


Figure 3.2: 3D model of femur in navigation 3D virtual space.

### **3.3.3. Establishing Safe Surgical Boundary**

The next step would be setting up the boundary of safe surgical volume as shown in Figure 3.3. The safe surgical volume is the milled area that confines to the volume of femoral stem 3D model. Femoral stem 3D CAD model is acquired via community online CAD model library (<http://grabcad.com/library/hip-replacement-prosthesis>). This is because no femoral stem implant can be obtained due to financial constraints. The 3D femoral stem model outline is transferred to be a boundary of the safe surgical volume. It is done after the femoral stem 3D model is properly positioned inside the 3D femur bone. The femoral head part of the femoral stem is excluded from the safe surgical boundary. It is excluded from the cross section at middle of femoral neck part of the stem. The burring motor is designed to stop once the burr tip reaches the boundary. Setting up the boundaries enables precise milling following the shape of the implant. The outline coordinate of the femoral implant is set so that whenever the burr tip coordinate is equal to any of the outline coordinate of the femoral implant; it will trigger the warning message of going beyond safe surgical area and stops the drill motor.

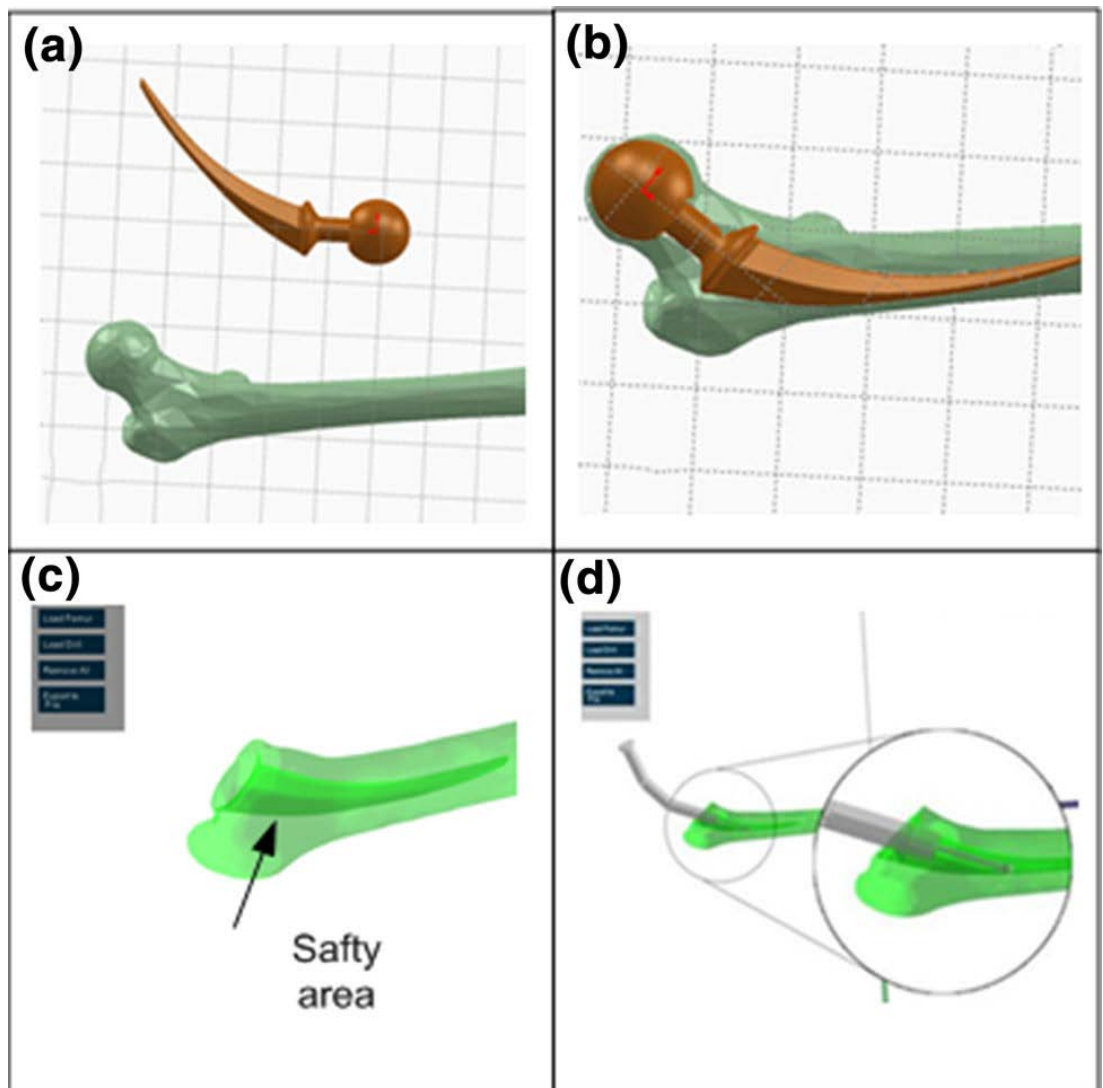


Figure 3.3: Setting up the boundary of the safe surgical volume (a) The femur and implant 3D models; (b) Position the femoral stem inside the 3D bone model; (c) Safety area is defined as the deeper green area; (d) The milling is guided by the safety boundary.

### **3.3.4. Importing the Surgical Tool 3D Model**

The following step is visualization of surgical tool 3D. The concept of the articulated drill is based on a three-bar kinematic chain. The articulated drill is able to bend to enable milling the curve shape of femoral stem, and the tool is rigid enough to make femoral canal drilling possible without buckling effect at the base. 3D CAD model of the articulated drill in .STL format is imported into the navigation system piece by piece. It is then assemble following the kinematics of articulated drill. At this point, the virtual 3D model is not movable as shown in Figure 3.4 since it can only move or bend when given stream input from hybrid tracking system. The 3D model did not include the motor box because the LED tracker is place at the base of articulated drill. Bending of joint 1 and joint 1 will follow the streaming input from the encoders.

### **3.3.5. Registration of Both 3D Models to the Tracking System**

This process is followed by the registration of both 3D models to the actual objects via the tracking system. Registration is done by aiming the burr tip to at least 3 points near greater trochanter to check and confirm that the articulated drill is registered and tracked. The points aimed were peak of greater trochanter, the superior surface at base of greater trochanter, and lateral surface at base of greater trochanter. The coordinates of the registration points were then registered to properly



locate and orient the surgical tool in relation to femur inside the navigation system. More registration points can be added by repeating the points location again and adding registration points at inferior surface and medial surface of base of greater trochanter.

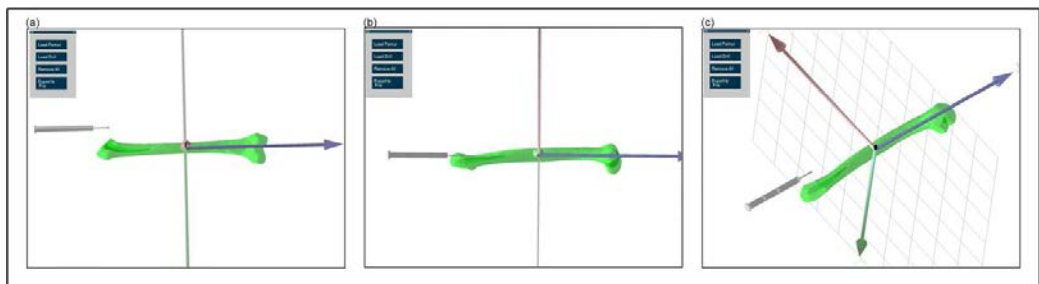


Figure 3.4: 3D model of both femur and articulated drill in navigation 3D virtual space.

The 3D model is the virtual objects (VO) in the guide system as shown in Figure 3.4. The VO has its coordinates and orientation mapped in the navigation system. These data are used to register the VO to the surgical objects (SO) which is carried out intra-operatively by the tracking system. This is done by transforming the coordinates and the orientation of the VO to follow those of the SO. This activation enables a real-time position tracking of the surgical objects virtually on the monitor. The SO is referenced by attaching dynamic referencing base (DRB) trackers to the base of articulated drill and the middle shaft of the femur bone. The optical tracking system consists of beacons of two infrared LED trackers and a small infrared camera at the middle of the LED trackers. They act as mobile/independent trackers and are attached to each surgical object

and the end-effector. The articulated drill sheath inside the bone is tracked by potentiometers attached at each joint of the sheath. They determine the position of the burr tip with reference to the base of the drill manipulator calculated by its forward kinematics. The potentiometers give each joint's bending angles. The joint bending angles data are then read by the navigation system as rotation angles for joint 1 and joint 2. The angle data, combined with the length of each segment, are then used to map the location of the articulated sheath and register it with its virtual object. This tracking system tracks and updates the virtual object to guide the surgical procedure.

### 3.3.6. Collision of Surgical Tool with Safe Surgical Boundary

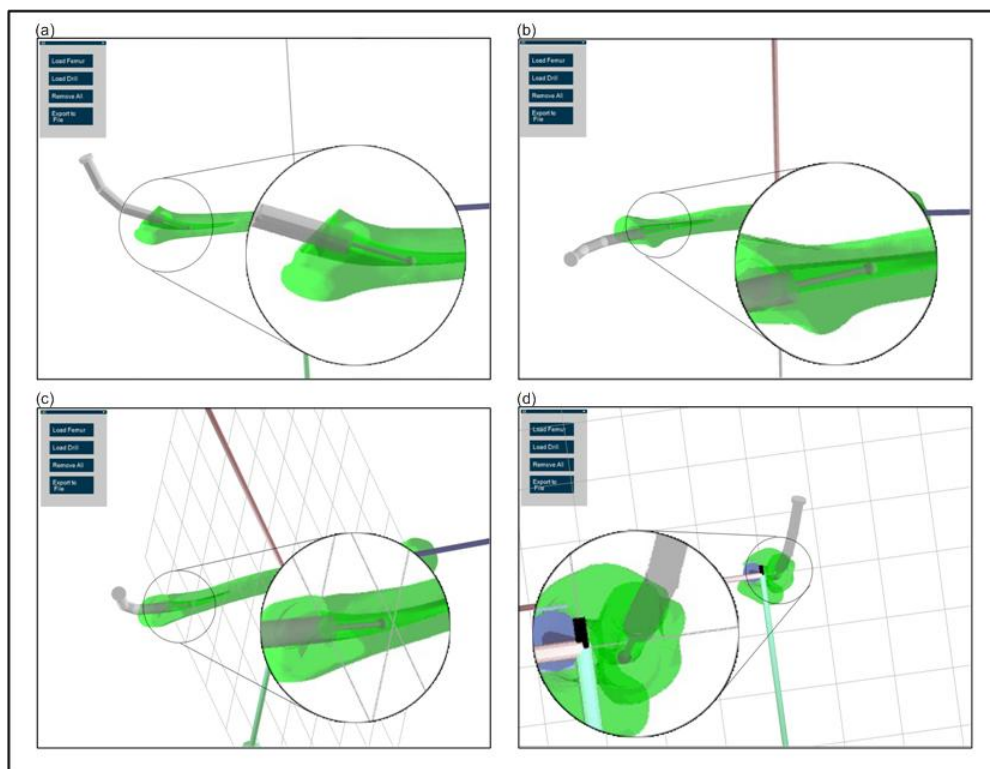


Figure 3.5: Manipulation and guiding the drilling process inside the bone within the safe surgical area defined by the femoral stem implant CAD model

Once the coordinates have been paired, the position tracking of the surgical object appears virtually on the monitor. The optical tracking system will track the position and orientation of both and the base of the articulated drill while the encoder tracking system will track the bending angle of the articulated drill. As shown in Figure 3.5, the articulated drill can be guided through a small space inside the bone. The positioning of the drill tip is calculated through the kinematics of the articulated drill. Milling inside the bone relies on the guidance of the navigation system.

The navigation system alerts the surgeon to when the milling tip touches the surgical boundary as shown in Figure 3.6. The green surgical boundary is a pre-planned area to guide the cutting for implantation of the femoral stem. A warning message to stop milling is triggered, and the drilling motor is switched off so that the surgeon will stop milling and take a step back to prevent over milling beyond the surgical boundary. This occurs when the coordinates of the milling tip overlap those of the surgical boundary. Since this navigation system does not indicate the depth of the mill due to priority over internal bone visualization, the extent of the milling can be checked by touching the mill tip inside the bone without switching on the drill motor. This step is called probe mode. If the extent of the cut triggers the warning message, then over milling has occurred and vice versa. To achieve accurate milling, we can enlarge the area in the navigation software and properly estimate the extent by virtual visualization of the milling tip next to the surgical boundary. However, the accuracy depends on the calibration and the tracking system. Once the milling is done, the femoral stem can be inserted to check for fitting. If the femoral stem is not properly fitted, the surgeon should check the area inside whether it has been milled completely or not by switching the drill tip into probe mode.

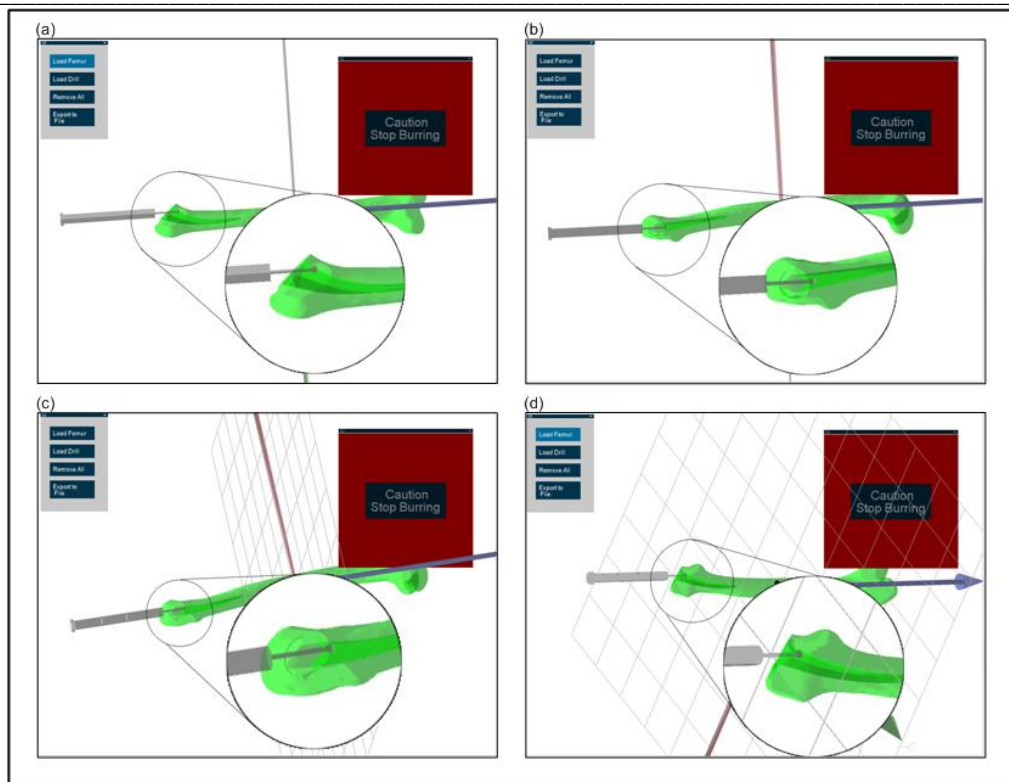


Figure 3.6: Error warning from navigation system whenever the mill tip made contact with the safe surgical boundary followed by the stopping of drill motor.

### 3.3.7. Summary of the Concept

The concept of this navigation system is illustrated in the flowchart in Figure 3.7 in reference to basic concept of CAOS (Nolte and Beutler, 2004). The end-effector (EE) consists of the articulated drill and its joints, both of which are tracked via the hybrid tracking system. The navigator (NAV) consists of a tracking camera (optical tracking) and potentiometer at articulated drill joints (position tracking). The NAV also tracks the surgical object (SO), a femur bone, via the optical tracking system. Streaming data from NAV are then registered to virtual objects (VOs) through the Articulated Drill navigation software. The VO is

obtained from two sources, which are CT scan images of the femur bone that have been reconstructed into a 3D model, and a 3D CAD model of a femoral stem and the articulated drill. These VOs have their own local coordinates, which are registered with the local coordinate system of surgical object (SO) and EE. The outcome in the navigation monitor would be trackable articulated drill and trackable femur bone with surgical boundary outlined. If these two objects' coordinates intersect with each other, it will trigger a warning message to stop milling as a result of the safety measure set to prohibit milling beyond the surgical boundary. The rendering of VO, registration step and safety warning system occurs in the navigation software.

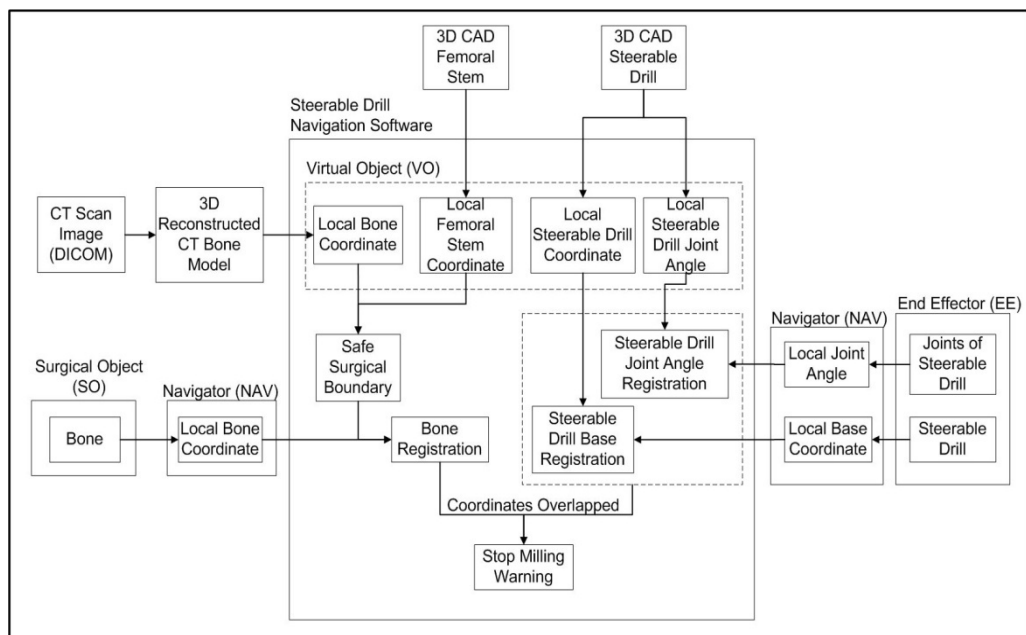


Figure 3.7: Concept of the navigation software in reference to basic concept of CAOS that divides the system into surgical object (SO), virtual object (VO), Navigation (NAV), and end effector (EE).

### **3.4. Conclusion**

The navigation system for articulated drill sheath was designed and developed. The navigation software was explained as part of the articulated drill navigation system. The navigation system is a multi-modality computer-aided integration system that provides guidance for a surgeon specifically during the procedure of total hip arthroplasty. The navigation software is being introduced as major component of the navigation system that is able to integrate optical tracking system and potentiometer tracking system, and therefore able to guide the steerable drill virtually.

By combining of the two tracking systems, i.e. the optical and potentiometer tracking system integrated by the navigation software, a hybrid navigation system is therefore introduced. This hybrid navigation system has the additional ability to track articulated drill inside the bone and able to define collision and overcome the limitation movement of 3D model of articulated drill sheath when drilling inside the bone.

Specifically, optical sensors in the optical tracking system enable this navigation software to track the location of objects outside the bone and also able to track bending angle of each joint in the articulated drill. Data Streaming from optical sensors acts as input for location tracking of surgical object such as the bone, and location tracking of end effector which is the base of articulated drill.

On the other hand, the rotary tracking system navigates further to show the location of the tip of articulated drill. As potentiometer are placed at each revolute joint of articulated drill in the three-bar linkage structure, thus inputting streams of bending angle values of each joint into the navigation software.



## **CHAPTER 4 -FORCE MEASUREMENT EXPERIMENT**

### **4.1. Introduction**

This chapter will describe the force measurement experiment of articulated drill system with the aim of understanding the static performance in variable configuration of the articulated drill system. The experiment is focusing on using milling orthogonal as the surgical bone cutting that cuts in parallel direction to the uncut surface with the tool approach is at the right angle to the uncut surface. This experiment was also done to test the capability of articulated drill system to sustain bending while milling in vertical and lateral configuration.

The measurement of force in milling in the experiment is based on action-reaction force. The test rig comprises of five components which are linear stage, articulated drill, bone holder platform, load cell, and bone sample holder will be assembled that will allow the measurement and acquisition of feedback force of the bone sample when mill by articulated drill.

### **4.2. Cutting Tool – Orthogonal Cutting**

Surgical bone cutting tools are consist of drilling, milling, and sawing. Each has different cutting methods, and different cutting force. Milling is an orthogonal cutting type that cuts in parallel direction to the uncut surface with the tool approach is at the right angle to the uncut surface. Studies on this orthogonal cutting have been published since the 1970s. The focus of study

was on influence of feed and rake angle on cutting force and chip morphology (Jacobs et al., 1974), study on fracture based chip formation model and linear correlation between specific energy and surface to volume ratio (Wiggins and Malkin, 1978), and study on influence of cutting speed and rake angle on cutting force (Krause, 1987). In these studies, it was stated that cutting force and specific cutting energy decreases with increase of cutting speed.

#### **4.2.1 Force model of bone cutting by spherical rotating tool**

Moghaddam et al (2008) did a study on voxel-based force modelling of orthogonal bone cutting by using spherical rotating tool such as burr. It cuts the bone by orthogonal cutting when each cutting element comes in contact with the bone piece. The cutting force is related to the size of chip formed after cutting. Their results showed that the force along the X axis ( $F_x$ ) is around 1 N (Figure 4.1) and the voxel size of 0.05mm results is closer to those of the analytical method with average absolute error of 6.8%. The result of voxel size 0.1mm has slightly higher average absolute error which is 14.4%. They concluded that the cutting force decreases as the number of teeth or spindle speed increases.

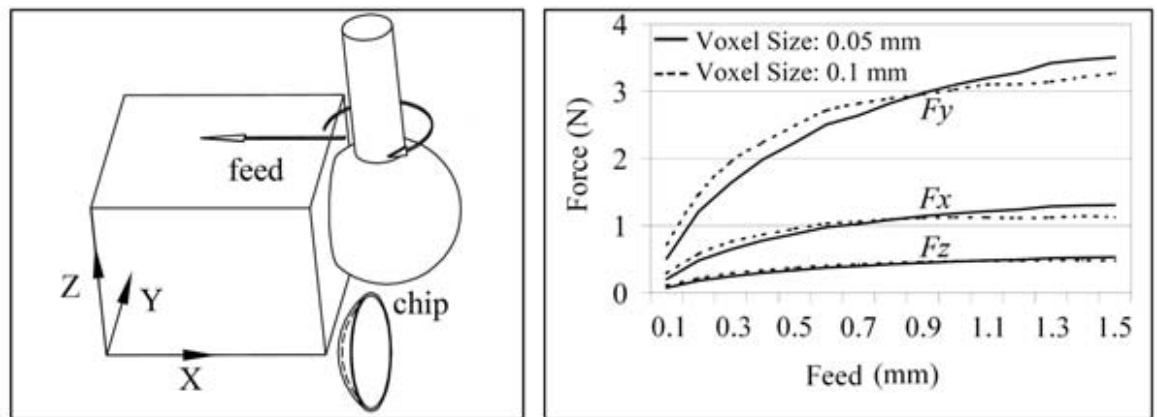


Figure 4.1: Simulation of a spherical tool with 6 cutting edges; (a) tool, bone, coordinates, feed direction, and the resulting chip, (b) simulation results for two voxel sizes (Moghaddam et al., 2008)

### 4.3. Experiment on Measurement of Reaction Force

The purpose of this experiment is to measure reaction force when milling in different bending configuration and rake angles and understanding the static performance of articulated drill system under different configurations. This experiment should be able to show which configuration is the best for milling bone with the articulated drill that has three bar and two linkages. The measurement of force in milling in this experiment is based on action-reaction force. The configurations of the articulated drill consist of variable degree under forward and lateral configurations. The cutting force will follow orthogonal cutting type due to the tip is a burr tip for milling.

#### 4.3.1 Action-Reaction Force

Forces acting on an object always act in pairs. One is the force acting on the object and another one is the opposing force from the

object in opposite direction. These two forces acting together are of equal amount of force. For example, a book on a table exerts downward force to the surface of the table due to gravity and the table exerts an equal amount of upward force on the book. The downward force from the book is called action force and the upward force from the table is called reaction force. This pair is called action-reaction force, and this is the basic of force acting on an object because there can never be a single force acting along without an opposing force. Action-reaction force is based on Newton's Third Law of Motion that states for every action force, there will be an equal and opposite reaction force. To put it in equation, the force of A on B is equal in magnitude and opposite in direction of the force of B on A as shown below.

$$F(AonB) = -F(BonA) \quad (\text{Eq. 1})$$

#### **4.3.2 Vertical Configuration**

The aim of this test is to measure the force required to mill the bone, in which the axis of the articulated drill is perpendicular to the surface plane of the bone and in the direction of axis perpendicular of the surface plane of the bone. This signifies the thrust cutting force of articulated drill system. The milling will be done in various total bending angle of the articulated drill. The bending direction of the articulated drill

is parallel to the surface plane of the bone. This test simulates the pushing action of the articulated drill (straight to bend) in milling the bone of the for femoral stem implantation. The result of this test is to evaluate the response force generated from the milling, which is the force required by the articulated drill tip towards the bone surface in order for the milling blade to mill the bone.

The test was performed within the articulated drill's maximum bending angle and specifically at 0° (Figure 4.2), 10° (Figure 4.3), 20° (Figure 4.4), and 30° (Figure 4.5). To achieve the desired bending angles, each joint angle was adjusted to half of the total bending angle and locked by the stall torque of the servo motor. The depth of milling was designed to be 1mm thickness. The milling was tested at a constant feed rate of 1mm/s and maximum drill motor speed of 30000 rpm.

The articulated drill will be mounting on a uniaxial linear stage by fixing the bottom surface of articulated drill's motor box to the linear stage mounting and it enables forward and reverse movement direction of articulated drill. In this configuration, the bone holder platform is placed at the end of linear stage, holding the bone sample parallel to linear stage axis. The bone holder platform is made so that the height of bone sample can be adjusted by adjusting the height of bone holder platform via screw threads. This is because as the articulated drill bends, the height of centre of the tip also changes. The bone sample holder is cube shape with hollowed centre to enable placement of 1cm<sup>3</sup> bone

sample. In between the bone holder platform and bone sample holder would be the position of load cell. The load cell is a 450N Dry Load Cell from BOSE Electroforce 3200 machine. This test will only utilize BOSE Electroforce 3200 load cell and its software for data acquisition only.

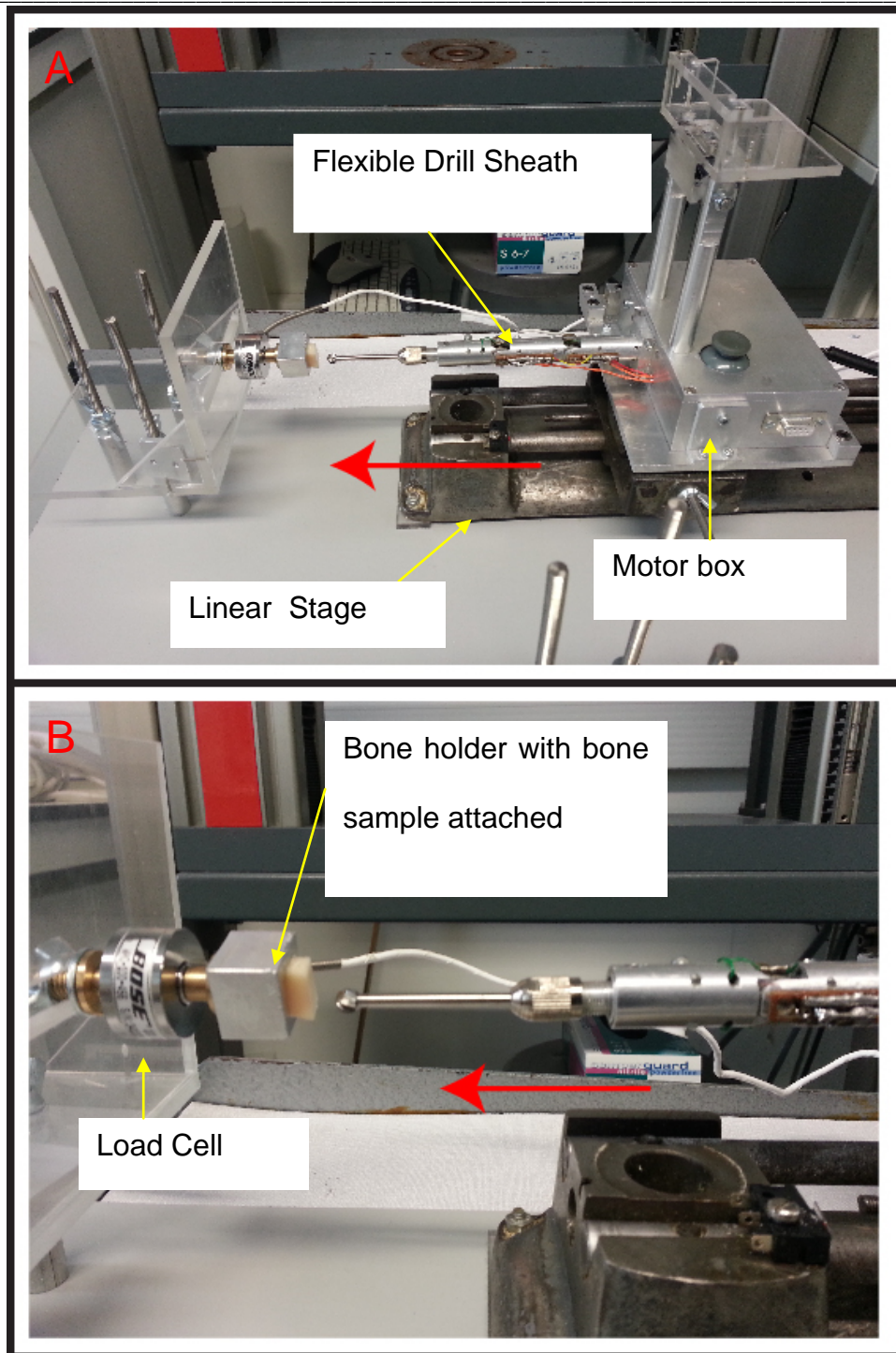


Figure 4.2: (A) Test rig setup for 0 degree in forward configuration; (B) Close up view of the burr tip position relative to bone sample surface. Red arrow in both pictures indicates direction of milling / linear stage during testing.

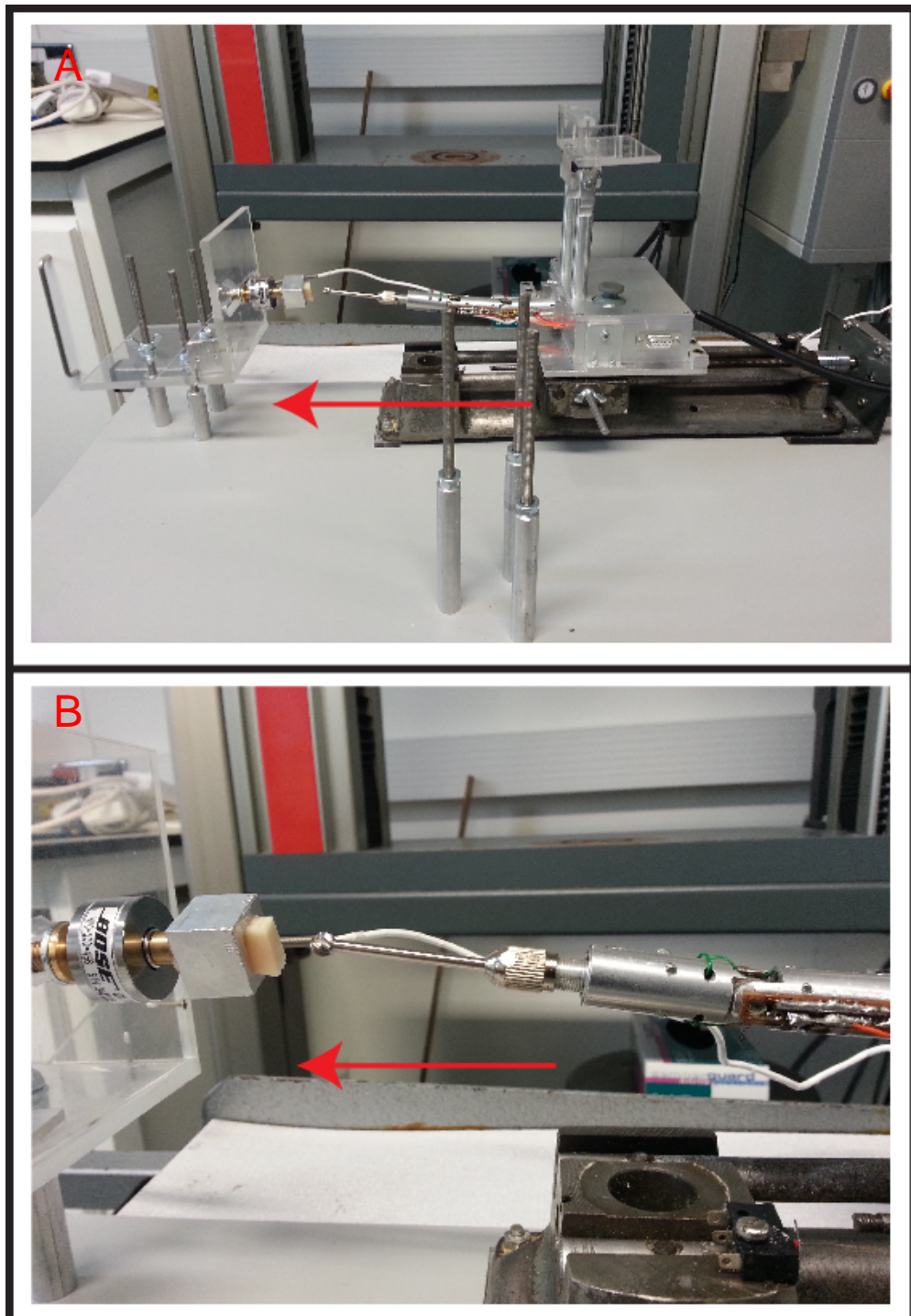


Figure 4.3: (A) Test rig setup for 10 degree in forward configuration; (B) Close up view of the burr tip position relative to bone sample surface. Red arrow in both pictures indicates direction of milling / linear stage during testing.



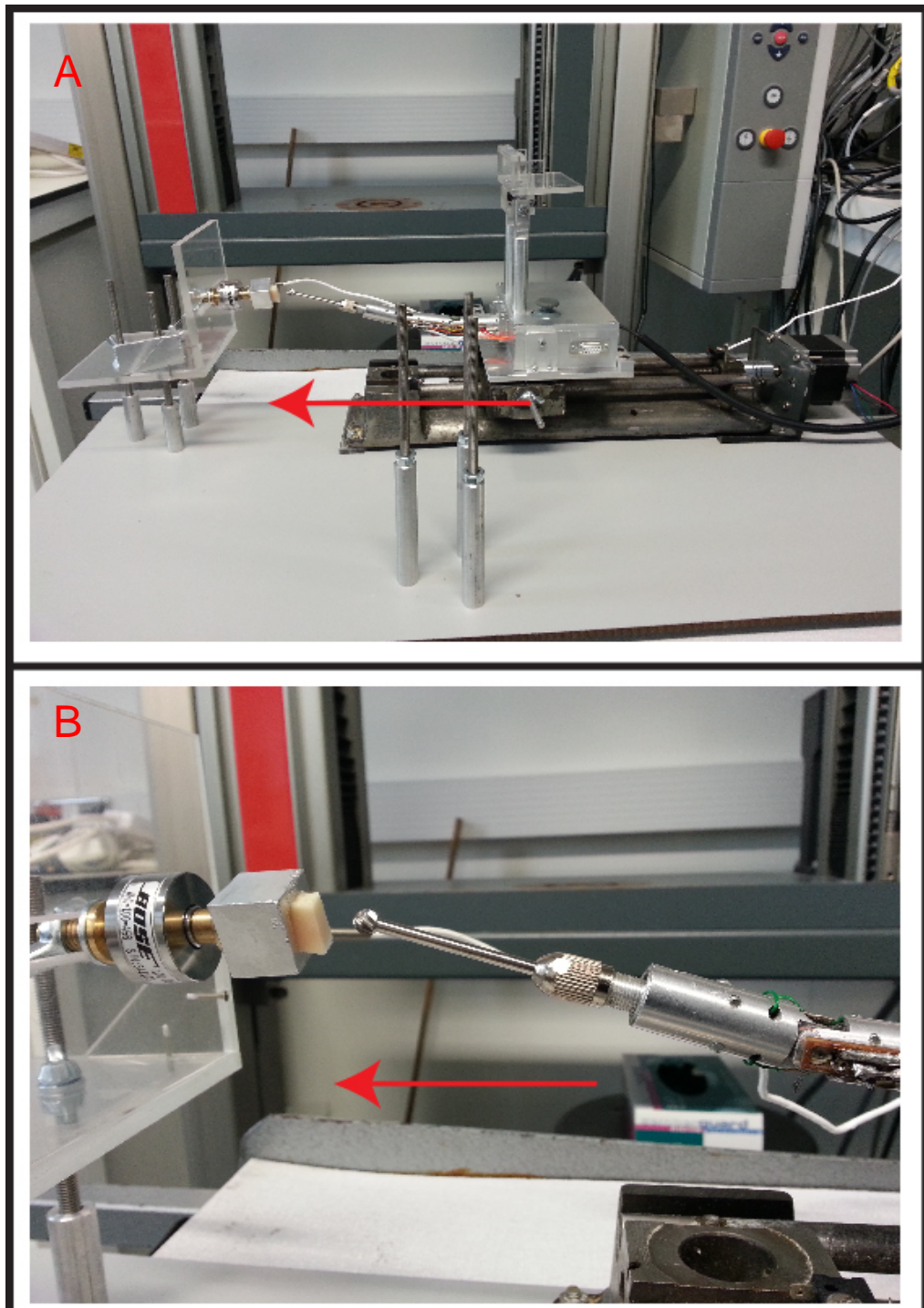


Figure 4.4: (A) Test rig setup for 20 degree in forward configuration; (B) Close up view of the burr tip position relative to bone sample surface. Red arrow in both pictures indicates direction of milling / linear stage during testing.

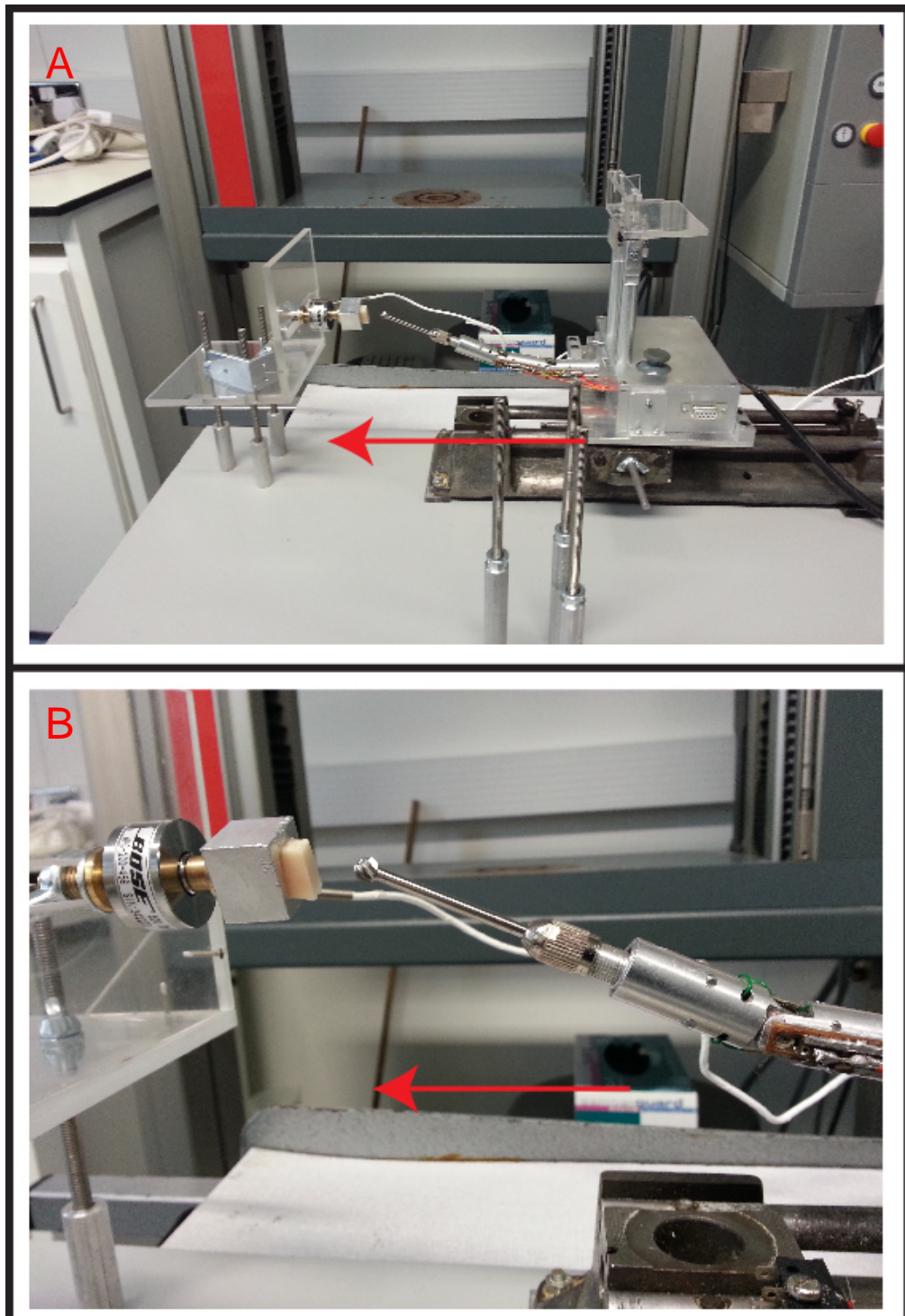


Figure 4.5: (A) Test rig setup for 30 degree in forward configuration; (B) Close up view of the burr tip position relative to bone sample surface. Red arrow in both pictures indicates direction of milling / linear stage during testing.

### **4.3.3 Lateral Configuration**

The aim of this test is to measure the force required to mill the bone with the axis of the articulated drill is parallel to the surface plane of the bone and in the direction of axis perpendicular of the surface plane of the bone. This signifies the orthogonal cutting force of the articulated drill system. The milling was performed in various total bending angles of the articulated drill. The bending direction of the articulated drill was perpendicular to the surface plane of the bone. These setups simulate the side-pulling action of the articulated drill (bend to straight) when milling the bone for femoral stem implantation. The result of this test demonstrates the forces generated from the milling, which is the force required by the articulated drill tip towards the bone surface in order for the milling blade to mill the bone.

The test will be done in articulated drill's total bending angle of 0° (Figure 4.6), 10° (Figure 4.7), 20° (Figure 4.8), and 30° (Figure 4.9). To achieve the desired bending angle, each joint angle is adjusted to half of total bending angle and locked by the stall torque of the servo motor. The depth of milling will be 1mm thickness. The milling will be done at constant feed rate of 1mm/s and maximum drill motor speed which is 30000RPM.

The articulated drill will be mounting on a uniaxial linear stage by fixing the side surface of articulated drill's motor box to the linear stage

mounting and it simulates upward and downward movement direction of articulated drill. In this configuration, the bone holder platform is placed at the side of linear stage, holding the bone sample parallel to linear stage axis. The bone holder platform is made so that the horizontal position of bone sample can be adjusted by adjusting the screw position on the slit of bone holder platform. This is because as the articulated drill bends, the horizontal position of centre of the tip also changes. The bone sample holder is cube shape with hollowed centre to enable placement of 1cm<sup>3</sup> bone sample. In between the bone holder platform and bone sample holder would be the position of load cell. The load cell is a 450N Dry Load Cell from BOSE Electroforce 3200 machine. This test will only utilize BOSE Electroforce 3200 load cell and its software for data acquisition only.

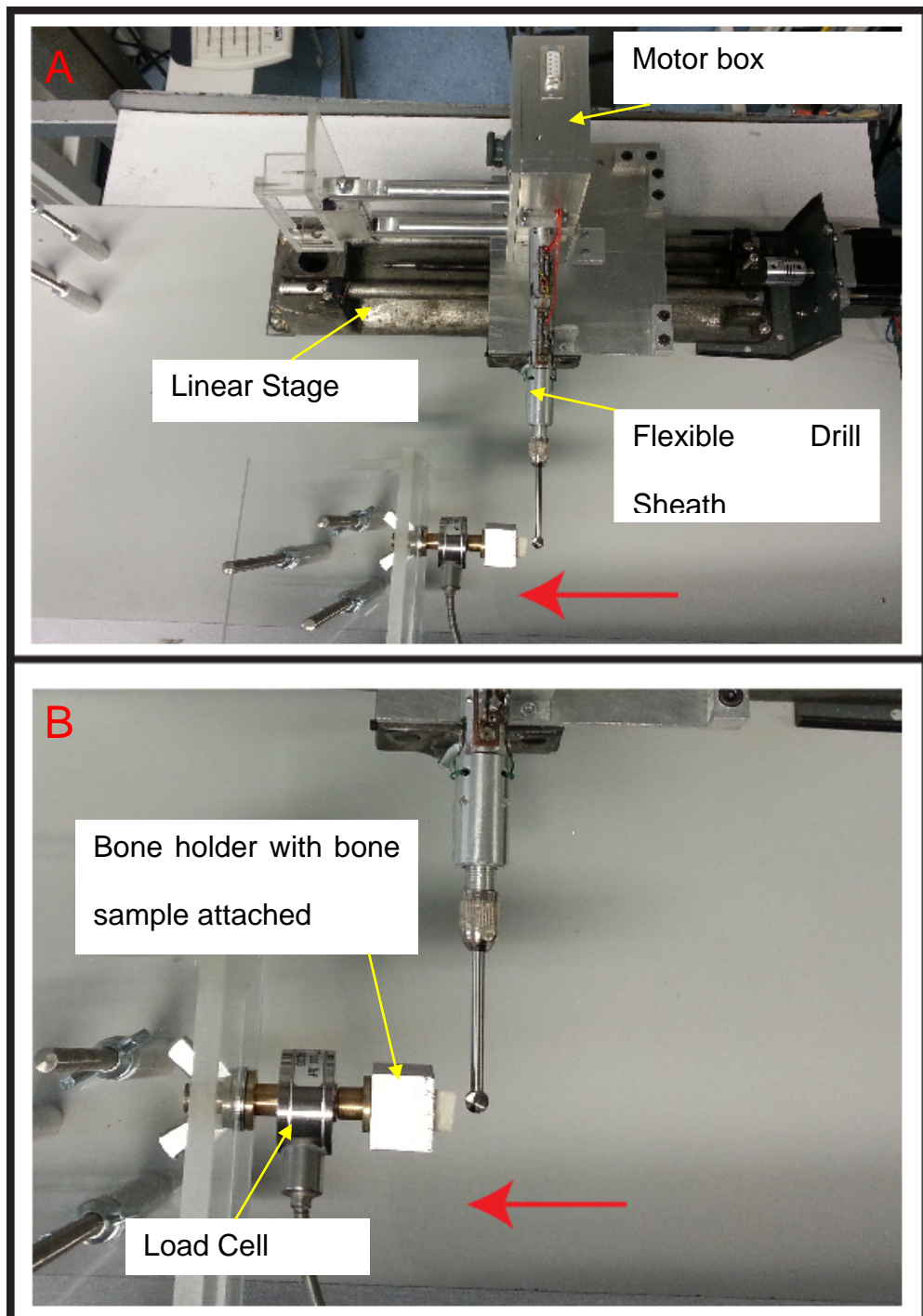


Figure 4.6: (A) Test rig setup for 0 degree in lateral configuration; (B) Close up view of the burr tip position relative to bone sample surface. Red arrow in both pictures indicates direction of milling / linear stage during testing.

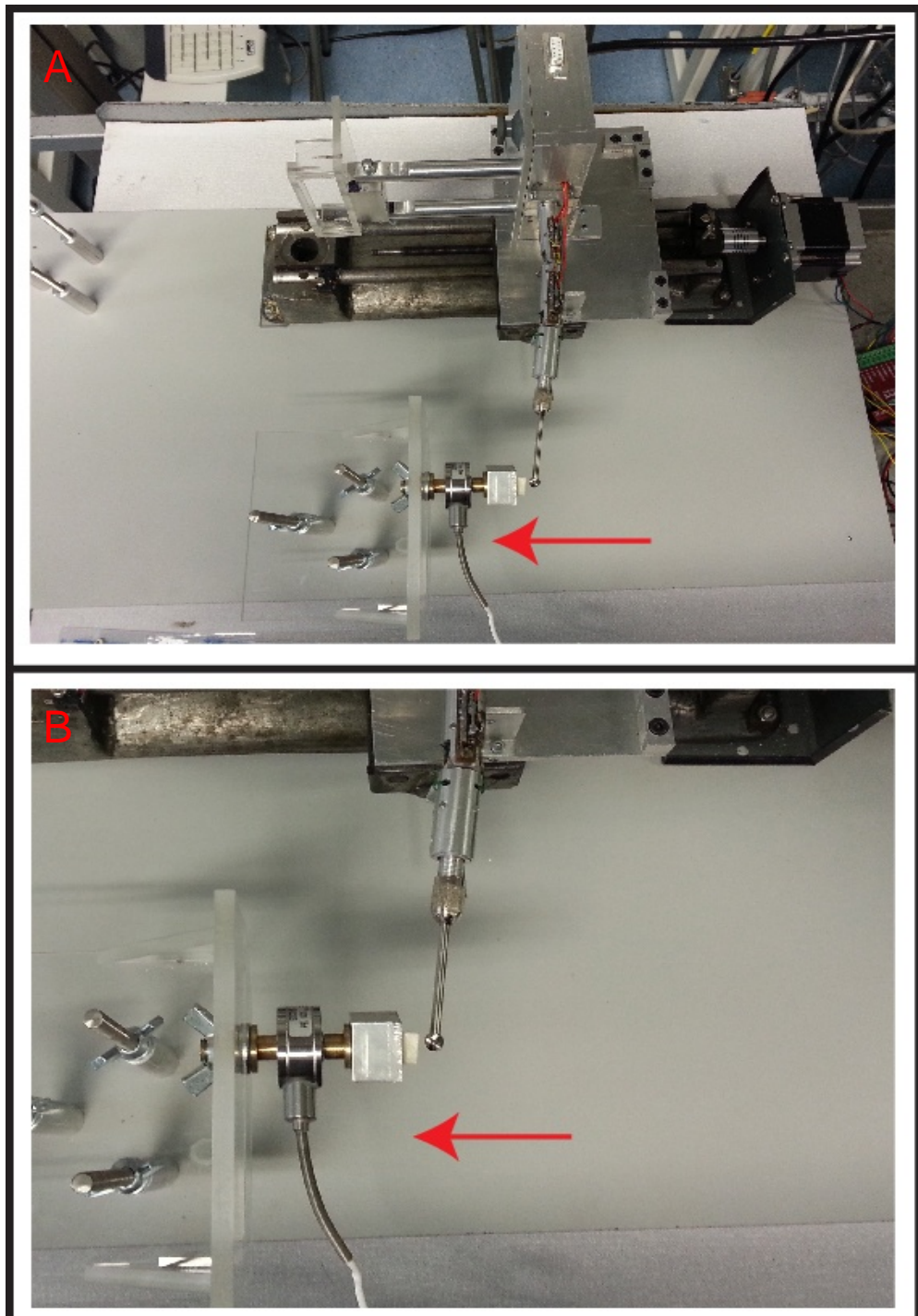


Figure 4.7: (A) Test rig setup for 10 degree in lateral configuration; (B) Close up view of the burr tip position relative to bone sample surface. Red arrow in both pictures indicates direction of milling / linear stage during testing.

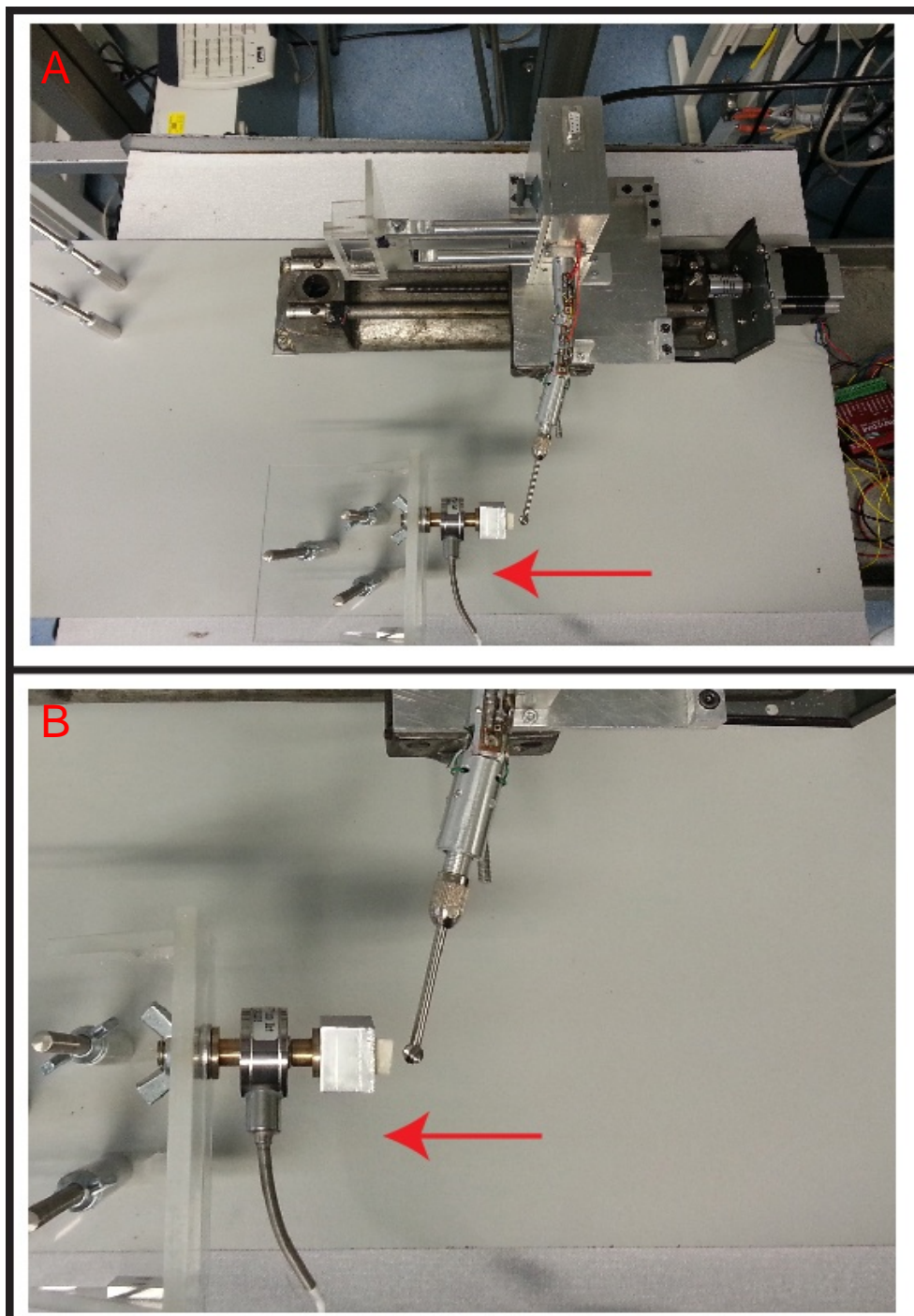


Figure 4.8: (A) Test rig setup for 20 degree in lateral configuration; (B) Close up view of the burr tip position relative to bone sample surface. Red arrow in both pictures indicates direction of milling / linear stage during testing.

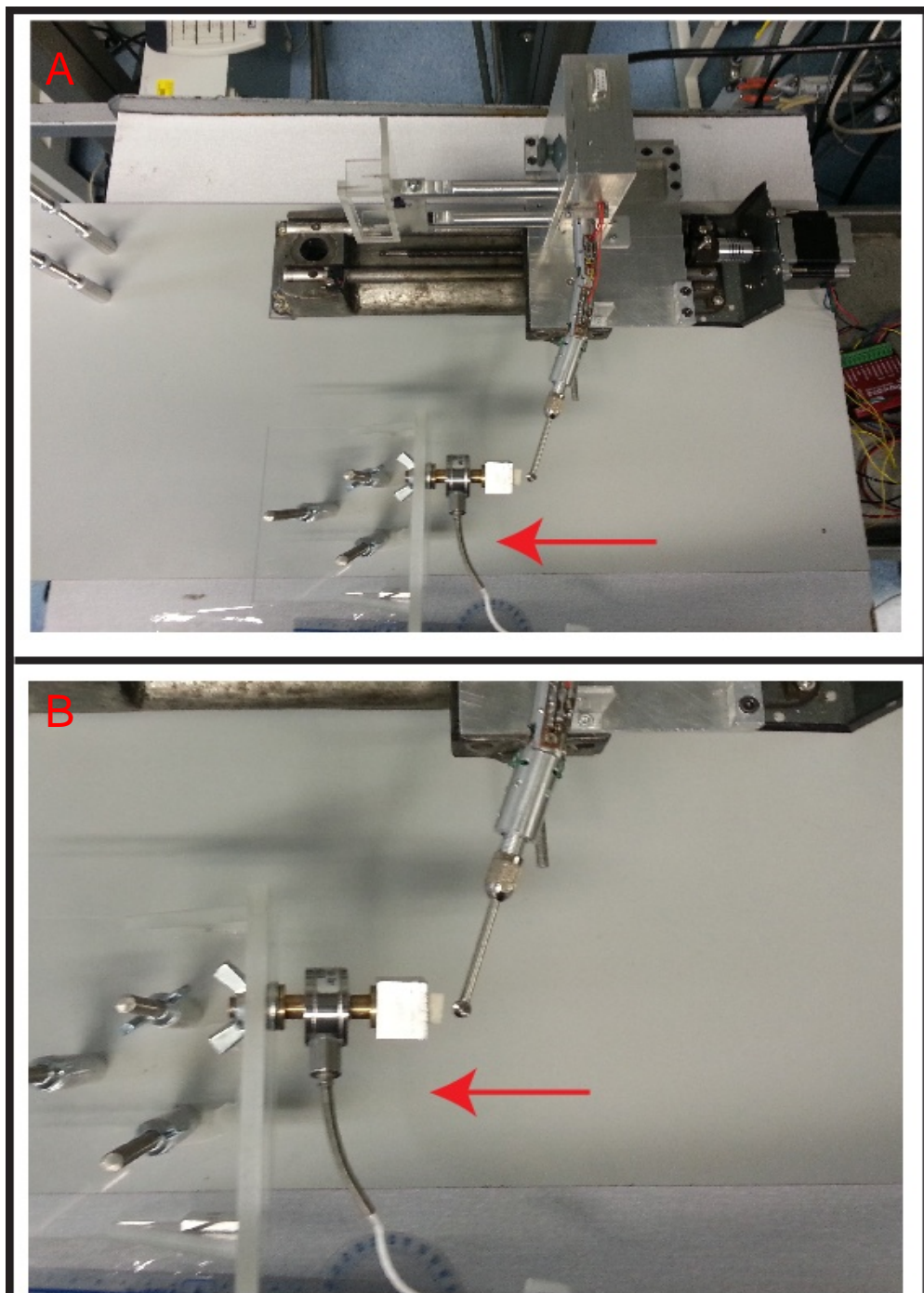


Figure 4.9: (A) Test rig setup for 30 degree in lateral configuration; (B) Close up view of the burr tip position relative to bone sample surface. Red arrow in both pictures indicates direction of milling / linear stage during testing.



#### **4.3.4 Assembly of the test rig**

The test rig comprises of five components which are linear stage, articulated drill, bone holder platform, load cell, and bone sample holder (Figure 4.2 (A)). These five components, when assemble will allow the measurement and acquisition of feedback force of the bone sample when mill by articulated drill. The articulated drill's motor box is attached to the linear stage that is fixed to a test rig platform and the bone holder platform is attached to three pylons fixing it to the test rig platform. The articulated drill can be attached to the linear stage in two configuration by which the bottom of the motor box is attached to the linear stage for vertical configuration (Figure 4.2 (A)) and the side of the motor box is attached to the linear stage for lateral configuration (Figure 4.6 (A)). The load cell is attached to the bone holder platform by tighten the load cell connector through a horizontal slit by a nut. The horizontal slit enables adjustment of the connector's position horizontally. The bone sample holder will hold a 1cm<sup>3</sup> bone sample that is cut from fresh bovine femur. The bone sample holder is attached to the load cell via second load cell connector. The linear stage motion is powered by a stepper motor with stepper motor controller that has micro stepping. Micro stepping is required since the motion occurs in millimetre range and the feed rate is only 1mm/s. The control of the linear stage is operated via computer terminal and engineered control. The load cell is connected to BOSE Electroforce DAX and computer unit to read and obtain the force

measured. The articulated drill is powered by a high-speed hand drill that is fixed to a table vice by attaching the end of flexible shaft of the articulated drill. The total bending angle to be measured is set and the centre of bone sample is aligned to the centre of mill bit tip. Once the test is finished, all bovine bone sample is disposed according to strict safety animal tissue disposal procedure and the test rig is cleaned and disinfected.

#### **4.3.5 Data Acquisition**

Data was collected by the BOSE Electroforce 3200 Data Acquisition Card and Software. It could measure force up to  $\pm 450$  N and had a sensitivity of less than a Newton. The test was set at hand drill speed of 3000 rpm, feed rate of 1mm/s, and milling depth of 1mm. The linear stage was set up so that the tip of mill bit is about 2mm from the surface of bone sample and was able to move 3mm back and forth. The force starts to record when the linear stage and the articulated drill start to run. Once one cycle of linear stage motion was completed, the recorded force readings were saved as a CSV file format. The tests were repeated with the maximum bending angle at 30 degree in both vertical and lateral configurations.

#### **4.3.6 Data Analysis**

Acquired data is imported into MATLAB for noise filtering and data visualization. Since the data is a time series data, moving average filter is used to remove the noise. The data was then analysed in a force vs. time graph; and the minimum peak value and the graph pattern were identified. Data visualization is consisting of graph of individual bending angle for both configuration and also combination of all bending angle for each configuration. The individual bending angle graph shows the graph pattern and minimum peak value while showing the changes of minimum peak values according to bending angles. The peak value is obtained when there is plateau phase and the highest value in the plateau phase is the peak.

### 4.3.7 Limitation of Experiment

There are limitations to this experiment and should be address in future research. The first limitation is this experiment only measure static performance of the articulated drill system. Therefore, it lacks the dynamic performance measurement of the system. The limitation is due to financial constraint on acquiring force sensors to be mounted directly on the device, and to acquire more bone sample in various size including a full bovine femur bone.

### 4.3.8 Results

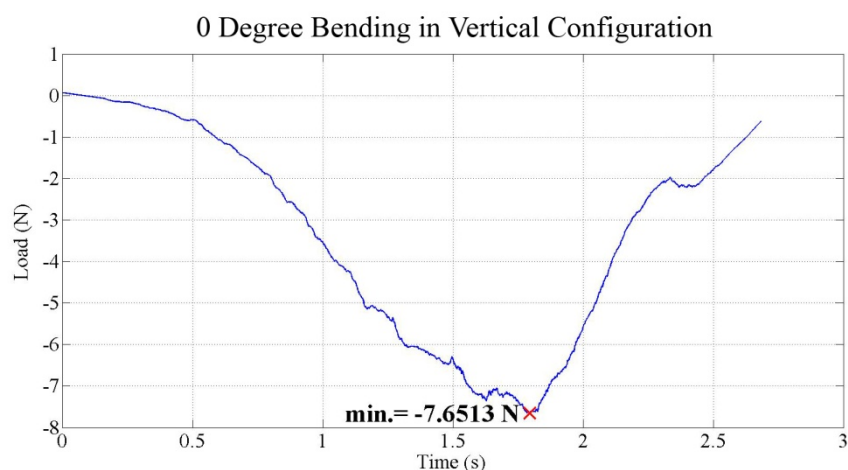


Figure 4.10: Force-Time Curve of 0 Degree Bending in Forward Configuration.

The force-time curves show the feedback force generated from 0 degree bending in forward configuration (Figure 4.10). The negative force value represents compression towards the load cell. The feedback force increases as the depth of milling increases until the peak minimum

value that is within plateau phase and later decreases as the mill tip moves backwards from the bone sample. From the force-time curves shown in Figure 1, the peak minimum value is -7.65N.

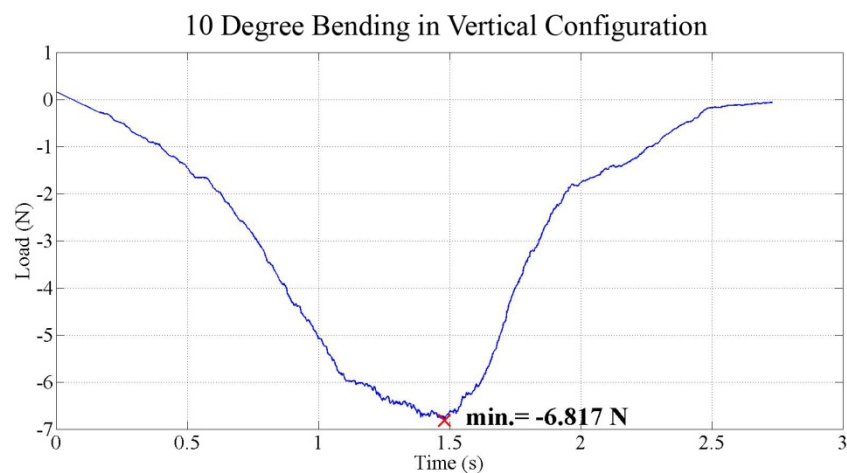


Figure 4.11: Force-Time Curve of 10 Degree Bending in Forward Configuration.

The force-time curves show the feedback force generated from 10 degree bending in forward configuration in Figure 4.11. The negative force value represents compression towards the load cell. The feedback force increases as the depth of milling increases until the peak minimum value that is within plateau phase and later decreases as the mill tip moves backwards from the bone sample. From the force-time curves shown in Figure 4.11, the peak minimum value is -6.82N.

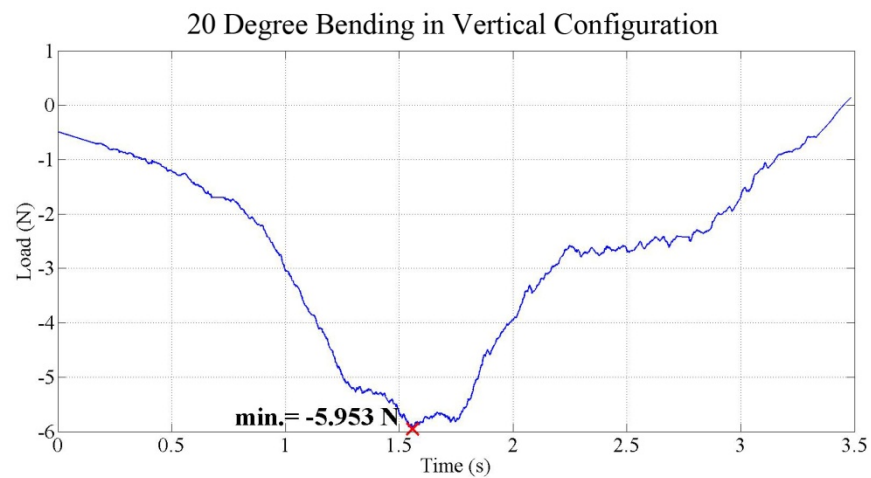


Figure 4.12: Force-Time Curve of 20 Degree Bending in Forward Configuration.

The force-time curves show the feedback force generated from 20 degree bending in forward configuration in Figure 4.12. The negative force value represents compression towards the load cell. The feedback force increases as the depth of milling increases until the peak minimum value that is within plateau phase and later decreases as the mill tip moves backwards from the bone sample. From the force-time curves shown in Figure 4.12, the peak minimum value is -5.95N.

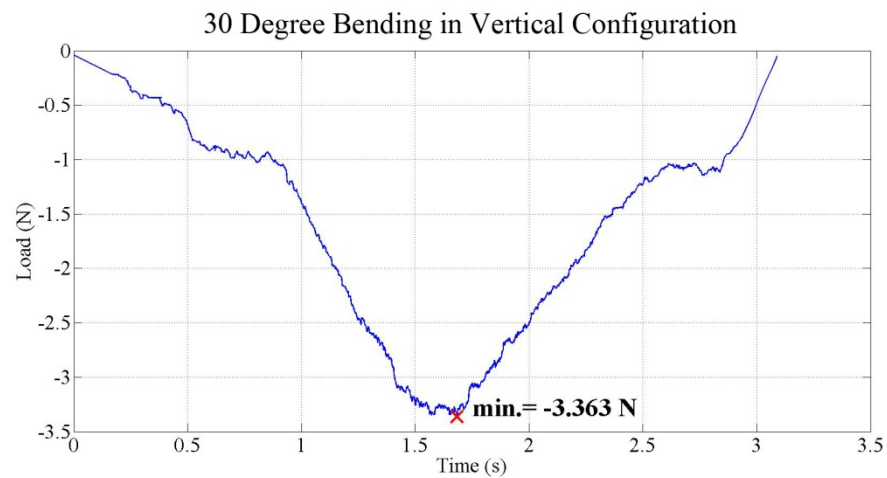


Figure 4.13: Force-Time Curve of 30 Degree Bending in Forward Configuration.

The force-time curves show the feedback force generated from 30 degree bending in forward configuration in Figure 4.13. The negative force value represents compression towards the load cell. The feedback force increases as the depth of milling increases until the peak minimum value that is within plateau phase and later decreases as the mill tip moves backwards from the bone sample. From the force-time curves shown in Figure 4.13, the peak minimum value is -3.36N.

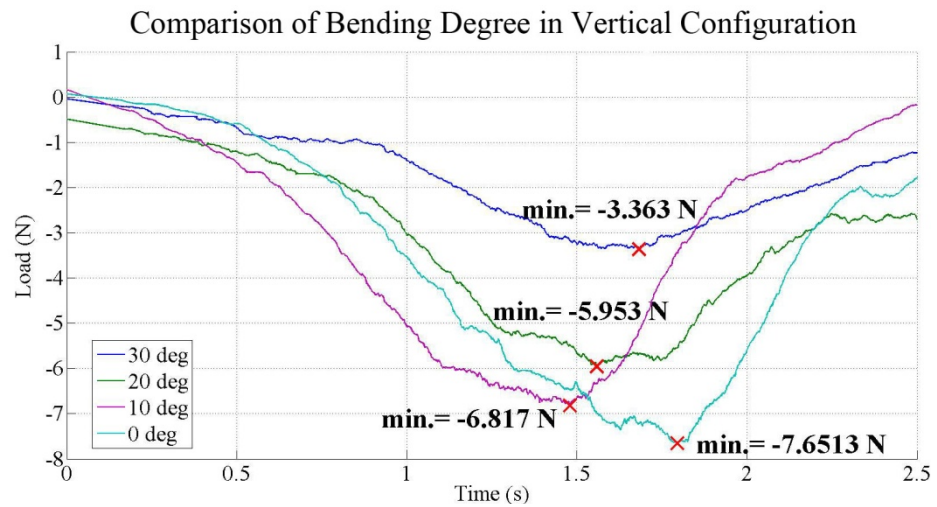


Figure 4.14: Force-Time Curve of Comparison of Bending Degree in Forward Configuration.

The force-time curves show the response forces generated in the vertical configuration at 0, 10, 20, and 30 degree bending in figure 4.14. The negative force values represent compression towards the load cell. The feedback force increases as the depth of milling increases until the peak minimum value that is within plateau phase and later decreases as the mill tip moves backwards from the bone sample.

From the force-time curves shown in Figure 4.14, the magnitude of the peak minimum value decreases as the bending angle increases from 0 degree to 30 degree. Lower negative force values in graph signify higher force needed to mill the bone sample. The results show that it is harder to mill at 0 degree bending when compare with higher bending angles in vertical configuration. This is expected since the mill bit cutting blade has the highest depth at the sides and the sides of mill bit has better cutting power compared to the front.



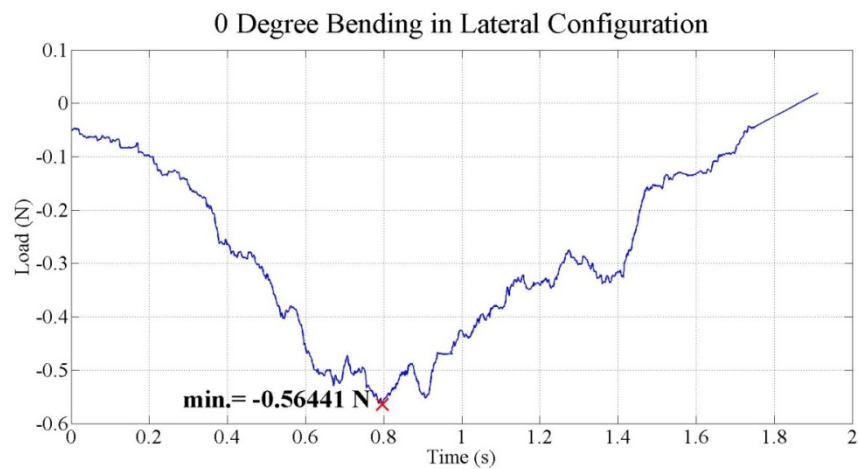


Figure 4.15: Force-Time Curve of 0 Degree Bending in Lateral Configuration.

The force-time curves show the feedback force generated from 0 degree bending in lateral configuration (Figure 4.15). The negative force value represents compression towards the load cell. The feedback force increases as the depth of milling increases until the peak minimum value that is within plateau phase and later decreases as the mill tip moves backwards from the bone sample. From the force-time curves shown in Figure 4.15, the peak minimum value is -0.56N.

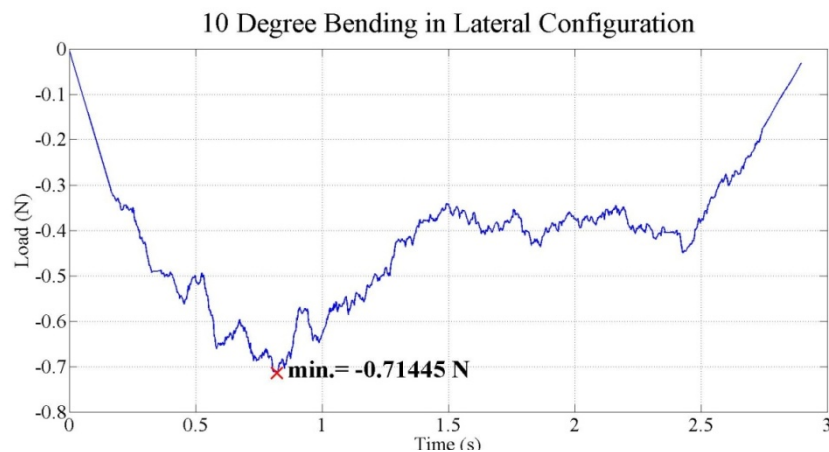


Figure 4.16: Force-Time Curve of 10 Degree Bending in Lateral Configuration.

The force-time curves show the feedback force generated from 10 degree bending in lateral configuration (Figure 4.16). The negative force value represents compression towards the load cell. The feedback force increases as the depth of milling increases until the peak minimum value that is within plateau phase and later decreases as the mill tip moves backwards from the bone sample. From the force-time curves shown in Figure 4.16, the peak minimum value is -0.71N.

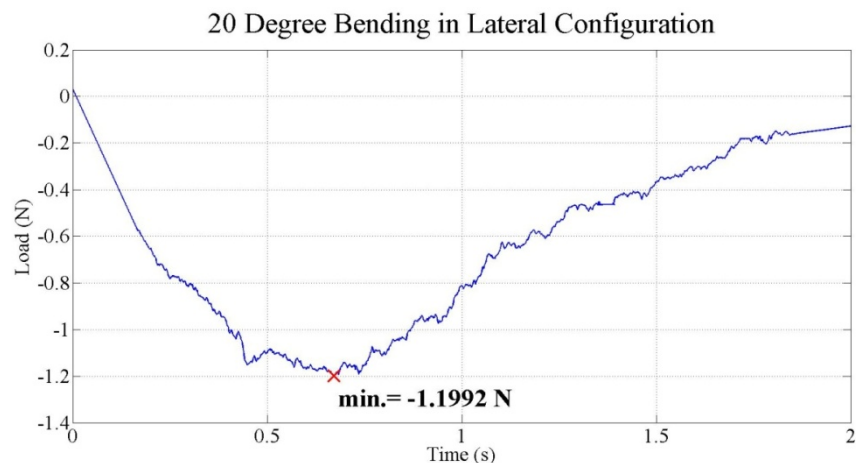


Figure 4.17: Force-Time Curve of 20 Degree Bending in Lateral Configuration.

The force-time curves show the feedback force generated from 20 degree bending in lateral configuration (Figure 4.17). The negative force value represents compression towards the load cell. The feedback force increases as the depth of milling increases until the peak minimum value that is within plateau phase and later decreases as the mill tip moves backwards from the bone sample. From the force-time curves shown in Figure 4.17, the peak minimum value is -1.20N.

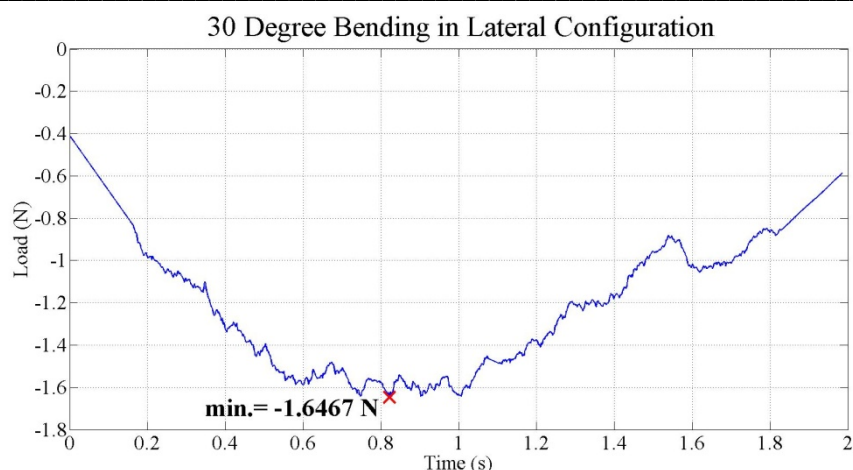


Figure 4.18: Force-Time Curve of 30 Degree Bending in Lateral Configuration.

The force-time curves show the feedback force generated from 30 degree bending in lateral configuration (Figure 4.18). The negative force value represents compression towards the load cell. The feedback force increases as the depth of milling increases until the peak minimum value that is within plateau phase and later decreases as the mill tip moves backwards from the bone sample. From the force-time curves shown in Figure 4.18, the peak minimum value is -1.65N.

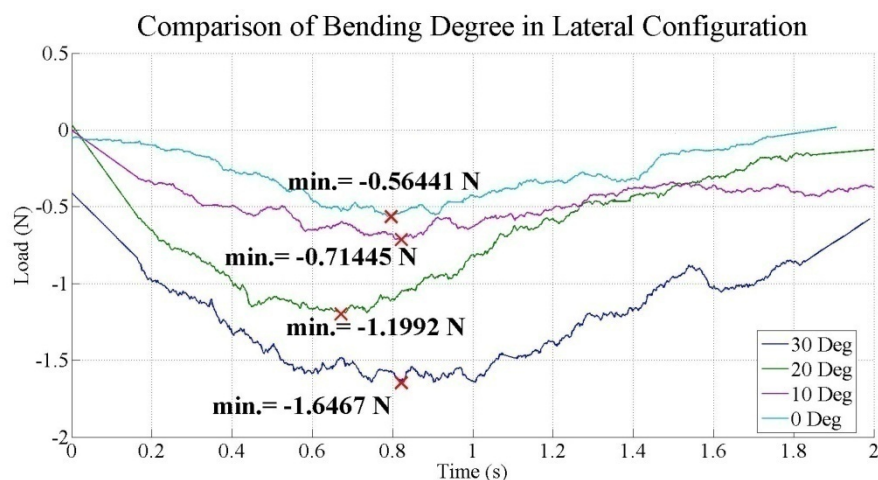


Figure 4.19: Force-Time Curve of Comparison of Bending Degree in Lateral Configuration.

The force-time curves in Figure 4.19 show the feedback force generated from lateral configuration in 0, 10, 20, and 30 degree bending (Figure 4.19). The negative force value represents compression towards the load cell. The feedback force increases as the depth of milling increases until the peak minimum value that is within plateau phase and later decreases as the mill tip moves backwards from the bone sample. From the force-time curves shown in Figure 4.19, the peak minimum value increases as the bending angle increases from 0 degree to 30 degrees. Lower negative force values in graph signify higher force needed to mill the bone sample. It shows that it is harder to mill in 30 degree bending when compare with lower bending angle in lateral configuration. This is expected since the mill bit cutting blade has the

highest depth at the sides and the sides of mill bit has better cutting power compared to the front.

#### **4.4. Conclusion**

Milling is an orthogonal cutting type that cuts in parallel direction to the uncut surface with the tool approach is at the right angle to the uncut surface. Studies that assume bone to have isotropic behaviour is common because it is adapted from numerous studies done in metal cutting simulation particularly metal alloys and it is found that bone exhibits some plasticity properties. Besides that, isotropic behaviour assumption bone modelling used two-dimensional simulation that has the advantage of computational efficiency. Studies that assume bone to have anisotropic behaviour is few because this approach requires three-dimensional modelling that is time consuming and can be complex. Despite being demonstrated to have behaviour similar to composite materials, study on composite cutting simulation is at the moment, limited to cutting force and lack prediction on temperature effect due to orthogonal cutting. Micro-scale modelling requires improvement because the early phase of predicted force development is less steep than the experimental results, and micro-scale modelling has the potential to predict the role of cement line, and micro crack propagations. Study on voxel-based force modelling of orthogonal bone cutting by using spherical rotating tool has been done. The results showed that the force

---

along the X axis is around 1 N, and the cutting force decreases as the number of teeth or spindle increases. Experiment on Measurement of Reaction Force has been done. The reaction force when milling in different bending configuration and rake angles has been measured, and the static performance of articulated drill system under different configurations has been understood. This experiment is done in vertical configuration and lateral configuration that followed orthogonal cutting type. Data was acquired by the BOSE Electroforce 3200 Data Acquisition Card and Software. Data was analysed, noise filtered, and visualized in MATLAB. Force-Time curve of each bending degree and comparison curve of all bending degree was plotted for both vertical configuration and lateral configuration. In vertical configuration, the magnitude of the peak minimum value decreased as the bending angle increased from 0 degree to 30 degree, which was -7.65 N, -6.82 N, -5.95 N, and -3.36 N respectively. Lower negative force values in graph signified higher force needed to mill the bone sample. The results showed that it is harder to mill at 0 degree bending when compared with higher bending angles in vertical configuration. In lateral configuration, the magnitude of the peak minimum value increased as the bending angle increased from 0 degree to 30 degrees, which were -0.56 N, -0.71 N, -1.20 N, and -1.65 N respectively. Lower negative force values in graph signified higher force needed to mill the bone sample. It showed that it is harder to mill in 30 degree bending when compare with lower bending angle in lateral configuration.

## **CHAPTER 5 - SYSTEM INTEGRATION AND EXPERIMENTS**

### **5.1. Introduction**

This chapter will describe the results obtained from experiments done on articulated drill system. It is divided into four topics in relation to previous chapter's experiments, namely System Integration; Encode Tracking Calibration; Experiment in Sawbones - 3D geometric analysis of the shape of the cut area; Experiment in sawbones - Accuracy Analysis/Symmetry Analysis

### **5.2. System integration**

This section presents an integrated articulated and steerable drill system in Figure 5.1 that can be used for evaluation experiments in sawbones. There are different levels of integration including mechanical assembly; embedded position sensing and optical tracking; mapping and navigation. In this system, the main emphasis of the mechanical integration is to ensure a reliable mechanical structure of the articulated drill manipulator and robust motor control. The mechanical structure will be designed for enough space for potentiometers embedded in the segments and on the handle optical tracking devices are mounted. Regarding the software integration, all imaging, tracking and virtual model software will be integrated into a unit framework of an easy to use and modular user-computer system. The navigation software shows a friendly graphics user interface, which



would make the surgical orientation and equipment handling easy for the surgeon.

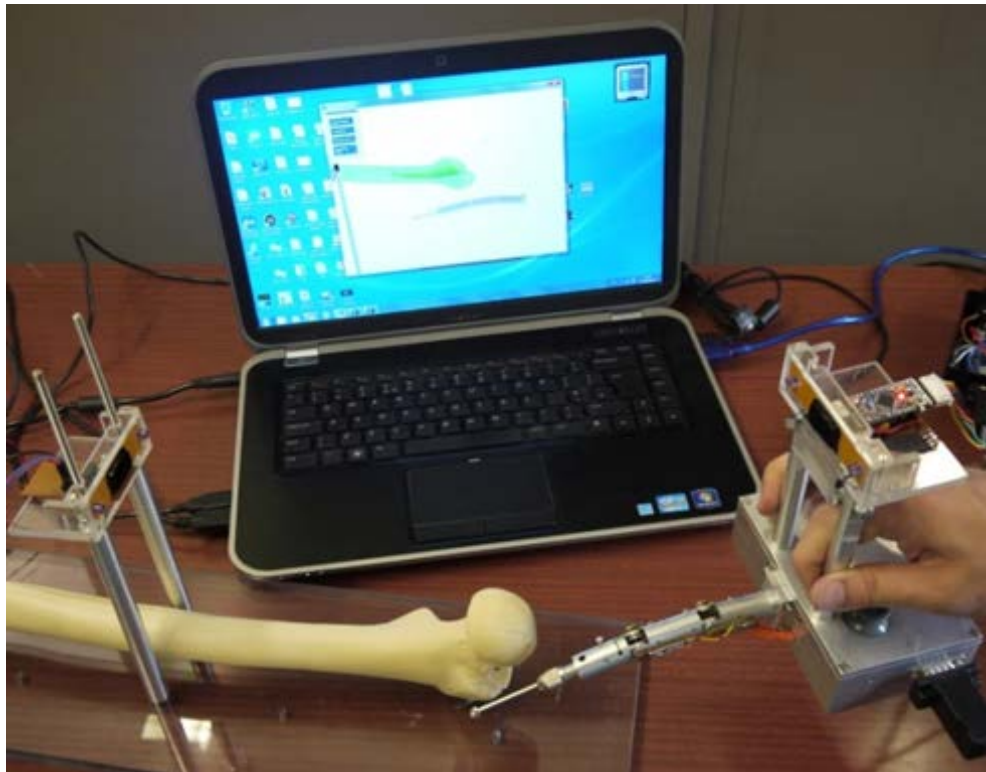


Figure 5.1: System integration for the articulated and steerable drill

### 5.3. Potentiometer tracking calibration

The encoder is calibrated by using a digital goniometer as a reference. The goniometer can be accurate up to 0.1 degree of measurement. The calibration is done by mapping the output voltage of the potentiometer for each degree of rotation. Zero degree is set when the articulated drill sheath is in straight configuration. Calibration is done for every degree in clockwise and counter-clockwise direction from the zero degree position. Calibration is

done for both joints separately. Angle measurements are taken from the navigation system and the average of the streamed data is taken as the measurement for each degree of rotation. The absolute percentage error of the calibrated potentiometer is calculated by comparing the calibrated angle values with the goniometer angle values. The absolute error is then plotted to a graph.

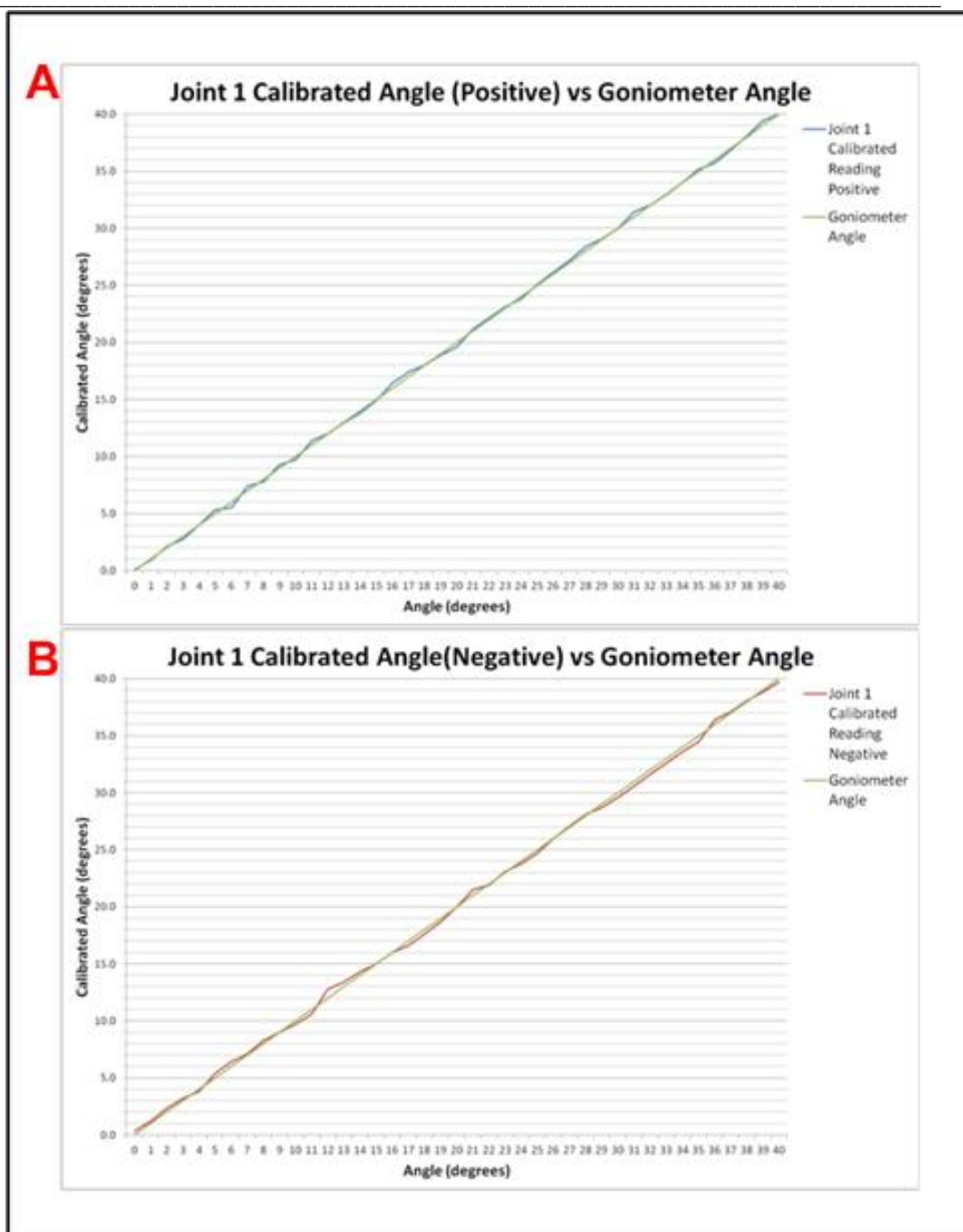


Figure 5.2: Joint 1 Calibrated Angle vs. Goniometer (A)Positive (B) Negative

Figure 5.2A and Figure 5.2B show the comparison between calibrated angle values of the potentiometer and the angles obtained from the digital

---

goniometer. Despite small deviation from the straight line of digital goniometer, the line that represents the calibrated value is almost the same with the goniometer line. They show that the potentiometer is calibrated almost perfectly against the digital goniometer values. In Figure 5.2A, there are clear deviations between the 5° until 11°. The potentiometer shaft is not sensitive enough to differentiate sub-degree precision up to 0.1°. Hence the voltage output varies from small change per sub-degree to bigger change per sub-degree. This is due to the usage of analogue potentiometer, which has some variation in output when it returns repeatedly to the same position and a small change of direction does not result in change in voltage output, hence it is not sensitive enough to detect small changes in the opposite direction. This also affects the readings in Figure 5.2B.

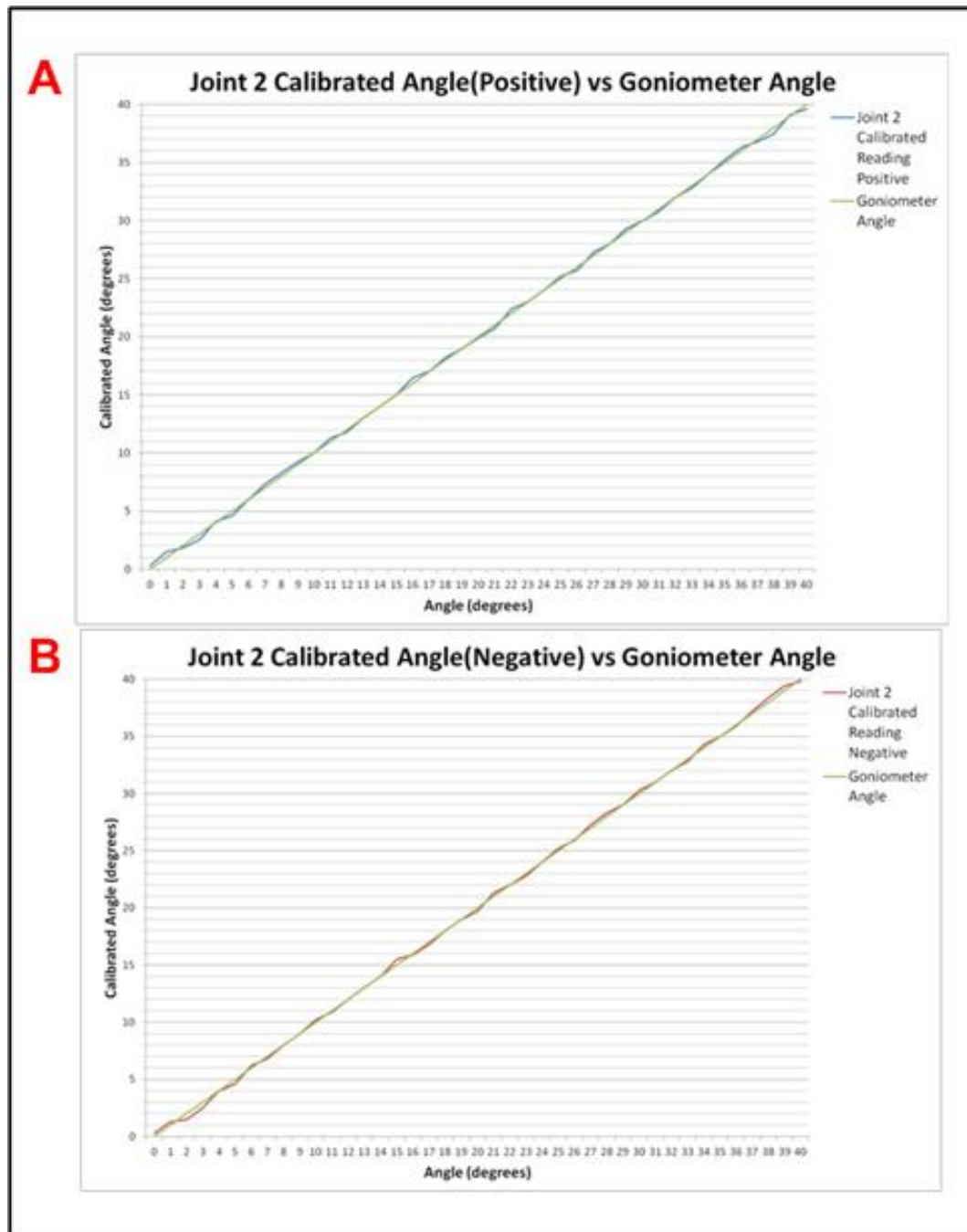


Figure 5.3: Joint 2 Calibrated Angle vs Goniometer (A) Positive (B) Negative

---

Comparison between the calibrated angle values of joint 2 (Figure 5.3) and the digital goniometer shows that the calibrated values have little deviation comparing to joint 1. However, in joint 2, deviation occurs in the first 10 degree of measurement. This represent the fact that joint 2 is not sensitive enough in measuring the angle from the starting zero-degree position. This is due to the sensitivity of the analogue potentiometer in producing change in voltage output for rotation angles of a few degrees from the stationary position.

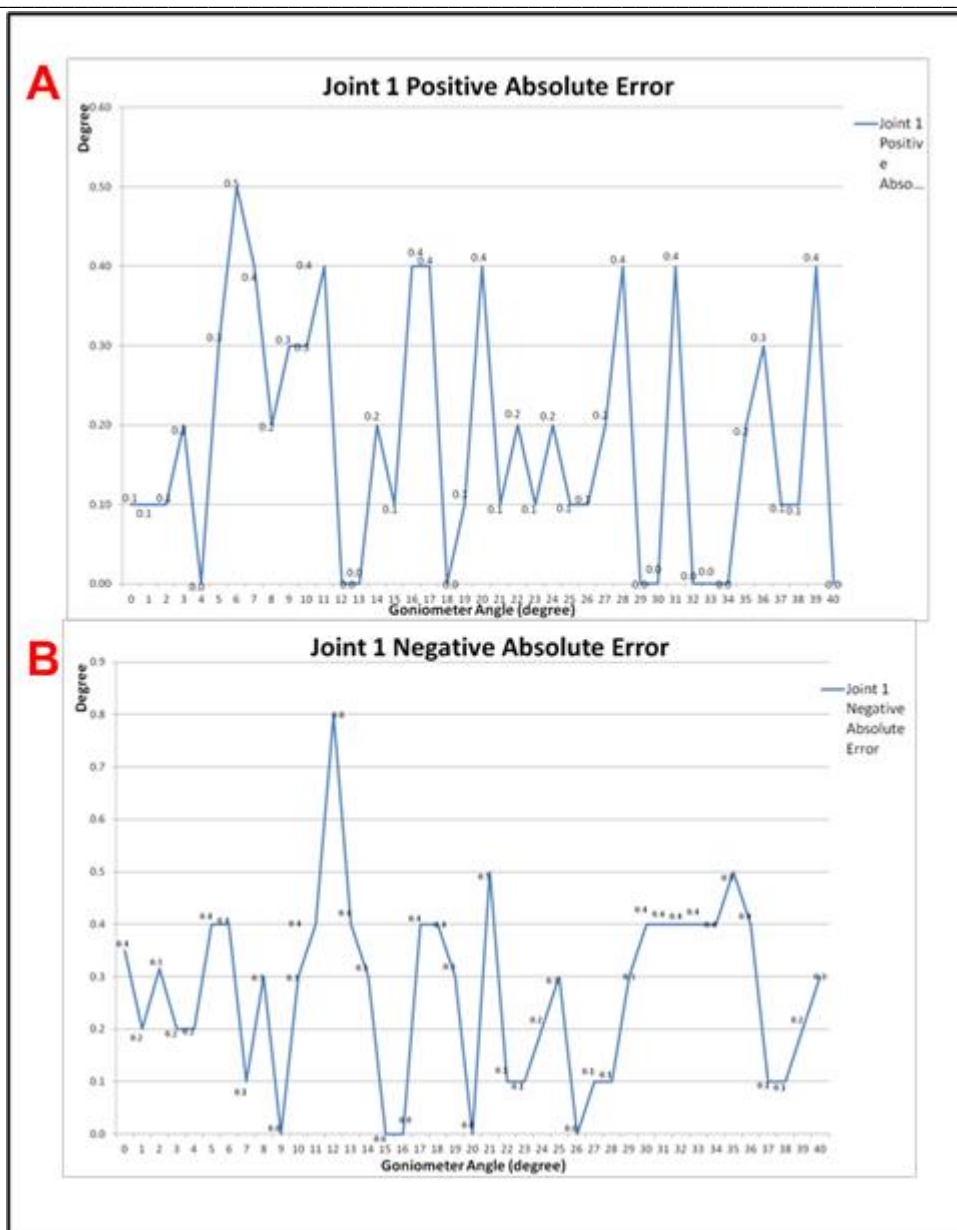


Figure 5.4: Joint 1 Absolute Error (A) Positive (B) Negative

Figure 5.4 shows the absolute error calculated for Joint 1 at positive and negative angle values relative to the digital goniometer angle value. Figure 5.4A shows that the absolute error value is less than 0.5°. In Figure 5.4B, there is one peak where the error value is greater than 0.5°. This

---

occurs at the calibrated value at  $12^\circ$  of measurement. This value is considered outlier since it is outside the cluster of values and there is no repeated value that is similar to it when comparing other measurement. The mean absolute error for joint 1 positive is  $0.2^\circ$  and joint 1 negative is  $0.3^\circ$ . Joint 1 negative has higher mean error than joint 1 positive is due to the outlier with value of  $0.8^\circ$ . Despite that, the error in joint 1 measurement is less than  $0.5^\circ$ , thus it has sub-degree precision in measuring the angle.



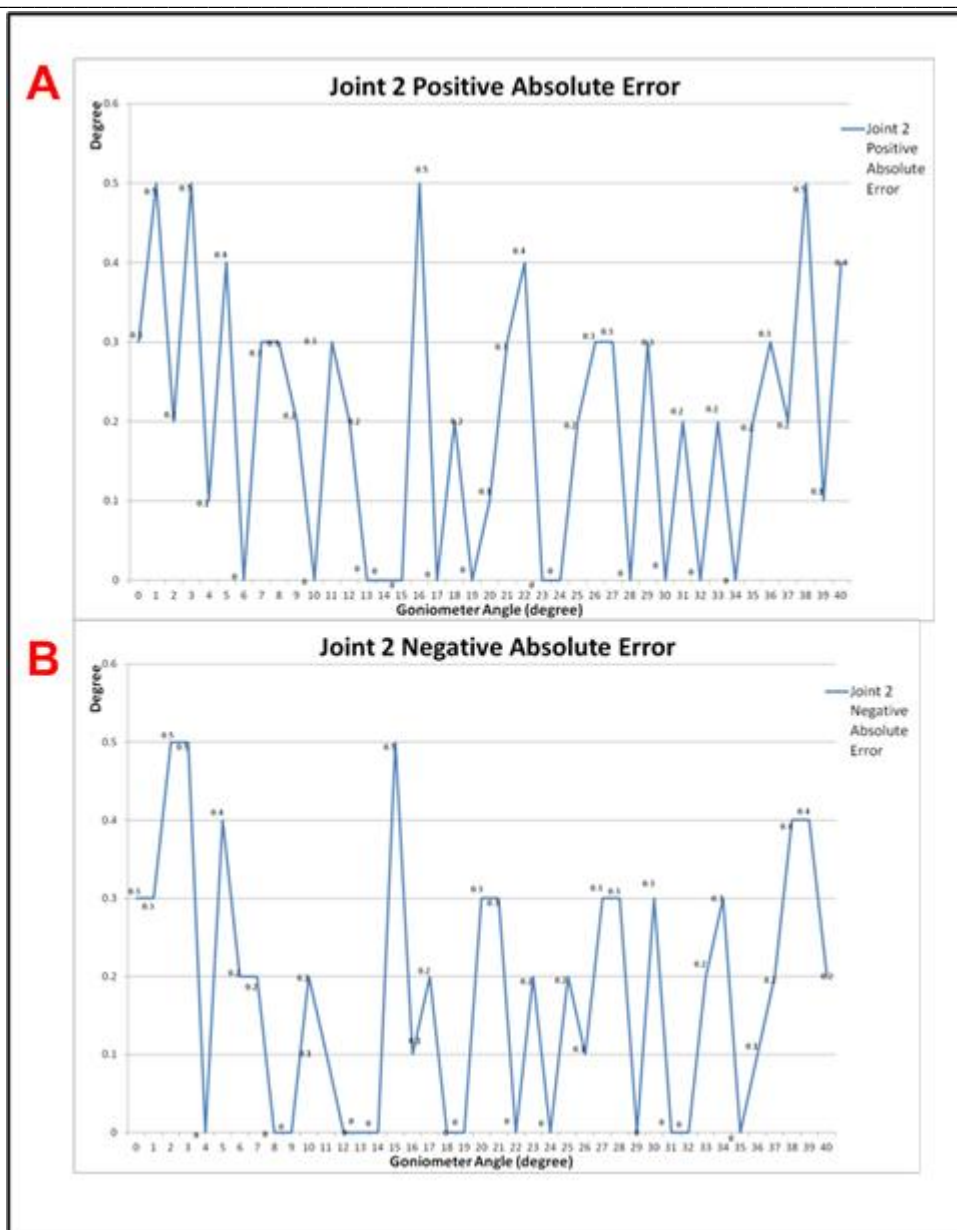


Figure 5.5: Joint 2 Absolute Error (A) Positive (B) Negative

Figure 5.5 shows the absolute error calculated for Joint 2 in positive and negative angle value relative to the digital goniometer angle value. Both figures show that Joint 2 has error of 0.5 degree or less. In Figure 5.5A, error value is higher in the first 5 degree and the last degree of measurement.

Similar to absolute error of Joint 1 negative value, there is spike of error value when measuring the 15th degree but the value does not exceed 0.5 degree of error. The mean absolute error for both positive and negative value for Joint 2 is 0.2 degree of error. This shows that joint 2 has sub degree precision of less than 0.5 degree in measuring the angle.

#### **5.4. Experiment in sawbones - (A) 3D geometric analysis of the shape of the cut area (B) Accuracy Analysis/Symmetry Analysis**

The tracking and navigation system of the articulated drill system has been tested in Sawbones. The first experiment was 3D geometric analysis of the shape of the cut area in comparison to femoral stem outline in pre-plan of navigation software is prepared to determine accuracy and repeatability of articulated drill system. This experiment was done to investigate the deviation of the cut area from the femoral stem outline in the pre-plan. This experiment is limited to cutting the curved shape of femoral stem inside femur only. The result of this experiment will be used for future research of articulated drill system.

The second experiment done was accuracy analysis/ symmetry analysis. This experiment was done to test the accuracy of articulated drill system in cutting the shape of femoral stem inside the femur sawbone.

#### 5.4.1 Materials and Methods

Sawbones were used to investigate the ability of the tracking and navigation of the robotic drill system to navigate and drill inside the femoral canal to produce a curved tunnel within the outline of the femoral stem. The sawbone was fixed at bone fixture rig by screws. Base optical tracking camera is fixed at the midpoint of the full length of sawbone and the mobile optical tracking camera is fixed at the motor box of articulated drill. Connection was made from the cameras and motor box to microcontroller box to stream tracking data to navigation software. A 6mm burr tip was attached to the chuck tip of articulated drill and a drill motor is connected to the flexible shaft of articulated drill.

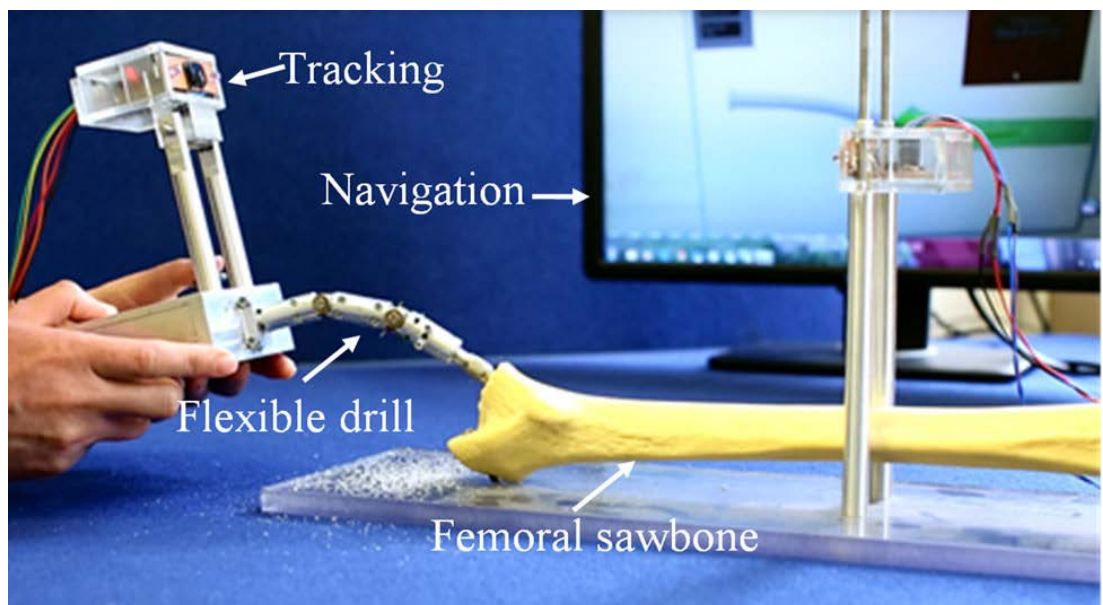


Figure 5.6: System setting for the articulated drill and its navigation system in a sawbone test rig.

In this test rig (Figure 5.6), the hip sawbone is fixed on a platform at which a tracking unit is placed at its geometric centre, providing the global coordinate information. The motor box of the articulated drill acts as a handle for the surgeon. As the first step of the test in the figure 5.7, the femur head is cut off. Then, the drill/bur tip is pushed forwards to mill the shape designed, while, the orientation and position is adjusted. During the procedure, the thumb stick is used to bend the articulated tip to the proper angle to fit in the curvature tunnelling. An optical tracking unit is mounted on the handle to provide 6 DOFs tracking information which refers to the location of the handle. During the cutting process, the movement of the drill tip comes from both hand movement at handle and the thumb stick, one at a time. After bending the drill tip at desired angle, the handle is moved to cut the bone until next angle adjustment of the drill tip via thumb stick. Both movements can also be done simultaneously because the handle is track via optical tracking system while the angle bending is track via potentiometer tracking system. However, due to delay of 20ms between hardware and software, and asynchronization at hardware level, only one movement can be done at a time to reduce error during movement.

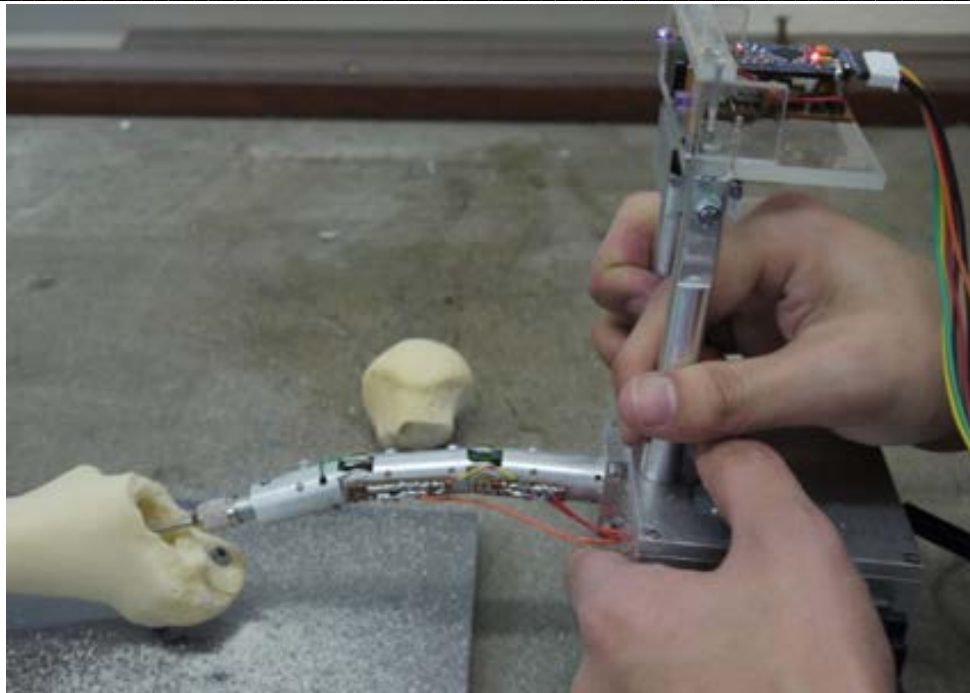


Figure 5.7: Manipulation using the articulated and steerable drill

Registration is done by aiming the burr tip to at least 3 points near greater trochanter to check and confirm that the articulated drill is registered and tracked as shown in Figure 5.8. The points aimed were peak of greater trochanter, the superior surface at base of greater trochanter, and lateral surface at base of greater trochanter. The coordinates of the registration points were then registered to properly locate and orient the surgical tool in relation to femur inside the navigation system. More registration points can be added by repeating the points location again and adding registration points at inferior surface and medial surface of base of greater trochanter. This method is possible due to the optical tracking system are able to measure depth between the LED cameras located at both the bone pin and at the motor box of

articulated drill. Motor drill was turned on and the femoral neck was milled to remove the femoral head. The femoral canal was milled by following visual feedback and pre-planned cut area from navigation software. Should the optical line of sight be blocked, the cutting will be interrupted and the registration process need to be repeated to reorient the drill tip.

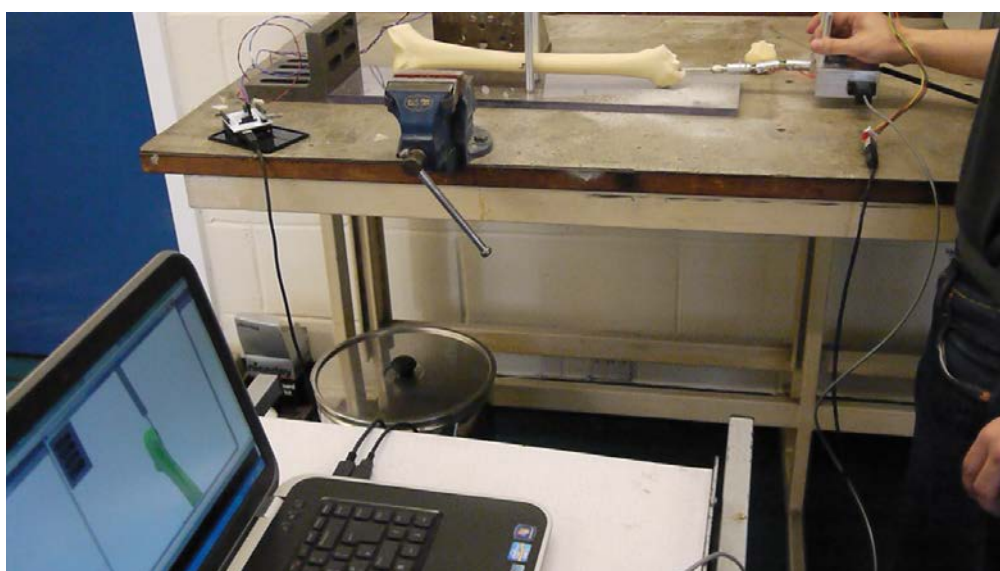


Figure 5.8: Registration of articulated drill to the optical tracking system.

The procedure is guided by the navigation system shown in the computer screen in Figure 5.9. Mapping enables surgeons to view virtually both the 3D model of femur and the 3D model of a femoral stem, thus enabling the surgeon to position the femoral stem inside the 3D bone model precisely. Also, both the femur model and the femoral stem's coordinates are linked together, providing a virtual interaction between

the models. Besides that, both the 3D model of femur and femoral stem's coordinate can be linked together enabling virtual interaction between the models.

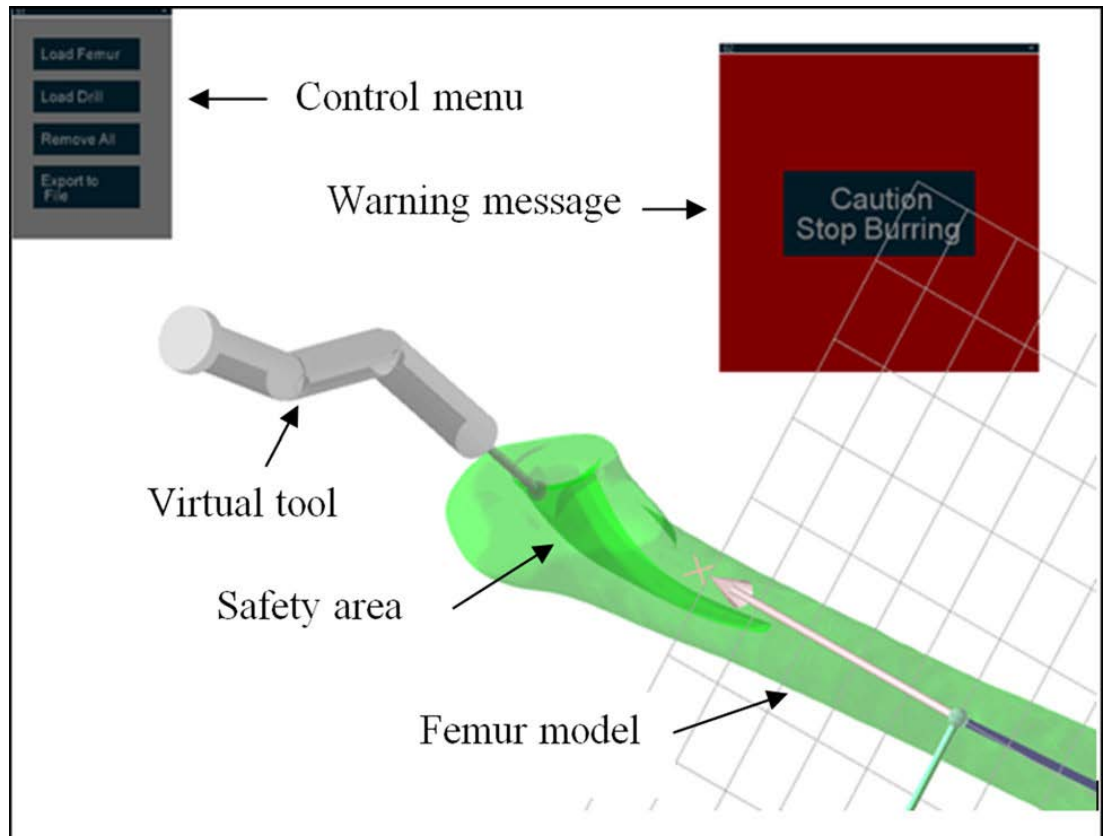


Figure 5.9:A graphical user interface (GUI) of a navigation system

A warning message will appear to note the surgeon when the drill/burr tip approach to the designed boundary. Through this open loop visual control system, a surgeon can switch the drill motor or link the system to an automatic switch to stop the bur/drill tip.

The milling was stopped whenever the 'Stop Milling Warning' was triggered and resumed after taking out the articulated drill from the femoral canal. Upon completion of milling (Figure 5.10 and 5.11), the sawbones were sent for CT scan imaging. DICOM CT images of the sawbone were then reconstructed into 3D digitized geometry by MIMICS (Materialize NV, Belgium) and saved as STL file format. The 3D digitized geometry of CT image of the sawbones was then imported into Geomagic Qualify 12 (Geomagic®) for analysis, and the boundary of the milled area was isolated from the whole geometry. The pre-planned cut area in STL file format was also imported into Geomagic Qualify 12 (Geomagic®). The pre-planned cut area was set as a reference template, while the boundary of the milled area was set as the test object. Alignment between the reference template and test object was made using two built-in alignment methods (best fit and manual) of Geomagic Qualify 12. The best fit alignment method uses an iterative closest point algorithm to best fit the objects. Next, 3D deviation analysis was performed to compare the milled area boundary and pre-planned cut area under a common coordinate and the chromatogram was generated automatically. The chromatogram represented the deviation of test object from reference template and deeper colour meant larger deviation. The range was set as  $\pm 5.0$  mm. Deep red represented +5.0 mm and dark blue represented -5.0 mm. The analysis provided maximum positive and



negative deviation, average positive and negative deviation, root mean square of deviation, and deviation distribution of points.

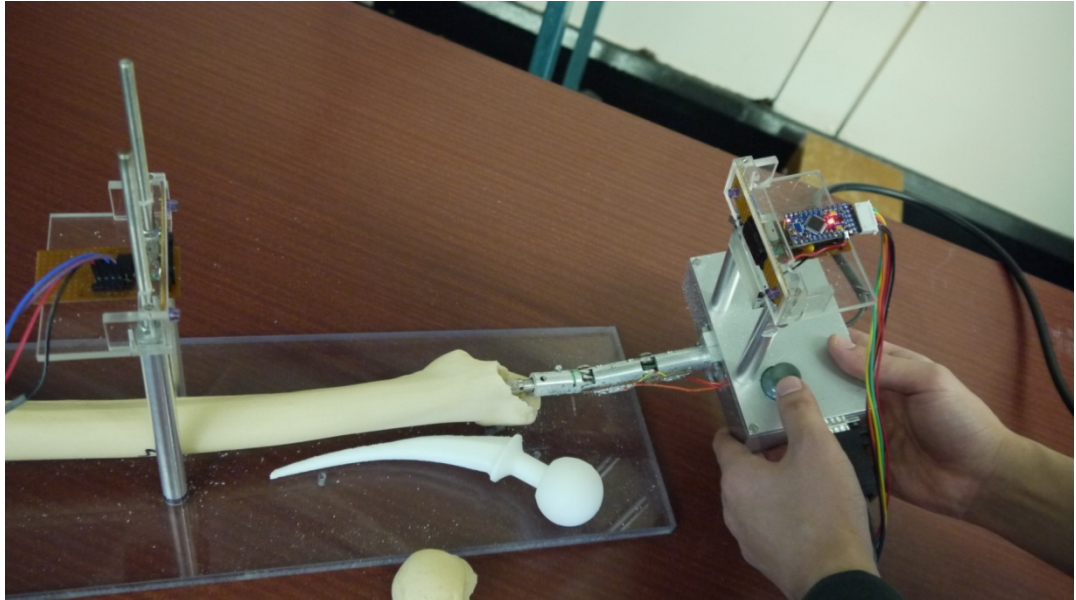


Figure 5.10: Completion of milling and fitting of implant.



Figure 5.11: Bone milling completed and ready to be sent for CT imaging.

#### 5.4.2 Results - (A) 3D geometric analysis of the shape of the cut area

An experiment was done on analysing the 3D geometric shape the actual cut area in relative to the 3D geometric shape of pre-planned cut area. The result data consists of deviation analysis and geometric chromatogram analysis.

The maximum positive and negative deviations; mean positive and negative deviations; and RMSD (root mean square of deviation) are shown in Table 5.1. The deviation distribution between cut area and outline of femoral stem from pre-plan of navigation software is shown in

Table 5.2. The percentages are categorized in steps of 1 mm. Figure 5.3, 5.4, 5.5 and 5.6 show the deviation colour map (DCM) generated from Geomagic Qualify after deviation analysis ranging from less than 1mm (green colour) deviation until 5 mm deviation (dark red and ark blue colour). The DCM is a visual representation of the distance in mm between cut area and outline of femoral stem from pre-plan of navigation software, where yellow colour, and light blue colour indicates positive, and negative deviation between 1 mm and 2 mm. Positive deviation value indicates outward deviation of cut area from outline of femoral stem and negative deviation value indicates inward deviation.

Cut Area	dmax(+) (mm)	dmax(-) (mm)	davg(+) (mm)	davg(-) (mm)	RMSD (mm)
Femur 1	3.653	-2.950	1.151	-0.762	1.065
Femur 2	4.393	-4.387	0.888	-0.925	1.085
Femur 3	4.848	-3.565	1.127	-0.759	0.864

Table 5.1: Summary of deviation analysis; dmax(+), maximum positive deviation; dmax(-), maximum negative deviation; davg(+), mean positive deviation; davg(-), mean negative deviation; RMSD, root mean square of deviation.

The data from Table 5.1 shows maximum positive (dmax(+)) and negative deviation (dmax(-)), mean positive (davg(+)) and negative deviation (davg(-)), and root mean square of deviation (RMSD).

Maximum positive deviation indicates overcut beyond the shape of the pre-planned 3D model. Maximum negative deviation indicates undercut beyond the shape of the pre-planned 3D model. Average positive deviation indicates the average deviation of overcutting beyond the shape of the pre-planned 3D model.

Average negative deviation indicates the average deviation of undercutting beyond the shape the pre-planned 3D model. Root mean square of deviation indicates error between actual cut 3D model and pre-planned cut 3D model. The highest value of  $d_{max}(+)$  is 4.848mm obtained from Femur 3 cut area while the lowest value of  $d_{max}(+)$  is 3.653mm obtained from Femur 1 cut area. This indicates that Femur 3 cut area has a point of overcut by 4.848mm, and Femur 1 has a point of overcut by 3.653mm, relative to the pre-planned 3D model. Besides that, throughout Femur 1 until Femur 3, the difference of 1.195 mm is calculated between highest and lowest value. This indicates that the maximum overcut obtained has a margin within 1.195 mm from either the highest or lowest value maximum positive deviation value when the experiment is repeated with a different sample. The highest value of  $d_{max}(-)$  is -4.387 mm obtained from Femur 2 cut area while the lowest value of  $d_{max}(-)$  is -2.950mm obtained from Femur 1 cut area. This indicates that Femur 2 cut area has a point of undercut by -4.387 mm, and Femur 1 has a point of undercut by -2.950 mm, relative to the pre-planned 3D model. Besides that, throughout Femur 1 until Femur 3, the

difference of 1.437 mm is calculated between highest and lowest value. This indicates that the maximum undercut obtained has a margin within 1.437 mm from either the highest or lowest maximum negative deviation value when the experiment is repeated with a different sample. The highest value of  $d_{avg}(+)$  is 1.151 mm obtained from Femur 1 cut area while the lowest  $d_{avg}(+)$  is 0.888 mm obtained from Femur 2 cut area. This indicates that, by average, Femur 1 cut area has overcut by 1.151 mm relative to the pre-planned 3D model, 0.263 mm more than Femur 2 cut area that has the lowest value. Besides that, this indicates that the average overcut obtained is within margin of 0.263 mm from either the highest or lowest average positive deviation value when the experiment is repeated again with another sample. The highest value of  $d_{avg}(-)$  is -0.952 mm obtained from Femur 2 cut area while the lowest value of  $d_{avg}(-)$  is -0.759 mm obtained from Femur 3 cut area. This indicates that, by average, Femur 2 has undercut by -0.952 mm relative to the pre-planned 3D model, 0.193 mm more than Femur 3 cut area that has the lowest value. Besides that, this indicates that the average undercut obtained is within margin of 0.193 mm from either the highest or lowest average positive deviation when the experiment is repeated again with another sample. Femur 2 has the highest value of RMSD, 1.085 mm while Femur 3 has the lowest value of RMSD, 0.864 mm. This indicates that Femur 2 cut area has higher error value in relative to the pre-planned 3D model, 0.221 mm more than Femur 3 cut area. Besides that,

this indicates that the error obtained is within margin of 0.221 mm from either the highest or lowest error value when the experiment is repeated again with another sample. Table 5.1 also show that overall, the error is close to 1 mm with average deviation of overcut and undercut, also close to 1mm.

Cut Area	% less than 1 mm	% between 1 mm and 2 mm	% between 2 mm and 3 mm	% between 3 mm and 4 mm	% more than 4 mm
Femur 1	54.636	33.489	10.473	1.401	0.00
Femur 2	64.097	29.907	4.782	0.785	0.429
Femur 3	48.462	43.36	7.177	0.963	0.038
Mean	55.732	35.585	7.477	1.050	0.156
SD	7.875	6.967	2.857	0.317	0.237

Table 5.2: Deviation distribution between femoral stem implant and cut area of femur sawbones.

Table 5.2 shows the deviation distribution between femoral stem implant and cut area of femur sawbones. The deviation distribution value is in percentage of points that deviates by distance of less than 1 mm, between 1 mm to 2 mm, between 2 mm to 3 mm, between 3 mm to 4 mm, and more than 4 mm. In comparing the geometry, 55.7% of the surface of cut area of femur sawbones was found to be within a deviation

of less than 1 mm, and 35.6% of the surface of cut area of femur sawbones was found to be within deviation of between 1 mm to 2 mm. This shows that 91.3% of the surface of cut area of femur sawbones was found to be within 2 mm and less. Only 8.7% of the surface of cut area of femur sawbones was found to be within more than 2 mm. This indicates that the majority of the surface of cut area of femur sawbones was deviated by up 2 mm from the femoral stem implant surface.

Figure 5.12 shows the isometric view of chromatogram of all three-cut area of femur sawbones. The colour ranges from green, which indicates less than 1 mm of deviation, to dark red or dark blue in colour, which indicates more than 5 mm of deviation, overcut or undercut respectively. This figure showed that there are similarities in area of overcut and undercut. Represented by blue a colour gradient, the undercut areas are clearly seen on the superior surface at the entrance of the cut area and the tip. These undercut areas contribute to the negative deviation value and distribution of negative deviation stated in table 5.1, and table 5.2. Represented by red colour gradient, the overcut areas are clearly seen on the inferior surface at the entrance of cut area and the tip, and on the superior surface at the middle section of the cut area. These overcut areas contribute to the positive deviation value and distribution of positive deviation stated in table 5.1, and table 5.2. However, there is widespread of green colour throughout the cut area surface, which indicates an overcut, or undercut of less than 1 mm from the pre-planned

3D model. In Figure 5.16 most deviations of between 2 mm and 3 mm and above appear in yellow colour in the lesser trochanter area.

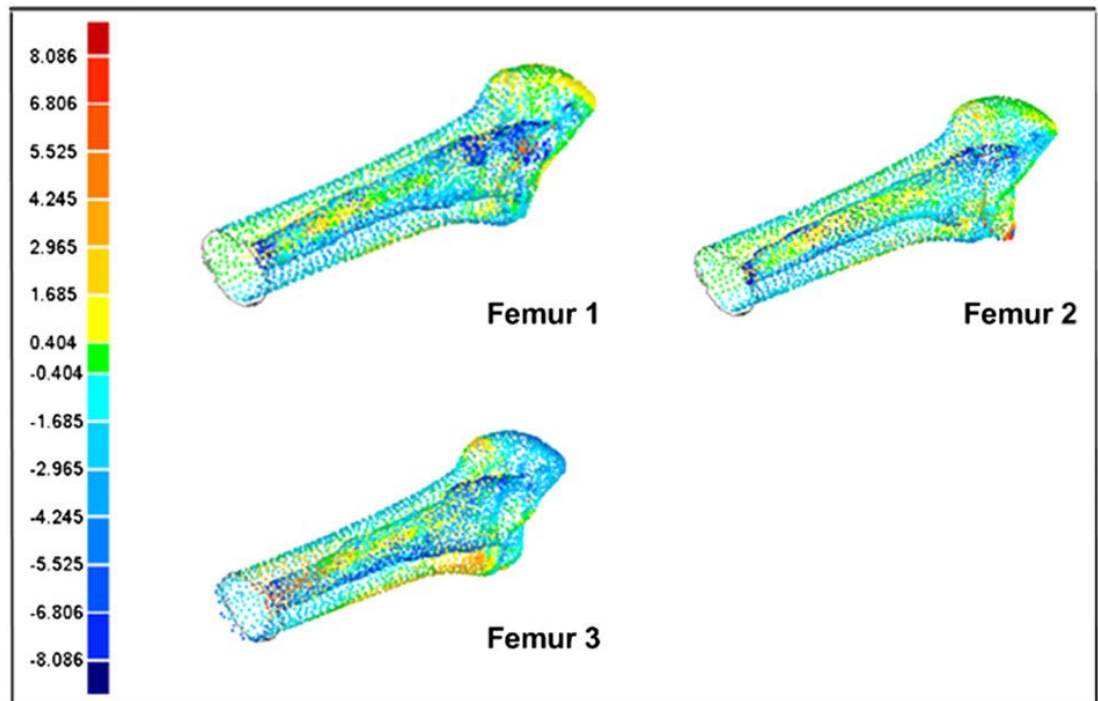


Figure 5.12: Isometric view of all three-cut area of femur sawbones and deviation colour map (DCM) (mm)

Figure 5.13, 5.14, and 5.15 shows the chromatogram of Femur 1, Femur 2, and Femur 3 cut area respectively in four views which is front, top, left, and isometric. The colour ranges from green that indicates less than 1 mm of deviation to dark red or dark blue in colour, which indicates more than 5 mm of deviation overcut, or undercut respectively. The front view in Figure 5.11 shows that Femur 1 has overcut at the middle section of superior surface, overcut at the tip section of inferior surface, overcut at the entry section of inferior surface, undercut at the entry section of superior surface, and undercut at the tip section of



superior surface. The front surface showed mixture of cut of less than 1 mm (green colour) and overcut of between 1 mm to 1.5 mm (yellow colour). The left view in Figure 5.13 shows that Femur 1 has two protrusions at the front surface of the cut area due to presence of overcut. It can be clearly seen that the peak of each protrusion was red in colour. Besides that, the middle section of superior surface overcut tapered and extended towards the tip of the cut area. The overcut at the entry section of inferior surface extended from midpoint of front surface until midpoint of back surface. The undercut at the entry section and tip section of superior surface was localized and did not extend. The top view in Figure 5.13 shows that Femur 1 has overcut at the middle section of superior surface that extended to the front surfaces. Besides that, there was an overcut at the tip section of back surface that extended to inferior surface of the cut area. The overcut at the entry section of inferior surface was located towards the back surface of the cut area. The front view in Figure 5.14 shows that Femur 2 has overcut at the tip section of inferior surface, overcut at the entry section of inferior surface, undercut at the entry section of superior surface, and undercut at the tip section of superior surface. The front surface showed small patches of overcut of between 1 mm to 1.5 mm (yellow colour). The left view in Figure 5.14 shows that Femur 2 has a protrusion at the back surface of the cut area due to presence of overcut. It can be clearly seen that the peak of the protrusion that was located middle and entry section is red in colour. Besides that,

the overcut at middle section was actually of inferior section and not superior section. The undercut at the entry section and tip section of superior surface was localized and did not extend. The top view in Figure 5.14 shows that Femur 2 has undercut at the tip section of superior surface that was focused at the front. The undercut at the entry section of superior surface was between 1 mm to 2 mm (light blue colour). The front view in Figure 5.15 shows that Femur 3 has overcut at the middle section of superior surface, overcut at the tip section of inferior surface, overcut at the entry section of inferior surface, and undercut at the entry section of superior surface. The front surface showed mixture of cut of less than 1 mm (green colour) and overcut of between 1 mm to 1.5 mm (yellow colour). The yellow colour extended from the entry section until middle section of the front surface. The left view in Figure 5.15 shows that Femur 3 has two protrusions at the front surface of the cut area due to presence of overcut. It can be clearly seen that one of the protrusion peaks is orange in colour and the other one is red in colour. Besides that, the middle section of superior surface shows an overcut protrusion with yellow colour overcut extended to the tip section. The overcut at the entry section of inferior surface localized at two points with one towards the front surface and the other one towards the back surface. The undercut at the entry section and tip section of superior surface is localized and did not extend, and the undercut is less than 2 mm (light blue colour). The top view in Figure 5.15 shows that Femur 3 has overcut

at the middle section of superior surface that extended to the one of the protrusions of the front surface. Besides that, there was an overcut that is localized at the tip section of inferior surface of the cut area.

Based on Figure 5.13, 5.14, and Figure 5.15, we can see that there are similarities in areas of overcut and undercut. The front view of all three figures showed that there was overcut at the tip section of inferior surface, overcut at the entry section of inferior surface, and undercut at the entry section of inferior surface. The front surface showed mixture of cut of less than 1 mm (green colour) and overcut of between 1 mm to 1.5 mm (yellow colour) but the size of yellow overcut area varies from small patches to extension of the yellow overcut over the middle section. The left view of all three figures showed that there were protrusions either at the front surface or the back surface. It also showed that the undercut at the entry section and tip section of superior surface are localized. These similarities signify the repetition of overcut and/or undercut at certain area in relative to the pre-planned 3D model.

The presence of overcut and undercut indicates inaccuracies in milling the shape of femoral stem. The cause would be the effect of backlash during milling that is not detected immediately due to delay of 20ms in tracking input and asynchronous of input data at hardware level between optical and potentiometer tracking system. This effect can be clearly seen on the protrusion peaks from the chromatogram. This effect

needs to be quantified and studied on further research and improvement are to be made at the structure of drill sheath, and the hybrid tracking system hardware.

The experiment was done by a single user with experience in orthopaedic procedures, thus was able to reduce the error due to user skills. However, further research can be done on repeating the experiment with several users. This could potentially highlight the weakness of this system and made improvements to the system.

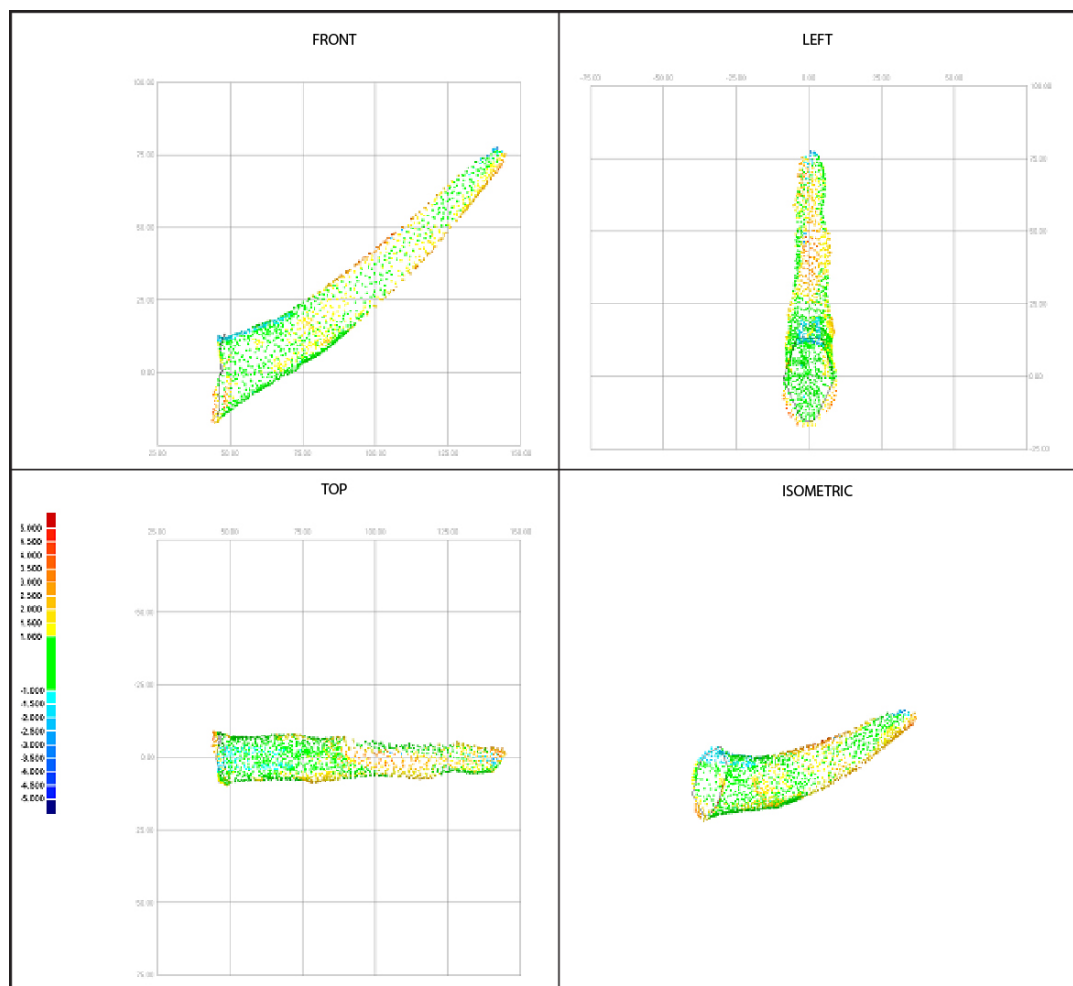


Figure 5.13: Deviation colour map (DCM) of cut area 1 of femur sawbones in four views.

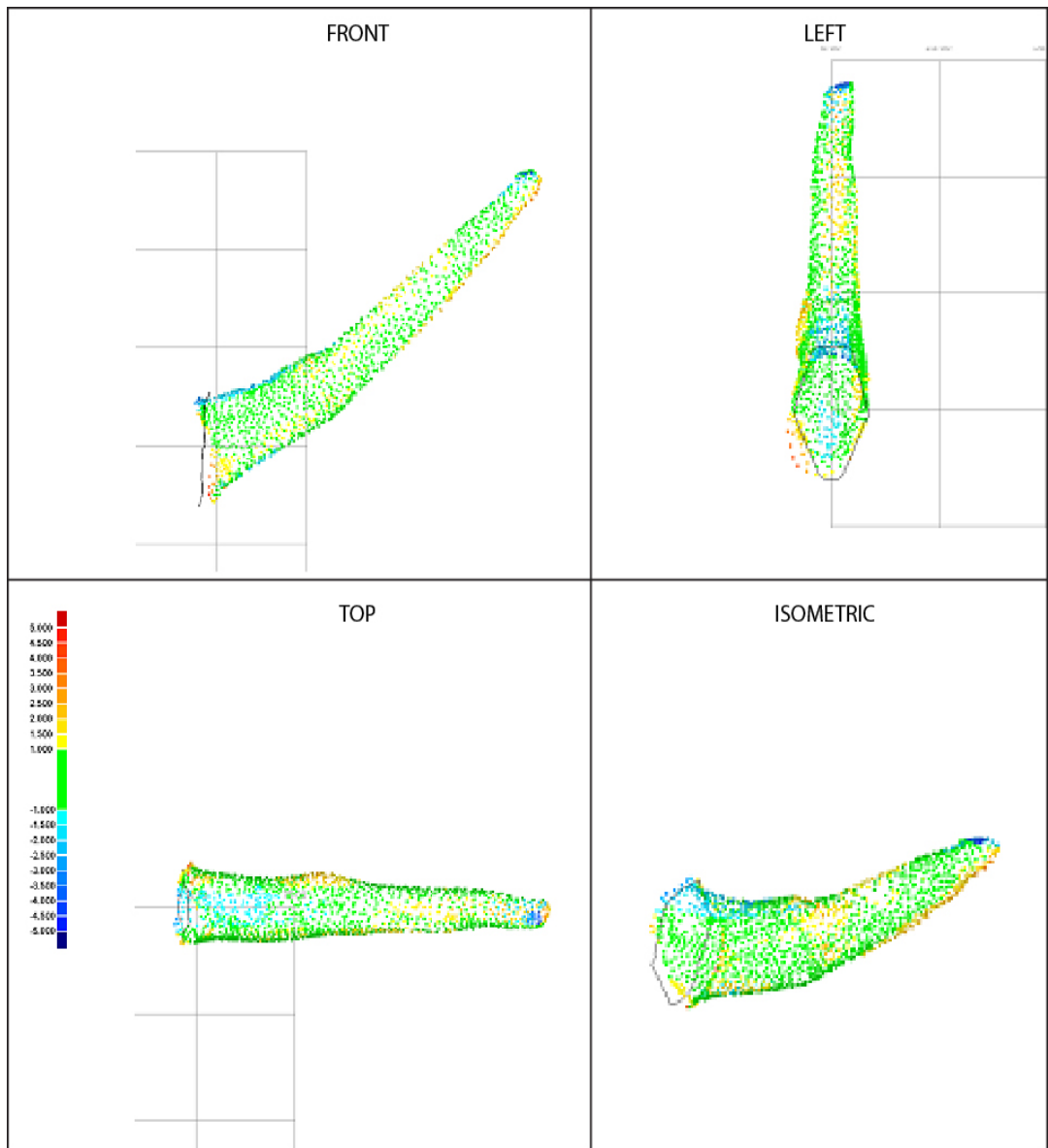


Figure 5.14: Deviation colour map (DCM) of cut area 2 of femur sawbones in four views.

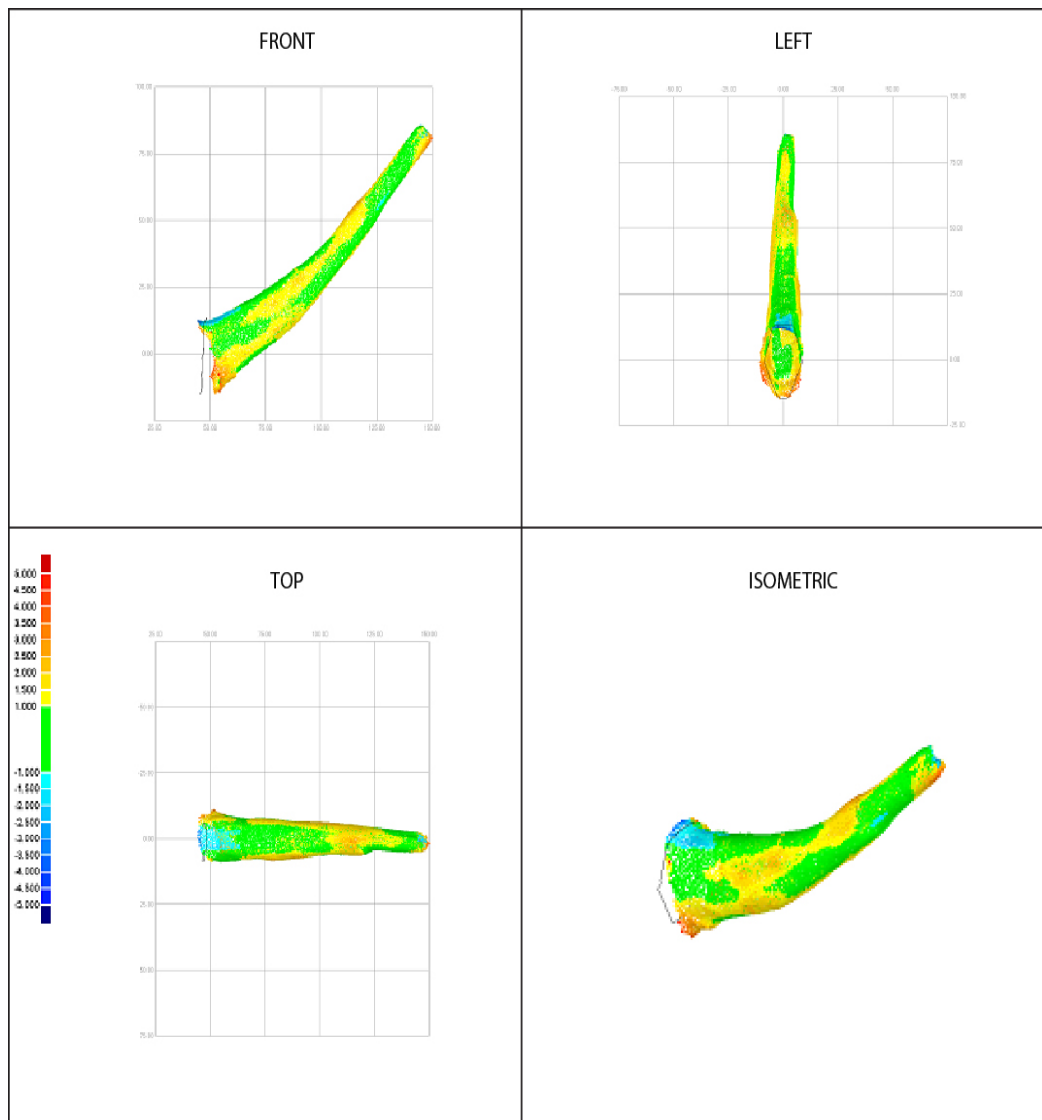


Figure 5.15: Deviation colour map (DCM) of cut area 3 of femur sawbones in four views.

### 5.4.3 Results - (B) Accuracy Analysis/Symmetry Analysis

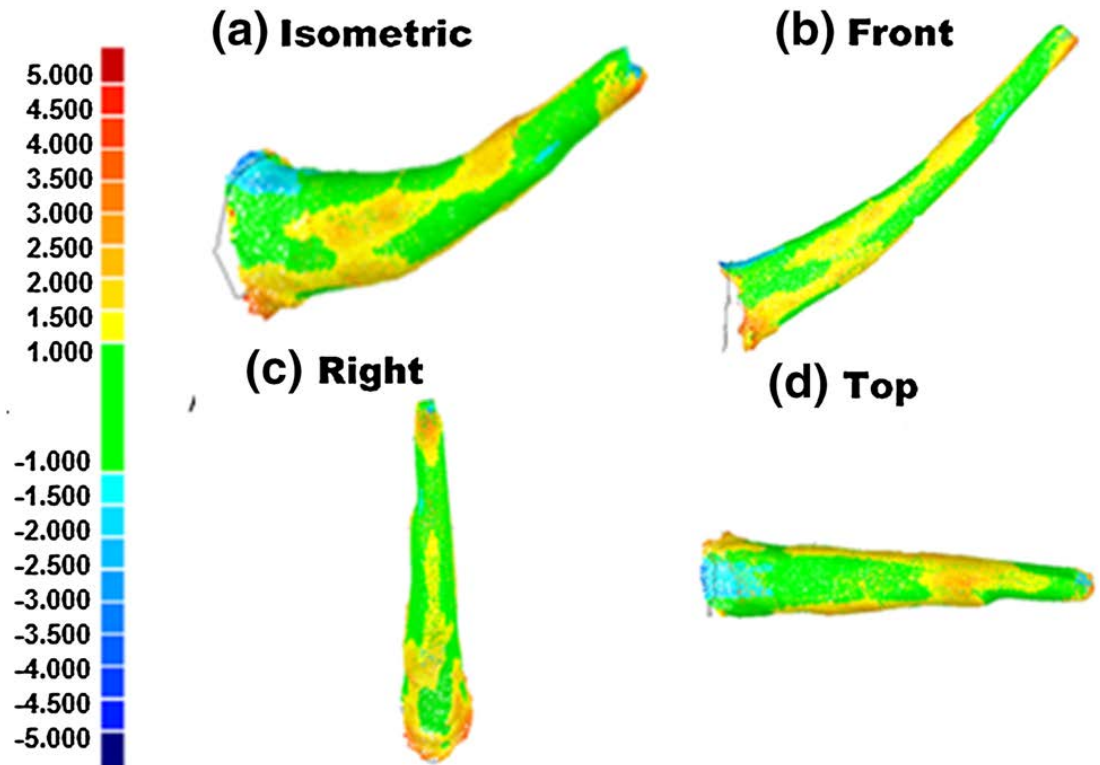


Figure 5.16: The chromatogram used for an analysis of the milling procedure.

Figure 5.16 show the chromatogram of Femur sawbone cut area respectively in four views which is front, top, left, and isometric. The colour ranges from green that indicates less than 1 mm of deviation to dark red or dark blue in colour, which indicates more than 5 mm of deviation overcut, or undercut respectively. The red sphere represents the point with highest value of overcut while the blue sphere represents the point with highest value of undercut. The front view in Figure 5.16 shows that Femur sawbone has overcut at the tip section of inferior

surface, overcut at the entry section of inferior surface, and undercut at the entry section of superior surface. The front surface showed mixture of cut of less than 1 mm (green colour) and overcut of between 1 mm to 1.5 mm (yellow colour). The yellow overcut is spread out at middle and entry section of the front surface. The right view in Figure 5.16 shows that it has two protrusions at the front surface of the cut area due to presence of overcut. It can be clearly seen that the peak of each protrusion was red in colour. Apart from that, it has overcut at the entry section of front and back surface, and it also has overcut at the tip section of the back surface. Besides that, the middle section of inferior surface overcut tapered and extended towards the entry section of the cut area. Besides that, the yellow overcut from the front surface extended to the middle section of superior surface. The top view in Figure 5.26 shows that Femur sawbone has overcut at the middle section of back surface, overcut at the entry section of the back surface and overcut at the tip section. Besides that, there was an undercut at the entry section of superior surface that is localized. There was a protrusion at the middle section of the front surface indicated by the red overcut area. The isometric view in Figure 5.16 showed the overcut at entry section of inferior surface is extended to the middle section of inferior surface and to the middle section of front surface. These similarities signify the repetition of overcut and/or undercut at certain area in relative to the pre-planned 3D model.



Result of 3D deviation analysis showed that the maximum positive deviation, maximum negative deviation, average deviation and standard deviation was 4.848 mm, -3.565 mm, 1.127/-0.759 mm, and 0.864 mm, respectively. Based on Figure 5.17, the percentage of point cloud data was 0.013%, 0.075%, 0.088 %, 0.313%, 0.925%, 1.988%, 48.462%, 23.818%, 16.629%, 5.151%, 1.625%, 0.625%, 0.250%, 0.013%, and 0.025% at percentage deviation of -4.000 ~ -3.501, -3.500 ~ -3.001, -3.000 ~ -2.501, -2.500 ~ -2.001, -2.000 ~ -1.501, -1.500 ~ -1.001, -1.000 - 1.000, 1.001 - 1.500, 1.501 - 2.000, 2.001 - 2.500, 2.501 - 3.000, 3.001 - 3.500, 3.501 - 4.000, 4.001 - 4.500, and 4.501 - 5.000, respectively. According to Figure 5.18, the percentage of point cloud data was 7.464%, 36.797%, 38.435%, and 11.228% at the standard deviation of -2.0 ~ -1.1, -1 ~0, 0.1 - 1.0 and 1.1 - 2.0 respectively.

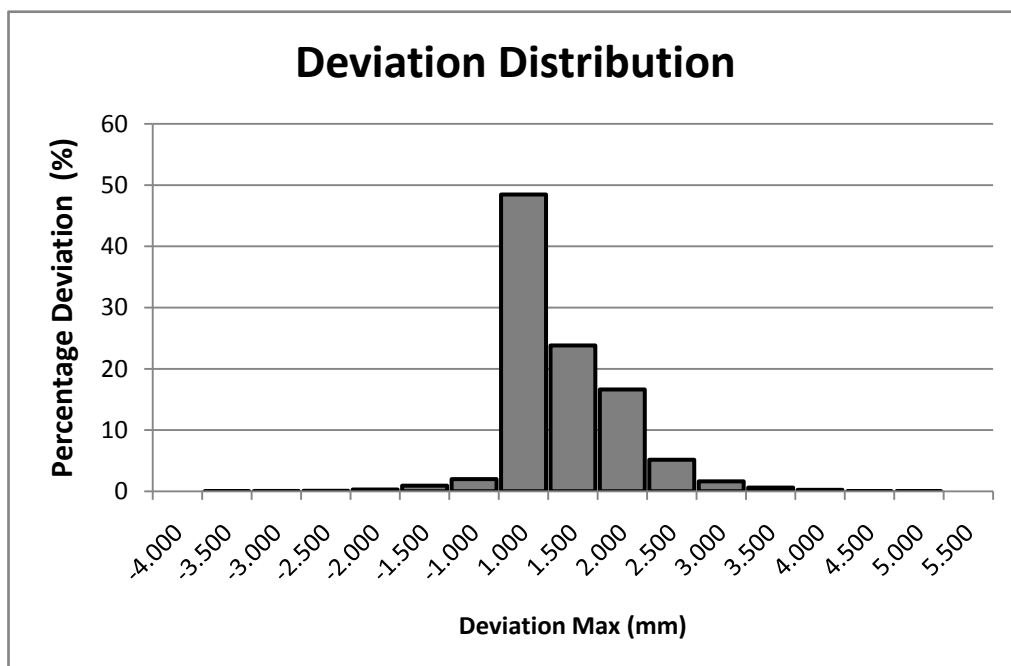


Figure 5.17: Percentage deviation distribution of point cloud data of cut area of femur sawbone.

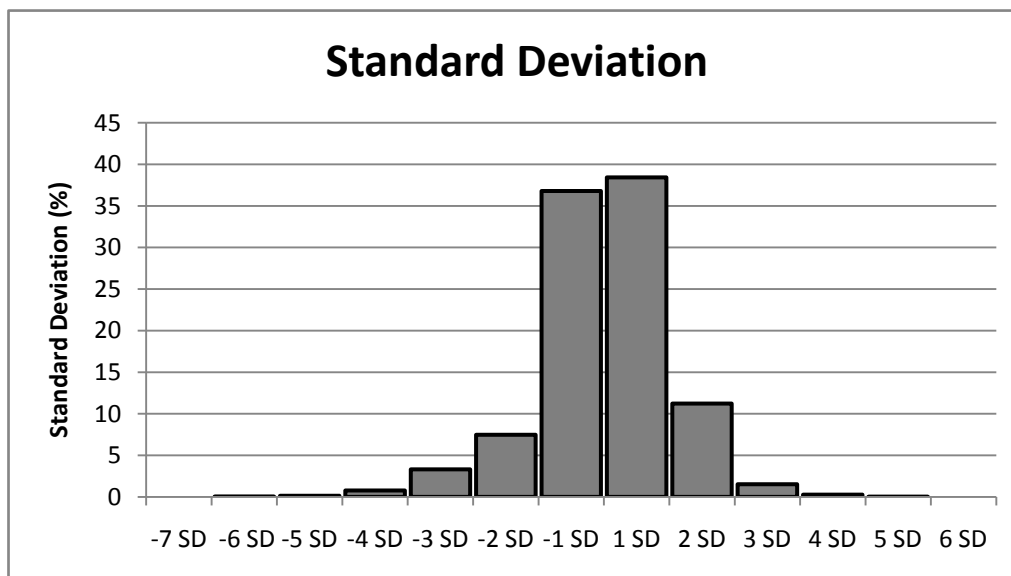


Figure 5.18: Standard deviation of point cloud data of cut area of femur sawbone.

## **5.5. Conclusion**

The articulated and steerable drill system was integrated and was used for evaluation experiments in sawbones. There are different levels of integration including mechanical assembly; embedded position sensing and optical tracking; mapping and navigation. The mechanical integration was to ensure a reliable mechanical structure of the articulated drill manipulator and robust motor control. The software integration, all imaging, tracking and virtual model software was integrated into a unit framework of an easy to use and modular user-computer system. The navigation software showed a friendly graphics user interface. The encoder was calibrated by using a digital goniometer as a reference. The calibration is done by mapping the output voltage of the potentiometer for each degree of rotation. Calibration is done for both joints separately. Before and after calibration, the angle measurements of the encoder are collected and plotted into a graph. The absolute percentage error of the calibrated potentiometer was calculated and was then plotted to a graph. The mean absolute error for joint 1 positive is  $0.2^\circ$  and that for joint 1 negative is  $0.3^\circ$ . The mean absolute error for both positive and negative value for Joint 2 is 0.2 degree of error. The error in joint 1 and joint 2 measurements were less than  $0.5^\circ$ , meaning that it has sub-degree precision in measuring the angle. 3D geometric analysis of the shape of the cut area experiment was done. The analysis of results confirmed that the tracking system is able to guide the articulated drill inside femoral, in which a deviation between cut area and outline of femoral stem

---

from navigation software was in range from  $-0.759$  mm to  $1.151$  mm. It was found that a small portion of the deviation is more than 2 mm ( $7.477 \pm 2.857\%$  deviation between 2 mm and 3 mm,  $1.050 \pm 0.317\%$  deviation between 3 mm and 4 mm, and  $0.156 \pm 0.237\%$  deviation above 4 mm). This means that the cut area was slightly deviated by up to 2 mm from the outline of femoral stem from navigation software. Accuracy Analysis/Symmetry Analysis experiment was done. The results showed that 75.232% of the point cloud data of the milled area boundary is within  $\pm 1$  SD (0.864 mm) of the pre-planned cut area; 93.924% of the point cloud data is within  $\pm 2$  SD (1.728 mm). This indicates that the majority of the cloud data from the geometric shape of the milling boundary is within 1.728 mm ( $\pm 2$  SD) in relation to the pre-planned cut area. Hence, the accuracy of the navigation system is within 1.728 mm.

## **CHAPTER 6 - DISCUSSION**

### **6.1. Static Performance of Articulated Drill System Under Different Configurations**

The main purpose of the experiment is to evaluate a new designed articulated drill for arthroplasty. The articulated drill manipulator combines a three-segments planar linkage as a sheath and a motor drive mechanism to allow an accurate control of bending angles for a flexible shaft mill bit. The articulated drill is able to tunnel a curved channel for accurate implant positioning for THA. It is essential that the drill produce sufficient force to cut bone materials at different configuration and bending angles. To prove the efficiency and implementation of the articulated drill, a test rig is designed to simulate major operation activity and measure the forces it generates for the required tasks.

Although there are lots of studies on milling force evaluation and related modelling studies for traditional rigid drilling for arthroplasty (Dillon et al., 2013, Alam et al., 2011, Lee et al., 2012, Al-Abdullah et al., 2018, Liao et al., 2019), there is no such research for a new articulated drill. In the study, we simulated two configurations by moving the mill tip in a forward direction and a lateral direction. In the test rig, the step motor was controlled by a slow and a constant speed and this pushed the articulated drill device, thus, the system was in equilibrium. From the basic static law, we suppose forward configuration generate larger force than lateral configuration, as a larger torque is required for lateral pushing control, and the presence of cutting

---

blade at lateral side of the tip. The results of this experiment support the hypothesis that the drill is sufficient to cut bone in orthopaedic surgery. From the Force-time curve at vertical configuration test in and lateral configuration test, the vertical configuration shows approximately 6 times larger forces than the lateral configuration at the different bending angles. However even in the harder lateral condition we found that the articulated drill have sufficient stiffness to cut a bone sample by a depth of 1mm. and hence meets the key requirement for the surgical task.

The articulated drill system cutting force and its static performance experiment produced force versus time data with varying peak force value that was dependent on the configuration of the drill and the degree of bending in each configuration. Looking at the data from forward configuration, the peak force value decreases as the degree of bending increases. This is because as the degree of bending increases, more of the burr tip cutting blade surface were in contact with the bone. This result in less reaction force produced in cutting the bone as the burr tip were able to remove bigger bone chip. Combined with high spindle speed, the bone was cut at a much faster rate, therefore less push force was needed to cut the bone. This was reflected by the decrease in reaction force measured as the bending angle increases. Looking at the zero-degree bending angle in forward configuration data, the force value was in negative is because the sensor is measuring compression force towards the load cell as the drill is push into the bone. The peak force value is measured at 7.65 N. It has high force value because at

---

zero-degree bending angle, only small portion of the burr tip cutting blade was in contact with the bone. Thus, forming smaller chip and the cutting rate is low resulting in the drill required to exert higher push force in order to cut the bone. The graph from Figure 4.10 showed that the force measured increased steadily until it reached the peak force value of 7.65 N. The graph showed jagged steps as the force is increasing to reach the peak force value. This is because despite lack of contact between burr tip cutting blade surface and the bone, increase in the push force enables better cut similar to drilling action. A small plateau formed as the force is reduced following peak force value was due to outliers and noise in raw data affecting the curve after filter is applied. Looking at the ten-degree bending angle in forward configuration data, the peak force value was measured at 6.82 N. The peak force value was lower than zero-degree bending angle peak force value. This is because more cutting blade surface was in contact with the bone hence increase in the cutting rate and reduce the push force needed as the burr tip increases its depth of cut. The graph in Figure 4.11 showed that the curve is better defined than zero-degree bending angle with minimal jagged steps as the force exerted increases. It reached a plateau stage near its peak force value. After reaching the peak force value, the curve reduced its amplitude gradually until it reached zero force value (articulated drill withdrawn away from the bone sample). Nearing the zero-force value, the curve became less steep. This occurred at about the same point as the less steep curve at the start of measurement as the force exerted increases. Looking at the twenty-

---

degree bending angle in forward configuration data, the peak force value was 5.95N. The curve in Figure 4.12 followed the same curve profile as previous bending angle data. It started with a steep inclining curve, followed by a plateau phase, and a steep declining curve. At the very early and very late period in the curve showed less steep curve that indicates beginning, and end of contact between the burr tip and the bone. The peak force value is lower than ten-degree bending angle because more cutting blade surface were in contact with the bone surface enabling more and bigger bone chip formation due to cut. Looking at the thirty-degree bending angle in forward configuration data, the peak force value was 3.36N. The curve in Figure 4.13 also followed the same curve profile as previous bending angle data. In this bending angle, it was much clear the reason for less steep curve at the beginning and the end of the curve, which was due to effect of stall torque of the servo motor and the compensation of servo motor to maintain the bending angle. In the beginning of the curve, as contact is made, the burr tip was pushed backward but the motor and stall torque of the motor corrected the angle back leading to steep curve. At the end of the curve, as the drill withdrawn from the bone, the compensation of the servo motor result in the burr tip was pushed forward followed by correction by the motor to return it back to the defined angle. Figure 4.14 showed the Force-Time curve of comparison of bending degree in forward configuration. It showed the pattern and profile of articulated drill bone cutting as the burr tip angle is varied. As stated before, all the curves have initiating phase (less steep), increasing



---

depth phase (more steep), plateau phase, withdrawing phase (more steep), and disengage phase (less steep). The peak force value was decreased as bending angle increase. This showed that the articulated drill was able to cut the bone easier in higher bending angle of forward configuration. This was expected since the higher bending angle resulted in more burr tip cutting blade at the side of burr tip to be in contact with the bone surface. The cutting blades at the side of burr tip also have higher depth compared to at the very tip of the burr. Therefore, the better cutting power at the sides of burr tip cause the reduced reaction force measured as more bone is cut at much faster rate. However, the peak force value was still higher than 1 N because this configuration followed the partial orthogonal cutting using burr tip. Theoretically, we can achieve the exact orthogonal cutting in this configuration by setting the bending angle to 90 degrees, but the articulated drill sheath has limit of thirty- degree bending angle as the maximum bending angle.

Looking at data from lateral configuration, the pattern and the profile of the force-time curve is the opposite of forward configuration. The peak force value increases as the degree of bending increases. This is because as the degree of bending increases, less of the burr tip cutting blade surfaces were in contact with the bone. This results in more reaction force produced in cutting the bone as the burr tip were not able to remove bigger bone chip. Besides that, the bone was cut at a much slower rate, therefore more push force was needed to cut the bone. This was reflected by the increase in

reaction force measured as the bending angle increases. Looking at the zero-degree bending angle in lateral configuration data, the peak force value was 0.56 N. The curve in lateral configuration have different profile compared to forward configuration as it lacks the initiating phase and disengage phase that is signified from section of less steep curve as shown in Figure 4.15. The curve is divided into three phase which was increasing depth phase, plateau phase, and withdrawing phase. In the withdrawal phase, there was slight increase in force measured as the curve went down. This is due to outliers in the noise before the filter is applied. Looking at ten-degree bending angle in lateral configuration data, the peak force value was 0.71N. The curve in Figure 4.16 followed the same curve profile as previous bending angle data. The peak force value was higher compared to zero-degree bending angle data. This is because in lateral configuration, zero-degree bending angle means that the bone surface will come in contact with the side of the burr tip and result in orthogonal cutting of the bone. As the bending angle increases, less cutting blade surface came into contact with the bone surface, thus resulting in partial orthogonal cutting that requires higher push force for cutting. Looking at twenty-degree bending angle in lateral configuration data, the peak force value was 1.20 N. The curve in Figure 4.17 followed the same curve profile as previous bending angle data. We can see that the peak force value was higher compared to previous bending angle data. It is much clearer from this bending angle curve that the lateral configuration curves have longer plateau phase compared to forward configuration data. Looking

---

at thirty-degree bending angle in lateral configuration data, the peak force value was 1.65 N. The curve in Figure 4.18 followed the same curve profile as previous bending angle data. Throughout the lateral configuration curve, there was no presence of less steep curve due to compensation of servo motor to maintain bending angle and servo motor stall torque. This is because the push force is not high enough to deflect the burr tip for any compensation to be made by the servo motor. Figure 4.19 showed the Force-Time curve of comparison of bending degree in lateral configuration. It showed the pattern and profile of articulated drill bone cutting as the burr tip angle is varied. As stated before, all the curves have increasing depth phase, longer plateau phase, and withdrawing phase. The peak force value was increased as bending angle increase. This showed that in higher bending angle of lateral configuration, it has become harder for the articulated drill to cut the bone. This was expected since the higher bending angle resulted in less burr tip cutting blade at the side of burr tip to be in contact with the bone surface. The cutting blades at the side of burr tip were also to have higher depth compared to at the very tip of the burr. Therefore, lesser cutting power was observed as the bending angle increases. The peak force value was lower than 1 N in zero and ten-degree bending angle, but the peak force value was above 1 N as the bending angle increases to 20 degrees and 30 degrees. Zero-degree bending angle in lateral configuration was the orthogonal cutting of the bone because the full sides of the burr tip were in contact with the bone surface. As the bending angle increases, it gradually

changes from orthogonal cutting at zero degree bending angle to drill cutting at ninety-degree bending angle on lateral configuration.

We suppose, at vertical configuration, more bending angles would generate less force as in equilibrium, large bending angles mean more lateral component force to generate torque. The opposite outcome would be obtained at lateral configuration. The measurement proved that at vertical configuration, the maximum force varied from 7.65N at 0 degrees to 3.363N at 30 degrees. At lateral configuration, the maximum force decreases from 1.464N at 30 degrees to 0.564N at 0 degrees. These results imply that at vertical configuration the capability of the articulated drill to cut the bone is the weakest. It also implies, more than thirty-degree bending at both configurations is not properly allowed by the design.

If the articulated drill was able to bend up to 90 degrees, beyond the design limit in vertical configuration, the force to be measured at bending angle 60, 70, 80, and 90 degrees would be similar to the force measured in 30, 20, 10, and 10 degrees bending angle in lateral configuration respectively. The same can be said for bending angle of 60, 70, 80, and 90 degrees in lateral configuration. We showed that the capability of the articulated drill to cut the bone is dependent on the bending angle and configuration. High bending angle in the vertical configuration and low bending angle in the lateral configuration have the best ability to cut the bone. The vertical configuration signifies the bone cutting ability of a push down the shaft action

when tunnelling, while the lateral configuration signifies the cutting ability of a pull or scraping action when tunnelling. This effect would be the opposite if we change the mill bit to standard drill bit.

The significance of our findings is that the milling behaviour of articulated drill in static condition is the same as milling with rigid mill tools. The cutting force and the ability of articulated drill to cut bone followed the orthogonal bone cutting modelling done by Moghaddam et al (2008).

Moghaddam et al (2008) did a study on voxel-based force modelling of orthogonal bone cutting by using spherical rotating tool such as burr which cuts the bone by orthogonal cutting when each cutting element comes in contact with the bone piece. Their results showed that the force along the X axis ( $F_x$ ) is around 1 N. They concluded that the cutting force decreases as the number of teeth or spindle speed increases. Our findings mentioned above have similar result to their force modelling result. At zero-degree bending of the lateral configuration, we found that the articulated burr cuts as an orthogonal cutting device with the highest number of teeth, and highest area of teeth that come in contact with the bone. Hence, our findings at zero-degree bending angle of lateral configuration have similar force measured. However, this is limited to depth cut of 1 mm at a rate of 1 mm/second. Further research on the variation of cut depth and cut rate is recommended

Another significance of our finding is the force measured in all configurations is less than the servo motor's stall torque in the articulated drill.

Therefore, the articulated drill is proved to have the ability to sustain its bending configuration when milling a bone. Should the servo motor's stall torque at less than the force measured, the articulated drill would not be able to maintain the bending angle and buckling would be more likely to happen. The buckling effect was minimized in the articulated drill via placement of bearings inside the sheath, limitation of the bending angle, and the high torque of the servo motor.

The principle weaknesses of our study are the less of dynamic measurement and biomechanical modelling in a complex surgical environment. Besides that, the study only measured force in single axis,  $F_x$  (direction of the articulated drill towards the bone). The remaining two force component axis,  $F_y$  and  $F_z$  were not measured because if the force data to be extrapolated until ninety-degree bending angle, we assumed that  $F_x$  in vertical configuration would have the same profile as  $F_z$  in lateral configuration; and  $F_x$  in lateral configuration would have the same profile as  $F_y$  and  $F_z$  in vertical configuration. This is because  $F_x$  in lateral configuration is milling in the direction perpendicular to the mill bit shaft axis, hence orthogonal cutting. The  $F_x$  in vertical configuration is milling in the direction parallel to the mill bit shaft axis, hence drill cutting. Besides that, the test rig is only set up at an ideal static model to avoid some more complex parameters such as vibration and impaction. Future studies should include more complex laboratory-based measurement and biomechanical modelling in a complex

surgical environment but if these proves satisfactory then the articulated drill should be tried in cadaveric specimens.

## **6.2. 3D Geometric Analysis of The Shape of The Cut Area**

The variations in geometric shape of the cut area in comparison with the outline of the femoral stem from the pre-plan of the navigation software were measured and presented using a deviation analysis (Table 5.1 and 5.2), and DCMs (Figure 5.16, 5.17, 5.18 and 5.19). The analysis of deviation confirmed that the tracking system is able to guide the articulated drill inside femoral, in which a deviation between cut area and outline of femoral stem from navigation software was in range of -0.759 mm to 1.151 mm in Table 5.1, and is slightly off from the acceptable clinical range of 1mm. Detailed deviation analysis quantified the deviation of cut area to outline of femoral stem from navigation software, and it was found that a small portion of deviation to be more than 2 mm ( $7.477 \pm 2.857\%$  deviation between 2 mm and 3 mm,  $1.050 \pm 0.317\%$  deviation between 3 mm and 4 mm, and  $0.156 \pm 0.237\%$  deviation above 4 mm). This means that the cut area was slightly deviated by up to 2 mm from the outline of femoral stem from navigation software. As seen in Figure 5.16, 5.17, 5.18 and 5.19, the significant proportion of these larger discrepancies came from the distal end of cut area and proximal brim of cut area. This is because the femoral stem outline had a tapered end and the mill bit used in this experiment was 6 mm mill bit, which unable to follow the tapered curvature less than 6 mm. The large discrepancies at the proximal brim of cut area was caused by chipping of the

sawbones due to difference in hardness between the sawbones' outer layer's resin and inner resin compound and structure. The outer layer's resin is harder and had a minimal hollowed structure, while the inner resin is softer with more hollowed structure. The RMS obtained showed indirect correlation with the magnitude of deviations and it signifies the accuracy of the system in milling the cut area. However, since it has indirect correlation with magnitude of deviations, high deviation regions (dark red and dark blue colour) at the distal end of cut area contributed to the larger value of RMS, hence reducing the accuracy of the system. Moreover, any noise or artefacts in the CT images, or manual segmentation of bones in MIMICS can also contribute to the higher deviation values. We also take note that even though CT slice thickness is 1.25 mm, the resolution within each slice was 0.918mm. Using the standard algorithm to reconstruct 3D CT model, by which it assumed the cross section to be in the middle of the slices and create stereo lithography (STL) 3D model by connecting geometry between cross sections. Thus, the precision was somewhere between 0.918mm and 1.25mm. Despite these factors contributed to the errors, the results indicate that the articulated drill system was able to mill a cut area inside femoral canal guided by navigation software of the system with accuracy less than 2.0mm. DCMs gave us visualisation of 3D deviation and highlighted regions of higher deviation. All three cut area had a higher deviation region towards the distal end and at proximal brim of the cut area (indicated by orange to dark red colour).



---

### **6.3. Accuracy Analysis/Symmetry Analysis**

The experiment result would be the first report about the application of digital scanning technology in comparing the milled area in the femoral canal to the outline of the femoral stem intended to be fit. There were variations of milled area due to sample used were sawbones which are more brittle than actual bone when milling. Sawbones tend to have bigger chip and break in bigger chunk resulting in some milled area to have bigger deviation than the outline of the femoral stem. Application of digital scanning technology particularly Computed Tomography Scan (CT Scan) has been used extensively in medical surgery in comparing pre and post-surgery and measuring the positioning and fitting of prosthesis (insert citation). However, there has yet any report of using such application in milling the femoral canal for femoral stem insertion. CT scanning is chosen apart from Magnetic Resonance Imaging (MRI) because CT scan images visualize the bone better than MRI. Although sawbone does not have the same physical properties of actual bone, some studies have reported usage of CT scan on sawbone and the acquired images are acceptable (insert citation). CT images obtained can be quickly rendered into 3D virtual model and converted to STL file format so that it can be stored and later, imported to Geomagic Qualify for comparing the deviation of milled area to the outline of femoral stem intended to be implanted. In this study, the femoral stem is created via rapid prototyping method from the femoral stem CAD model. Despite not

having the same surface smoothness as the metal implant, rapid prototype version of femoral stem is cheaper and faster to obtain for research purposes.

The accuracy of milled area relative to outline of femoral stem was evaluated using Geomagic Qualify software. This software has the ability to compare two 3D objects and establish a 3D deviation profile for the test object from reference template. In this study, we successfully cut an area inside the sawbone according to the shape of femoral stem outline used with good accuracy and shape. It has been found in Figure 5.28 that 75.232% of the point cloud data were within  $\pm 1$  SD and 93.924% of point cloud data were within  $\pm 2$  SD. This indicates that majority of cloud data from the geometric shape of milled area boundary is within 1.728mm (2 SD) to the pre-planned cut area. Hence, the accuracy of the navigation system is within 1.728mm.

However, there was still 1.813% of the point cloud data exceeding the positive deviation value, and 4.264% exceeding the negative deviation value. The analysis of the results by Geomagic Qualify software analysis showed that there was greater degree of error at the distal end of cut area and proximal part of cut area. The main reason is the femoral stem used is the tapered femoral stem that has diameter of less than 6mm towards the end of tapered tip. Nevertheless, the mill bit used has a diameter of 6mm hence the smallest cut in terms of diameter can only be 6mm. This resulted in the distal tip of cut area having greater error due to the mill bit cannot mill the bone smaller than 6mm diameter. The large discrepancies at the proximal part of

---

the cut area is caused by chipping of the sawbones due to the difference in hardness between the sawbones' outer layer's resin and the inner resin compound. The outer layer's resin is harder and had a minimal hollowed structure, while the inner resin is softer with more a hollowed structure. The error at distal end of cut area can be corrected by changing into smaller mill bit size. However, due to financial constraints, we only have the 6mm mill bit. This error is similar to 'imperfect drilling characteristics' noted in study done by Bumm et al.(2005) on robotic-assisted skull base surgery. Apart from that, a possible reason for reducing the accuracy of the system is its setting of their DRBs. In the sawbones experiment, one tracking unit is fixed in the femur as a DRB. As the SO in real clinical setting could be moving, such non-fixed SO would affect the positioning accuracy. Thus, an additional fixed tracking unit is introduced to be a globe reference for the system to track both DRBs attached in the patient's femur and the surgical drill. Besides that, robot kinematic error, and mill bit deflection due to surgeon's applied force as shown in study done by Li et.al.(2007) that involves flexible tool, could also be the factors contributing to the errors mentioned above. Besides that, study done by Khorasani et al. (2016) state that tool deflection during milling could leads to dimensional error, and reduction in the surface quality of milled area. These errors can be reduced by incorporating the haptic-feedback system that restricts motion of articulated drill sheath, stop the motor, or retracts the milling bit whenever the milling bit touch the safe surgical boundary. Incorporating haptic-feedback system may require additional hardware

---

and/or extension hardware in order to properly restrict the motion of articulated drill sheath and retracts the milling bit. The haptic-feedback system can improve the milling accuracy, hence femoral stem positioning to about 1mm as reported in study done on ROBODOC total hip arthroplasty (Kazanzides, 1999, Schulz et al., 2007, Netravali et al., 2016). Apart from that, these errors can be further reduced by using a potentiometer system that is better than potentiometer such as Fiber Bragg grating sensors (Mishra et al., 2011, Payo et al., 2009), or high definition optical potentiometer system (Mihelj et al., 2019). Dimensional error due to deflection can be reduced by improving the articulated drill sheath stiffness and utilizing an active compensation method such as estimation of mill bit deflection by measuring the applied force by surgeon.

The femoral stem implant is a solid body which will fit into a cavity. It will sit where the area of the cavity comes in contact first and that will be the majority of the contact area. Although the accuracy of the navigation system is 1.728 mm, the difference is small since the defect is on the inner side of the aim (-1 SD) as shown in Figure 5.28. This error results in a cavity which is 1 mm less than the implant dimensions, thus reducing the chance of burring the cortex too much, and the implant will have a nice press fit stability if the implant is an uncemented implant (Mazoochian et al., 2004, Berahmani et al., 2018). If the femoral stem implant is a cemented implant, the accuracy

of 1.728 mm is good since there is space of nearly 2 mm for filling the cement and press to fit the implant into the desired position.

#### **6.4. Limitation of the Research**

##### **a. Limitation of the Hardware**

The design of the articulated drill system has some limitations that is due to financial and size constraints. The limitations are:

- the articulated drill system bending is only limited to 1 degree of freedom from the motor base. This is because of limited amount of metal and materials that can be acquired from available funding.
- only single servo is controlling the bending, connected to two wires that produce opposing action when the motor turns. This is because the size of servo motor that has high stall torque is quite large for the scale of articulated drill system as a whole.
- potentiometers are used instead of potentiometers due to size and space constraint of the design. The rotary disc diameter is more than 15mm, which is the average diameter of femoral canal.
- only 6mm burr tip is used instead of variable size of burr tip. This is because of insufficient funds to purchase different size of burr tip used for surgery.

## **b. Limitation of the Software**

The software development has limitations in terms of functions, and data acquisition and processing. The limitations are:-

- Synchronization of both data from optical tracking and potentiometer tracking are not properly synchronize using synchronization board. The most recent data from both tracking system are paired at software level.
- The refresh rate and latency test to confirm the manufacturer specifications was not done and to be included in future research.

## **c. Limitation of the Experiments/Testing**

Experiments done has some limitations that opens up opportunity for future research. The limitations are:

- The 3D geometric analysis and accuracy analysis experiment is done using sawbones instead of cadaveric bone. This is because the price of cadaveric bone is beyond the budget available
- Positional accuracy of the end effector with respect to the base coordinate was not measured. This affects the accuracy of the system. This is because this research is proof of concept research and the positional accuracy of the end effector is to be included in future research on optimization of the system.

- The force measurement experiment is a static experiment. Dynamic response experiments can be further done in future research.
- The force measured is from single axis to simplify the test.
- Vibration and impaction test was not done that open up an area for future research.

### **6.5. Conclusion**

In total hip arthroplasty, CAOS is currently practiced only with acetabular cup positioning and orientation while femoral stem positioning still using hand-rasping method instead of femoral milling. The emergence of robotic micro-tools give opportunity for development of articulated drill tip integrated into robotic surgical system. The benefits include utilization of femoral milling in MIS total hip arthroplasty, tunnel drilling in ACL reconstruction, milling in revision of arthroplasty, and drilling in head and neck surgery. Due to the fact that articulated drill tip is not trackable via optical tracking system, this project focus on developing hybrid mapping and navigation system for tracking articulated drill tip by using both optical and potentiometer tracking system. The articulated drill sheath has been manufactured. It consists of multiple rigid bodies that act as sheath to a flexible shaft with micro chuck attach at the end. The outer diameter of the sheath is designed to be 14.42mm so that it can fit the medullary cavity of femur. The sheath has one degree of freedom (DOF) that is control via wire at the bottom of it. The mapping system for tracking has been developed in

---

JAVA processing language. It supports 3-axis navigation panning, rotating, zooming, area zooming, return to specific camera view, 2D grid, and 3-axis legend. This will then be integrated with the tracking system and be synchronized the virtual object motion with surgical object. Tracking and navigation system is still under development and final phase of the project will commenced after completing it. The results of Static Performance of Articulated Drill System under Different Configurations experiment support the hypothesis that the drill is sufficient to cut bone in orthopaedic surgery. The measurement at vertical configuration, larger bending angles generated less force as in equilibrium. The maximum force decreased from 7.65N at 0 degree to 3.363N at 30 degree. The opposite outcome was obtained in lateral configuration data. The maximum force increased from 0.564N at 0 degree to 1.464N at 30 degree. These results imply that at vertical configuration the capability of the articulated drill to cut the bone is the weakest. It also implies, more than thirty-degree bending at both configurations is not properly allowed by the design. High bending angle in the vertical configuration and low bending angle in the lateral configuration have the best ability to cut the bone. The significance of these findings is that the milling behaviour of the articulated drill in static conditions is the same as when milling with a rigid mill tool. The cutting force and the ability of the articulated drill to cut bone followed the orthogonal bone cutting modelling, which results showed that the force along the X axis is around 1 N. However, this is limited to depth cut of 1 mm at a rate of 1 mm/second. Further



research on the variation of cut depth and cut rate is recommended. Another significance of our finding is the buckling effect is minimized in the articulated drill via placement of bearings inside the sheath, limitation of the bending angle, and the high torque of the servo motor. The test rig is only a set up at an ideal static model to avoid some more complex parameters such as vibration and impaction. Future studies should include more complex laboratory-based measurement and biomechanical modelling in a complex surgical environment but if these proves satisfactory then the articulated burr should be tried in cadaveric specimens. On the basis of the 3D Geometric Analysis of The Shape of The Cut Area study, we conclude that articulated drill system was able to mill inside femoral guided by the tracking and navigation system. The accuracy of this concept is less than 2mm. The majority of the deviation is less than 2mm, with only small portion of deviation to be more than 2 mm ( $7.477 \pm 2.857\%$  deviation between 2 mm and 3 mm,  $1.050 \pm 0.317 \%$  deviation between 3 mm and 4 mm, and  $0.156 \pm 0.237\%$  deviation above 4 mm). The result obtained from this study may have significant value in research pertaining femoral canal milling in the application of computer-assisted orthopaedic surgery to total hip arthroplasty following the approach of minimally invasive surgery (MIS). The application of CAOS in MIS total hip arthroplasty is limited, at the moment, to acetabular cup placement and biomechanical alignment. The application of CAOS in femoral stem placement is not yet available due to lack of extensive research to track milling tools inside the femoral canal in CAOS total hip arthroplasty under

---

MIS approach. The Accuracy Analysis/Symmetry Analysis study reports the navigation system of articulated drill navigation system for femoral stem placement in total hip arthroplasty. The navigation system has the potential to help surgeon in tracking articulated drill or any flexible tools inside the bone by which are not trackable by the optical tracking system. The mill cut area of navigation system is evaluated using Geomagic Qualify software that can compare 3D deviation between two 3D models. This study uses the safe surgical boundary from the navigation system as one of 3D models with the other 3D model is reconstructed from CT scan images of sawbone post-milling using the articulated drill navigation system. This study indicates that the navigation system has the accuracy within 1.728mm in guiding the articulated drill sheath to mill inside the femoral canal following the pre-planned cut area with safe surgical boundary. There is 6.077% of point cloud data beyond the deviation value that indicates error of the navigation system in milling the cut area. This system can be further improved by incorporating haptic-feedback system, Fiber Bragg grading sensor, and active compensation system to reduce errors due to deflections of mill bit during milling inside femoral canal.

## **CHAPTER 7: FUTURE RESEARCH**

### **7.1. Hardware**

The future research of the articulated drill system's hardware that has been identified are:

- Research on increasing the degree of freedom of the bending of articulated drill sheath. This will have the potential to improve functionality and reduce accidental blockage of clear line of sight of the optical tracking system.
- Research on fitting and utilizing multiple high torque servo motor to individually control each wire.
- Potentiometer gives out analog signal and has some inaccuracies. Research on using digital component for joint angle tracking has potential to improve accuracy of the system.
- Research on effects of different burr tip or other cutting tip in milling inside the bone with articulated drill system.

### **7.2. Software**

The navigation software of this system can be further improved by:

- Integrating synchronization board and algorithm in the software to enable real-time synchronize tracking from hybrid tracking system
- Measurement and improvement on the refresh rate, and latency of the software.

### **7.3. Experimentation**

Further experimentation can be done on articulated drill system with hybrid navigation system such as:

- Experimentation using cadaveric femur on 3D geometric analysis and accuracy analysis
- Measuring the positional accuracy of end effector in respect to base coordinate and improvements to the accuracy.
- Dynamic response experimentation on cutting force of articulated drill system in various configuration
- Measurement of cutting force on all three axes in various configuration.
- Experimentation on effect of vibration and impaction to the articulated drill system.

---

## REFERENCES

- ABBOTT, J. J., MARAYONG, P. & OKAMURA, A. M. 2007. Haptic virtual fixtures for robot-assisted manipulation. *Robotics research*. Springer.
- ABITBOL, J., GENDRON, D., LAURIN, C. & BEAULIEU, M. 1990. Gluteal nerve damage following total hip arthroplasty: a prospective analysis. *The Journal of arthroplasty*, 5, 319-322.
- ADAMOVICH, S. V., MERIANS, A. S., BOIAN, R., LEWIS, J. A., TREMAINE, M., BURDEA, G. S., RECCE, M. & POIZNER, H. 2005. A virtual reality—based exercise system for hand rehabilitation post-stroke. *Presence: Teleoperators and Virtual Environments*, 14, 161-174.
- ADVINCULA, A. P. & SONG, A. 2007. The role of robotic surgery in gynecology. *Current Opinion in Obstetrics and Gynecology*, 19, 331-336.
- AL-ABDULLAH, K. I. A.-L., ABDI, H., LIM, C. P. & YASSIN, W. A. 2018. Force and temperature modelling of bone milling using artificial neural networks. *Measurement*, 116, 25-37.
- ALAM, K., MITROFANOV, A. & SILBERSCHMIDT, V. V. 2011. Experimental investigations of forces and torque in conventional and ultrasonically-assisted drilling of cortical bone. *Medical Engineering and Physics*, 33, 234-239.
- ALAMBEIGI, F., WANG, Y., SEFATI, S., GAO, C., MURPHY, R. J., IORDACHITA, I., TAYLOR, R. H., KHANUJA, H. & ARMAND, M. 2017. A curved-drilling approach in core decompression of the femoral head osteonecrosis using a continuum manipulator. *IEEE Robotics and Automation Letters*, 2, 1480-1487.
- ALEXANDER, J. H., MAYERSON, J. L. & SCHARSCHMIDT, T. J. 2018. Guided Pelvic Resections in Tumor Surgery. *Techniques in Orthopaedics*, 33, 158-165.
- ALLEN, M. W., MYERTHALL, S. L. & JACOFISKY, D. J. 2018. Robotics in Total Hip Arthroplasty—A Current Review. *The Journal of Hip Surgery*, 2, 076-080.
- AMIOT, L.-P., LABELLE, H., DEGUISE, J. A., SATI, M., BRODEUR, P. & RIVARD, C.-H. 1995. Computer-Assisted Pedicle Screw Fixation- A Feasibility Study. *Spine*, 20, 1208-1212.
- AMSTUTZ, H. & MAKI, S. 1978. Complications of trochanteric osteotomy in total hip replacement. *The Journal of Bone & Joint Surgery*, 60, 214-216.
- ARAND, M., HARTWIG, E., KINZL, L. & GEBHARD, F. 2001. Spinal navigation in cervical fractures—A preliminary clinical study on Judet-osteosynthesis of the axis. *Computer Aided Surgery*, 6, 170-175.
- ARCHER, J. E., MAY, P. L. & JEYS, L. M. 2015. CAOS in Paediatric Bone Tumour Surgery. *Journal of Bone and Soft Tissue Tumors Sep-Dec*, 1, 17-21.
- ARMAND, M., GRUPP, R., MURPHY, R., HEGMAN, R., ARMIGER, R., TAYLOR, R., MCARTHUR, B. & LEPISTO, J. 2018. Biomechanical guidance system for periacetabular osteotomy. *Intelligent Orthopaedics*. Springer.
- BAE, D. K. & SONG, S. J. 2011. Computer assisted navigation in knee arthroplasty. *Clinics in orthopedic surgery*, 3, 259-267.
- BANCHETTI, R., DARI, S., RICCIARINI, M. E., LUP, D., CARPINTERI, F., CATANI, F. & CALDORA, P. 2018. Comparison of conventional versus robotic-assisted total hip arthroplasty using the Mako system: An Italian retrospective study. *Journal of Health and Social Sciences*, 3, 37-48.
- BANKS, S. A. 2009. Haptic robotics enable a systems approach to design of a minimally invasive modular knee arthroplasty. *Am J Orthop (Belle Mead NJ)*, 38, 23-27.

- 
- BARGAR, W. L., BAUER, A. & BÖRNER, M. 1998. Primary and revision total hip replacement using the Robodoc (R) system. *Clinical orthopaedics and related research*, 354, 82-91.
- BASDOGAN, C. & SRINIVASAN, M. A. 2002. Haptic rendering in virtual environments. *Handbook of virtual environments*, 117-134.
- BEASLEY, R. A. 2012. Medical Robots: Current Systems and Research Directions. *Journal of Robotics*, 2012, 14.
- BELL, S. W., ANTHONY, I., JONES, B., MACLEAN, A., ROWE, P. & BLYTH, M. 2016. Improved accuracy of component positioning with robotic-assisted unicompartmental knee arthroplasty: data from a prospective, randomized controlled study. *JBJS*, 98, 627-635.
- BERAHMANI, S., HENDRIKS, M., DE JONG, J. J., VAN DEN BERGH, J. P., MAAL, T., JANSSEN, D. & VERDONSCHOT, N. 2018. Evaluation of interference fit and bone damage of an uncemented femoral knee implant. *Clinical biomechanics*, 51, 1-9.
- BERGSTRÖM, B., LINDBERG, L., PERSSON, B. M. & ÖNNERFÄLT, R. 1973. Complications after total hip arthroplasty according to Charnley in a Swedish series of cases. *Clinical orthopaedics and related research*, 95, 91-95.
- BERRY, D. J., BERGER, R. A., CALLAGHAN, J. J., DORR, L. D., DUWELIUS, P. J., HARTZBAND, M. A., LIEBERMAN, J. R. & MEARS, D. C. 2003. Symposium: Minimally Invasive Total Hip Arthroplasty Development, Early Results, and a Critical Analysis\*. *The Journal of Bone & Joint Surgery*, 85, 2235-2246.
- BETTINI, A., MARAYONG, P., LANG, S., OKAMURA, A. M. & HAGER, G. D. 2004. Vision-assisted control for manipulation using virtual fixtures. *Robotics, IEEE Transactions on*, 20, 953-966.
- BOWYER, S. A., DAVIES, B. L. & RODRIGUEZ Y BAENA, F. 2014. Active constraints/virtual fixtures: A survey. *Robotics, IEEE Transactions on*, 30, 138-157.
- BOZZIO, A. E., HU, X. & LIEBERMAN, I. H. 2019. Robotics in Spine Surgery: Uses in Development. *Robotics in Knee and Hip Arthroplasty*. Springer.
- BRETT, P. N. 2007. Moving on from surgical robotics to robotic micro-tools in surgery. *14th International Conference on Mechatronics and Machine Vision in Practice*. IEEE.
- BRISSON, G., KANADE, T., DIGIOIA, A. & JARAMAZ, B. Year. Precision freehand sculpting of bone. *In: International Conference on Medical Image Computing and Computer-Assisted Intervention*, 2004. Springer, 105-112.
- BROWN, R. A. 1979. A computerized tomography-computer graphics approach to stereotaxic localization. *Journal of neurosurgery*, 50, 715-720.
- BUECHEL, F. & CONDITT, M. 2016. Robotic-Arm Assisted Unicompartmental Knee Arthroplasty (MAKO). *Minimally Invasive Surgery in Orthopedics*, 1281-1305.
- BUKOWSKI, B., ANDERSON, P., KHLOPAS, A., CHUGHTAI, M. & MONT, M. 2016. Improved Functional Outcomes with Robotic Compared with Manual Total Hip Arthroplasty. *Surgical technology international*, 29, 303-308.
- BUMM, K., WURM, J., RACHINGER, J., DANNENMANN, T., BOHR, C., FAHLBUSCH, R., IRO, H. & NIMSKY, C. 2005. An automated robotic approach with redundant navigation for minimal invasive extended transsphenoidal skull base surgery. *min-Minimally Invasive Neurosurgery*, 48, 159-164.
- CHANG, J.-D., KIM, I.-S., BHARDWAJ, A. M. & BADAMI, R. N. 2017. The Evolution of Computer-Assisted Total Hip Arthroplasty and Relevant Applications. *Hip & pelvis*, 29, 1-14.

- 
- CHEN, C.-L., HAN, P.-F., ZHANG, Z.-L., SUN, X.-J. & LV, Z. 2019. Clinical efficacy of OrthoPilot navigation system versus conventional manual total hip arthroplasty: A systematic review and meta-analysis. *Journal of International Medical Research*, 47, 505-514.
- CHEN, Y., XU, W., LI, Z., SONG, S., LIM, C. M., WANG, Y. & REN, H. 2016. Safety-enhanced motion planning for flexible surgical manipulator using neural dynamics. *IEEE Transactions on Control Systems Technology*, 25, 1711-1723.
- CHENG, T., PAN, X.-Y., MAO, X., ZHANG, G.-Y. & ZHANG, X.-L. 2012. Little clinical advantage of computer-assisted navigation over conventional instrumentation in primary total knee arthroplasty at early follow-up. *The Knee*, 19, 237-245.
- CHRIST, A., PONZIO, D., PITTA, M., CARROLL, K., MUIR, J. M. & SCULCO, P. K. 2018. Minimal increase in total hip arthroplasty surgical procedural time with the use of a novel surgical navigation tool. *The open orthopaedics journal*, 12, 389.
- CLAVÉ, A., FAZILLEAU, F., CHEVAL, D., WILLIAMS, T., LEFÈVRE, C. & STINDEL, E. 2015. Comparison of the reliability of leg length and offset data generated by three hip replacement CAOS systems using EOS™ imaging. *Orthopaedics & Traumatology: Surgery & Research*, 101, 647-653.
- DAI, Y., ANGIBAUD, L., JUNG, A., HAMAD, C., BERTRAND, F., STULBERG, B. & HUDDLESTON, J. Year. Computer-assisted total knee arthroplasty: impact of surgeon experience on the ability to achieve surgical resection goals. *In: Orthopaedic Proceedings*, 2017. The British Editorial Society of Bone & Joint Surgery, 90-90.
- DAI, Y., CUI, Q., BOLOGNESI, M., WELLMAN, S., SEYLER, T., NAJMABADI, Y., BOLCH, C. & LIU, D. 2018. "Standard" Versus "Challenging" Patients-Perioperative Outcomes using Computer-Assisted Total Knee Arthroplasty. *EPiC Series in Health Sciences*, 2, 24-27.
- DARIO, P., CARROZZA, M. C., MARCACCI, M., D'ATTANASIO, S., MAGNAMI, B., TONET, O. & MEGALI, G. 2000. A novel mechatronic tool for computer-assisted arthroscopy. *IEEE Transactions on Information Technology in Biomedicine*, 4, 15-29.
- DARIO, P., SCUOLA SUPERIORE SANT'ANNA, P., ITALY & PAGGETTI, C. T., NELLY; PAPA, E.; CIUCCI, T.; CARROZZA, MARIA CHIARA; MARCACCI, MAURIZIO 1997. A miniature steerable end-effector for application in an integrated system for computer-assisted arthroscopy. *International Conference on Robotics and Automation* Albuquerque, New Mexico: IEEE.
- DAVID, O., RUSSOTTO, F.-X., SIMOES, M. D. S. & MEASSON, Y. 2014. Collision avoidance, virtual guides and advanced supervisory control teleoperation techniques for high-tech construction: Framework design. *Automation in Construction*, 44, 63-72.
- DEEP, K. 2018. Imageless Computer-Assisted Navigation for Total Hip Arthroplasty. *Computer Assisted Orthopaedic Surgery for Hip and Knee*. Springer.
- DENHAVIT, J. & HARTENBERG, S. 1955. A kinematic notation for lower-pair mechanisms based on matrices. *ASME J. Appl. Mech.*, 215-221.
- DEREK F AMANATULLAH, M., PHD, PAUL E DI CESARE, M., B SONNY BAL, M., WILLIAM L JAFFE, M., JAMES J MCCARTHY, M., STEVEN I RABIN, M., FRANCISCO TALAVERA, P., PHD & SANTARAM VALLURUPALLI, M. 2014. *Minimally Invasive Total Hip Arthroplasty Technique* [Online]. Medscape. Available: <http://emedicine.medscape.com/article/2000333-technique> [Accessed 2015].
- DIGIOIA, A. M., JARAMAZ, B., BLACKWELL, M., SIMON, D. A., MORGAN, F., MOODY, J. E., NIKOU, C., COLGAN, B. D., ASTON, C. A. & LABARCA, R. S. 1998a. Image guided navigation system to measure intraoperatively acetabular implant alignment. *Clinical orthopaedics and related research*, 355, 8-22.

- DIGIOIA, A. M. I., JARAMAZ, B. & COLGAN, B. D. 1998b. Computer Assisted Orthopaedic Surgery: Image Guided and Robotic Assistive Technologies. *Clinical Orthopaedics & Related Research*, 354, 8-16.
- DIGIOIA III, A. M., PLAKSEYCHUK, A. Y., LEVISON, T. J. & JARAMAZ, B. 2003. Mini-incision technique for total hip arthroplasty with navigation. *The Journal of Arthroplasty*, 18, 123-128.
- DILLON, N. P., KRATCHMAN, L. B., DIETRICH, M. S., LABADIE, R. F., WEBSTER III, R. J. & WITHROW, T. J. 2013. An experimental evaluation of the force requirements for robotic mastoidectomy. *Otology & neurotology: official publication of the American Otological Society, American Neurotology Society [and] European Academy of Otology and Neurotology*, 34, e93.
- DORR, L. D. 2009. CAOS: Greater Precision, Doubtful Clinical Benefit—Opposes. *Seminars in Arthroplasty*, 20, 60-61.
- DUQUE, S. G., GORREPATI, R., KESAVABHOTLA, K., HUANG, C. & BOOCKVAR, J. A. 2014. Endoscopic endonasal transphenoidal surgery using the BrainLAB® Headband for navigation without rigid fixation. *Journal of Neurological Surgery Part A: Central European Neurosurgery*, 75, 267-269.
- FAN, M., LIU, Y. & TIAN, W. 2018. Internal fixation in upper cervical spinal surgery: a randomized controlled study. *EPiC Series in Health Sciences*, 2, 51-55.
- FERNANDES, J. J. & SELVAKUMAR, A. 2018. Kinematic and Dynamic Analysis of 3PUU Parallel Manipulator for Medical Applications. *Procedia computer science*, 133, 604-611.
- FIANI, B., QUADRI, S. A., FAROOQUI, M., CATHEL, A., BERMAN, B., NOEL, J. & SIDDIQI, J. 2018. Impact of robot-assisted spine surgery on health care quality and neurosurgical economics: a systemic review. *Neurosurgical review*, 1-9.
- FIGUEROA, F., WAKELIN, E., TWIGGS, J. & FRITSCH, B. 2019. Comparison between navigated reported position and postoperative computed tomography to evaluate accuracy in a robotic navigation system in total knee arthroplasty. *The Knee*.
- FOMEKONG, E., SAFI, S. E. & RAFTOPOULOS, C. 2017. Spine navigation based on 3-dimensional robotic fluoroscopy for accurate percutaneous pedicle screw placement: a prospective study of 66 consecutive cases. *World neurosurgery*, 108, 76-83.
- FUJII, Y., FUJIWARA, K., ENDOU, H., TETSUNAGA, T., MIYAKE, T., YAMADA, K., OZAKI, T., ABE, N., SUGITA, N. & MITSUISHI, M. Year. THE INFLUENCE OF THE SURGICAL APPROACH TO THE ACCURACY OF NEWLY DEVELOPED CT-BASED NAVIGATION SYSTEM IN THA. *In: Orthopaedic Proceedings*, 2017. The British Editorial Society of Bone & Joint Surgery, 124-124.
- GLOSSOP, N. D., HU, R. W. & RANDLE, J. A. 1996. Computer-Aided Pedicle Screw Placement Using Frameless Stereotaxis. *Spine*, 21, 2026-2034.
- GONZALEZ, G., MEDELLIN, H. I., LIM, T., RITCHIE, J. M. & SUNG, R. C. Year. 3D object representation for physics simulation engines and its effect on virtual assembly tasks. *In: ASME 2012 International Design Engineering Technical Conferences and Computers and Information in Engineering Conference*, 2012. American Society of Mechanical Engineers, 1449-1459.
- HAAS, S. B., LEHMAN, A. P. & COOK, S. 2005. *Total Knee Arthroplasty: A Guide to Get Better Performance*, Springer Medizin Verlag Heidelberg.



- 
- HAFEZ, M. A., SEEL, M. J., JARAMAZ, B. & DIGIOIA III, A. M. 2006. Navigation in minimally invasive total knee arthroplasty and total hip arthroplasty. *Operative Techniques in Orthopaedics*, 16, 207-210.
- HAMLIN, B., BARRETT, M. & JIRANEK, W. 2005. The Role of Computer Assisted Surgery in Minimally Invasive Joint Replacement Surgery. *Seminars in Arthroplasty*, 16, 239-247.
- HAN, P. F., CHEN, C. L., ZHANG, Z. L., HAN, Y. C., WEI, L., LI, P. C. & WEI, X. C. 2019. Robotics-assisted versus conventional manual approaches for total hip arthroplasty: A systematic review and meta-analysis of comparative studies. *The International Journal of Medical Robotics and Computer Assisted Surgery*, e1990.
- HARAGUCHI, D., KANNO, T., TADANO, K. & KAWASHIMA, K. 2015. A pneumatically driven surgical manipulator with a flexible distal joint capable of force sensing. *IEEE/ASME Transactions on Mechatronics*, 20, 2950-2961.
- HU, T., WANG, Y., MA, B., ZHANG, F., SUN, J., ZHENG, M. & PAN, R. Year. A Passive Snake-like Arm Based on Wire-driven Mechanism for Laparoscopic Surgery. In: IOP Conference Series: Materials Science and Engineering, 2018. IOP Publishing, 012058.
- HUSSAIN, A., MALIK, A., HALIM, M. & ALI, A. 2014. The use of robotics in surgery: a review. *International journal of clinical practice*, 68, 1376-1382.
- IBRAHIM, K., RAMADAN, A., FANNI, M., KOBAYASHI, Y., ABO-ISMAIL, A. & FUJIE, M. G. 2015. Development of a new 4-DOF endoscopic parallel manipulator based on screw theory for laparoscopic surgery. *Mechatronics*, 28, 4-17.
- IMAI, N., TAKUBO, R., SUZUKI, H., SHIMADA, H., MIYASAKA, D., TSUCHIYA, K. & ENDO, N. 2018. Accuracy of acetabular cup placement using CT-based navigation in total hip arthroplasty: Comparison between obese and non-obese patients. *Journal of Orthopaedic Science*.
- JACOBS, C., POPE, M., BERRY, J. & HOAGLUND, F. 1974. A study of the bone machining process—orthogonal cutting. *Journal of biomechanics*, 7, 131-136.
- JACOFISKY, D. J. & ALLEN, M. 2016. Robotics in arthroplasty: a comprehensive review. *The Journal of arthroplasty*, 31, 2353-2363.
- JAKOPEC, M., HARRIS, S., RODRIGUEZ Y BAENA, F., GOMES, P., COBB, J. & DAVIES, B. 2001. The first clinical application of a “hands-on” robotic knee surgery system. *Computer Aided Surgery*, 6, 329-339.
- JAKOPEC, M., HARRIS, S. J., RODRIGUEZ Y BAENA, F., GOMES, P. & DAVIES, B. L. 2003. The Acrobot® system for total knee replacement. *Industrial Robot: An International Journal*, 30, 61-66.
- JARAMAZ, B. & NIKOU, C. 2012. Precision freehand sculpting for unicondylar knee replacement: design and experimental validation. *Biomedizinische Technik/Biomedical Engineering*, 57, 293-299.
- JENNY, J.-Y., BOERI, C., DOSCH, J.-C., USCATU, M. & CIOBANU, E. 2009. Navigated non-image-based positioning of the acetabulum during total hip replacement. *International orthopaedics*, 33, 83-87.
- JERABEK, S., CARROLL, K., MARATT, J., MAYMAN, D. & PADGETT, D. Year. Accuracy of cup positioning and achieving desired hip length and offset following robotic THA. In: 14th annual CAOS Meeting, 2014.
- JI, D., KANG, T. H., SHIM, S., LEE, S. & HONG, J. 2019. Wire-driven flexible manipulator with constrained spherical joints for minimally invasive surgery. *International journal of computer assisted radiology and surgery*, 1-13.

- 
- JIMÉNEZ, P., THOMAS, F. & TORRAS, C. 2001. 3D collision detection: a survey. *Computers & Graphics*, 25, 269-285.
- JOLLES, B., GENOUD, P. & HOFFMEYER, P. Year. Accuracy of computer-assisted cup placement in total hip arthroplasty. *In: International Congress Series*, 2001. Elsevier, 314-318.
- JOLLES, B. M. & BOGOCH, E. R. 2006. Posterior versus lateral surgical approach for total hip arthroplasty in adults with osteoarthritis. *Cochrane Database Syst Rev*, 3.
- JOSKOWICZ, L. & HAZAN, E. J. 2016. Computer aided orthopaedic surgery: incremental shift or paradigm change? : Elsevier.
- KAGIYAMA, Y., OTOMARU, I., TAKAO, M., SUGANO, N., NAKAMOTO, M., YOKOTA, F., TOMIYAMA, N., TADA, Y. & SATO, Y. 2016. CT-based automated planning of acetabular cup for total hip arthroplasty (THA) based on hybrid use of two statistical atlases. *International journal of computer assisted radiology and surgery*, 11, 2253-2271.
- KANLIĆ, E. M., DELAROSA, F. & PIRELA-CRUZ, M. 2006. Computer assisted orthopaedic surgery--CAOS. *Bosn J Basic Med Sci*, 6, 7-13.
- KAOUK, J. H., HABER, G.-P., AUTORINO, R., CROUZET, S., OUZZANE, A., FLAMAND, V. & VILLERS, A. 2014. A novel robotic system for single-port urologic surgery: first clinical investigation. *European urology*, 66, 1033-1043.
- KAZANZIDES, P. Year. Robot Assisted Surgery: The ROBODOC® Experience. *In: INTERNATIONAL SYMPOSIUM ON ROBOTICS*, 1999. unknown, 281-286.
- KHORASANI, A. M., GIBSON, I., CHEGINI, N. G., GOLDBERG, M., GHASEMI, A. H. & LITTLEFAIR, G. 2016. An improved static model for tool deflection in machining of Ti-6Al-4V acetabular shell produced by selective laser melting. *Measurement*, 92, 534-544.
- KIM, H. J., YOON, J.-R., CHOI, G. W. & YANG, J.-H. 2016. Imageless navigation versus conventional open wedge high tibial osteotomy: a meta-analysis of comparative studies. *Knee surgery & related research*, 28, 16.
- KLEIN, G. R., AUSTIN, M. S., SMITH, E. B. & HOZACK, W. J. 2006. Total knee arthroplasty using computer-assisted navigation in patients with deformities of the femur and tibia. *The Journal of arthroplasty*, 21, 284-288.
- KLEIN, G. R., JAMES, D. & LONNER, J. H. 2019. Total Knee Arthroplasty Technique: ROSA® Knee. *Robotics in Knee and Hip Arthroplasty*. Springer.
- KOENIG, J. A. & PLASKOS, C. 2019. Total Knee Arthroplasty Technique: OMNIBotics. *Robotics in Knee and Hip Arthroplasty*. Springer.
- KRAUSE, W. 1987. Orthogonal bone cutting: saw design and operating characteristics. *Journal of Biomechanical Engineering*, 109, 263-271.
- KUANG, S., TANG, Y., LIN, A., YU, S. & SUN, L. 2018. Intelligent Control for Human-Robot Cooperation in Orthopedics Surgery. *Intelligent Orthopaedics*. Springer.
- LAINE, T., LUND, T., YLIKOSKI, M., LOHIKOSKI, J. & SCHLENZKA, D. 2000. Accuracy of pedicle screw insertion with and without computer assistance: a randomised controlled clinical study in 100 consecutive patients. *European Spine*, 9, 235-240.
- LANG, J., MANNAVA, S., FLOYD, A., GODDARD, M., SMITH, B., MOFIDI, A., M SEYLER, T. & JINNAH, R. 2011. Robotic systems in orthopaedic surgery. *Journal of Bone & Joint Surgery, British Volume*, 93, 1296-1299.

- 
- LANG, Z., TIAN, W., LIU, Y., LIU, B., YUAN, Q. & SUN, Y. 2016. Minimally invasive pedicle screw fixation using intraoperative 3-dimensional fluoroscopy-based navigation (CAMISS Technique) for hangman fracture. *Spine*, 41, 39-45.
- LANGLOTZ, F., BÄCHLER, R., BERLEMANN, U., NOLTE, L.-P. & GANZ, R. 1998. Computer assistance for pelvic osteotomies. *Clinical orthopaedics and related research*, 354, 92-102.
- LAU, K., LEUNG, E. Y., POON, C. C., CHIU, P. W., LAU, J. Y. & YAM, Y. Year. Motion Compensation of Tendon-Sheath Driven Continuum Manipulator for Endoscopic Surgery. *In: MATEC Web of Conferences*, 2015. EDP Sciences, 04007.
- LAVALLEE, S. 1996. *Registration for Computer-Integrated Surgery: Methodology, State of the Art*, Cambridge, MIT Press.
- LAVALLÉE, S., SAUTOT, P., TROCCAZ, J., CINQUIN, P. & MERLOZ, P. 1995. Computer-Assisted Spine Surgery: A Technique for Accurate Transpedicular Screw Fixation Using CT Data and a 3-D Optical Localizer. *Computer Aided Surgery*, 1, 65-73.
- LEE, B. H., KUM, D. H., KIM, Y., CHO, H. & WANG, J. H. 2016. Clinical advantages of image-free navigation system using surface-based registration in anatomical anterior cruciate ligament reconstruction. *Knee Surgery, Sports Traumatology, Arthroscopy*, 24, 3556-3564.
- LEE, J., GOZEN, B. A. & OZDOGANLAR, O. B. 2012. Modeling and experimentation of bone drilling forces. *Journal of biomechanics*, 45, 1076-1083.
- LEELASESTAPORN, C. 2018. Robotic UKA. *Computer Assisted Orthopaedic Surgery for Hip and Knee*. Springer.
- LEVISON, T. J., MOODY, J. E., JARAMAZ, B., NIKOU, C. & DIGIOIA, A. M. Year. Surgical navigation for THR: A report on clinical trial utilizing HipNav. *In: International Conference on Medical Image Computing and Computer-Assisted Intervention*, 2000. Springer, 1185-1187.
- LI, M., ISHII, M. & TAYLOR, R. H. 2007. Spatial motion constraints using virtual fixtures generated by anatomy. *Robotics, IEEE Transactions on*, 23, 4-19.
- LI, M., KAPOOR, A. & TAYLOR, R. H. Year. A constrained optimization approach to virtual fixtures. *In: Intelligent Robots and Systems, 2005.(IROS 2005). 2005 IEEE/RSJ International Conference on*, 2005. IEEE, 1408-1413.
- LI, M. & OKAMURA, A. M. Year. Recognition of operator motions for real-time assistance using virtual fixtures. *In: Haptic Interfaces for Virtual Environment and Teleoperator Systems, 2003. HAPTICS 2003. Proceedings. 11th Symposium on*, 2003. IEEE, 125-131.
- LI, Z., CHIU, P. W. & DU, R. Year. Design and kinematic modeling of a concentric wire-driven mechanism targeted for minimally invasive surgery. *In: 2016 IEEE/RSJ International Conference on Intelligent Robots and Systems (IROS), 2016. IEEE*, 310-316.
- LI, Z., WU, L., REN, H. & YU, H. 2017. Kinematic comparison of surgical tendon-driven manipulators and concentric tube manipulators. *Mechanism and Machine Theory*, 107, 148-165.
- LIAO, Z., AXINTE, D. & GAO, D. 2019. On modelling of cutting force and temperature in bone milling. *Journal of Materials Processing Technology*, 266, 627-638.
- LIN, F., LIM, D., WIXSON, R. L., MILOS, S., HENDRIX, R. W. & MAKHSOUS, M. 2011. Limitations of imageless computer-assisted navigation for total hip arthroplasty. *The Journal of arthroplasty*, 26, 596-605.

- 
- LIOW, M. H. L., CHIN, P. L., PANG, H. N., TAY, D. K.-J. & YEO, S.-J. 2017. THINK surgical TSolution-One®(Robodoc) total knee arthroplasty. *SICOT-J*, 3.
- LIU, N., BERGELES, C. & YANG, G.-Z. Year. Design and analysis of a wire-driven flexible manipulator for bronchoscopic interventions. *In: 2016 IEEE International Conference on Robotics and Automation (ICRA), 2016. IEEE, 4058-4063.*
- LIU, Z., GAO, Y. & CAI, L. 2015. Imageless navigation versus traditional method in total hip arthroplasty: A meta-analysis. *International Journal of Surgery*, 21, 122-127.
- LONNER, J. H. 2009. Indications for unicompartmental knee arthroplasty and rationale for robotic arm-assisted technology. *Am J Orthop (Belle Mead NJ)*, 38, 3-6.
- LONNER, J. H. 2016. Robotically assisted unicompartmental knee arthroplasty with a handheld image-free sculpting tool. *Orthopedic Clinics*, 47, 29-40.
- LONNER, J. H. & KLEMENT, M. R. 2019. Robotic-assisted Medial Unicompartmental Knee Arthroplasty: Options and Outcomes. *JAAOS-Journal of the American Academy of Orthopaedic Surgeons*, 27, e207-e214.
- LONNER, J. H., SMITH, J. R., PICARD, F., HAMLIN, B., ROWE, P. J. & RICHES, P. E. 2015. High degree of accuracy of a novel image-free handheld robot for unicondylar knee arthroplasty in a cadaveric study. *Clinical Orthopaedics and Related Research®*, 473, 206-212.
- MAILLET, P., NAHUM, B., BLONDEL, L., POIGNET, P. & DOMBRE, E. Year. BRIGIT, a robotized tool guide for orthopedic surgery. *In: Proceedings of the 2005 IEEE International Conference on Robotics and Automation, 2005. IEEE, 211-216.*
- MARECIK, S. J., CHAUDHRY, V., JAN, A., PEARL, R. K., PARK, J. J. & PRASAD, L. M. 2007. A comparison of robotic, laparoscopic, and hand-sewn intestinal sutured anastomoses performed by residents. *The American journal of surgery*, 193, 349-355.
- MARTELLI, M., MARCACCI, M., NOFRINI, L., PALOMBARA, F. L., MALVISI, A., IACONO, F., VENDRUSCOLO, P. & PIERANTONI, M. 2000. Computer- and Robot-Assisted Total Knee Replacement: Analysis of a New Surgical Procedure. *Annals of Biomedical Engineering*, 28, 1146-1153.
- MAZOOCHIAN, F., PELLENGAHR, C., HUBER, A., KIRCHER, J., REFIOR, H. J. & JANSSON, V. 2004. Low accuracy of stem implantation in THR using the CASPAR-system anteversion measurements in 10 hips. *Acta Orthopaedica Scandinavica*, 75, 261-264.
- MIHELJ, M., BAJD, T., UDE, A., LENARČIČ, J., STANOVNIK, A., MUNIH, M., REJC, J. & ŠLAJPAH, S. 2019. Robot Sensors. *Robotics*. Springer.
- MILLAR, L. J., BANGER, M., ROWE, P. J., BLYTH, M., JONES, B. & MACLEAN, A. 2018. O 017-A five-year follow up of gait in robotic assisted vs conventional unicompartmental knee arthroplasty. *Gait & posture*, 65, 31-32.
- MIN, B.-W., SONG, K.-S., BAE, K.-C., CHO, C.-H., KANG, C.-H. & KIM, S.-Y. 2008. The Effect of Stem Alignment on Results of Total Hip Arthroplasty with a Cementless Tapered-Wedge Femoral Component. *Journal of Arthroplasty*, 23, 418-423.
- MISHRA, V., SINGH, N., TIWARI, U. & KAPUR, P. 2011. Fiber grating sensors in medicine: Current and emerging applications. *Sensors and Actuators A: Physical*, 167, 279-290.
- MOGHADDAM, M., NAHVI, A., ARBABTAFTI, M. & MAHVASH, M. 2008. A physically realistic voxel-based method for haptic simulation of bone machining. *Haptics: Perception, Devices and Scenarios*. Springer.

- 
- MOLLI, R. G., ANDERSON, K. C., BUEHLER, K. C. & MARKEL, D. C. 2011. Computer-assisted navigation software advancements improve the accuracy of total knee arthroplasty. *The Journal of arthroplasty*, 26, 432-438.
- MOLLOY, S., AFTAB, S., PATEL, A., BUTLER, J., BALAJI, V., WILSON, L. & LEE, R. Year. THE BRITISH EXPERIENCE OF PEDICLE SCREW INSERTION USING THE O-ARM® IMAGING SYSTEM AND STEALTHSTATION® NAVIGATION SYSTEM. *In: Orthopaedic Proceedings*, 2014. The British Editorial Society of Bone & Joint Surgery, 30-30.
- MOORE, K. L., DALLEY, A. F. & AGUR, A. M. 2013. *Clinically oriented anatomy*, Lippincott Williams & Wilkins.
- MUNUERA, L. & GARCIA-CIMBRELO, E. 1992. The femoral component in low-friction arthroplasty after ten years. *Clinical orthopaedics and related research*, 279, 163-175.
- NAKAZAWA, A., NANRI, K., HARADA, K., TANAKA, S., NUKARIYA, H., KUROSE, Y., SHONO, N., NAKATOMI, H., MORITA, A. & WATANABE, E. Year. Feedback methods for collision avoidance using virtual fixtures for robotic neurosurgery in deep and narrow spaces. *In: 2016 6th IEEE International Conference on Biomedical Robotics and Biomechanics (BioRob)*, 2016. IEEE, 247-252.
- NAWABI, D. H., CONDITT, M. A., RANAWAT, A. S., DUNBAR, N. J., JONES, J., BANKS, S. & PADGETT, D. E. 2013. Haptically guided robotic technology in total hip arthroplasty: a cadaveric investigation. *Proceedings of the Institution of Mechanical Engineers, Part H: Journal of Engineering in Medicine*, 227, 302-309.
- NETRAVALI, N. A., BÖRNER, M. & BARGAR, W. L. 2016. The Use of ROBODOC in Total Hip and Knee Arthroplasty. *Computer-Assisted Musculoskeletal Surgery*. Springer.
- NETTER, F. H. 2014. *Atlas of human anatomy*, Elsevier Health Sciences.
- NISHIHARA, S., SUGANO, N., NISHII, T., MIKI, H., NAKAMURA, N. & YOSHIKAWA, H. 2006. Comparison Between Hand Rasping and Robotic Milling for Stem Implantation in Cementless Total Hip Arthroplasty. *The Journal of Arthroplasty*, 21, 957-966.
- NISHIHARA, S., SUGANO, N., NISHII, T., TANAKA, H., NAKAMURA, N., YOSHIKAWA, H. & OCHI, T. 2004. Clinical accuracy evaluation of femoral canal preparation using the ROBODOC system. *Journal of Orthopaedic Science*, 9, 452-461.
- NOLTE, L. P. & BEUTLER, T. 2004. Basic Principles of CAOS. *International Journal of the Care of the Injured*, 35, 6-16.
- PAPROSKY, W. G., MUIR, J. M. & SOSTAK, J. R. 2019. Imageless Navigation Accurately Measures Component Orientation during Total Hip Arthroplasty: A Comparison with Postoperative Radiographs. *The Journal of Hip Surgery*.
- PARK, J. W., CHOI, J., PARK, Y. & SUN, K. 2011. Haptic virtual fixture for robotic cardiac catheter navigation. *Artificial organs*, 35, 1127-1131.
- PARRATTE, S., ARGENSON, J., FLECHER, X. & AUBANIAC, J. 2007. [Computer-assisted surgery for acetabular cup positioning in total hip arthroplasty: comparative prospective randomized study]. *Revue de chirurgie orthopedique et reparatrice de l'appareil moteur*, 93, 238-246.
- PARRATTE, S., PRICE, A., JEYS, L., JACKSON, W. & CLARKE, H. D. 2019. Accuracy of a new robotically-assisted technique for Total Knee Arthroplasty: a cadaveric study. *The Journal of arthroplasty*.
- PAYANDEH, S. & STANISIC, Z. Year. On application of virtual fixtures as an aid for telemanipulation and training. *In: Haptic Interfaces for Virtual Environment and*

- 
- Teleoperator Systems, 2002. HAPTICS 2002. Proceedings. 10th Symposium on, 2002. IEEE, 18-23.
- PAYNE, C. J., GRAS, G., HUGHES, M., NATHWANI, D. & YANG, G.-Z. Year. A hand-held flexible mechatronic device for arthroscopy. *In: 2015 IEEE/RSJ International Conference on Intelligent Robots and Systems (IROS), 2015. IEEE, 817-823.*
- PAYO, I., FELIU, V. & CORTÁZAR, O. D. 2009. Fibre Bragg grating (FBG) sensor system for highly flexible single-link robots. *Sensors and Actuators A: Physical, 150, 24-39.*
- PERETS, I., WALSH, J., MU, B., MANSOR, Y., YUEN, L. & DOMB, B. 2018a. Does robotic-arm assisted total hip arthroplasty benefit short-term clinical outcomes? A pair match-controlled study. *EPiC Series in Health Sciences, 2, 157-162.*
- PERETS, I., WALSH, J. P., CLOSE, M. R., MU, B. H., YUEN, L. C. & DOMB, B. G. 2018b. Robot-assisted total hip arthroplasty: Clinical outcomes and complication rate. *The International Journal of Medical Robotics and Computer Assisted Surgery, 14, e1912.*
- PFLUGI, S., LERCH, T., VASIREDDY, R., BOEMKE, N., TANNAST, M., ECKER, T. M., SIEBENROCK, K. & ZHENG, G. 2017. Augmented Marker Tracking For Peri-Acetabular Osteotomy Surgery: A Cadaver Study. *EPiC Series in Health Sciences, 1, 54-57.*
- PITTO, R., MALAK, S. & ANDERSON, I. 2009. Accuracy of a computer-assisted navigation system in resurfacing hip arthroplasty. *International orthopaedics, 33, 391-395.*
- PLAWESKI, S., ROSSI, J., MERLOZ, P. & JULLIARD, R. 2011. Analysis of anatomic positioning in computer-assisted and conventional anterior cruciate ligament reconstruction. *Orthopaedics & Traumatology: Surgery & Research, 97, S80-S85.*
- PLINKERT, P. & LÖWENHEIM, H. 2009. Trends and Perspectives in Minimally Invasive Surgery in Otorhinolaryngology-Head and Neck Surgery. *The Laryngoscope, 107, 1483-1489.*
- POZO, A. S. D., ESCANO, J. M. & BORDONS, C. Year. Simulator for control and automation using an interactive and configurable 3D virtual environment. *In: SICE Annual Conference (SICE), 2012 Proceedings of, 2012. IEEE, 2268-2273.*
- QIANG YUAN, M., WU, J., LIU, Y., YONGGANG XING, M., ZHANG, Y. & TIAN, W. 2018. Robot-assisted screw fixation in upper cervical spine using TiRobot system: an accurate and reliable procedure. *CAOS, 2, 242-247.*
- QIAO, F., LI, D., JIN, Z., GAO, Y., ZHOU, T., HE, J. & CHENG, L. 2015. Application of 3D printed customized external fixator in fracture reduction. *Injury, 46, 1150-1155.*
- QIN, J., XU, Z., DAI, J., CHEN, D., XU, X., SONG, K., SHI, D. & JIANG, Q. 2018. New technique: practical procedure of robotic arm-assisted (MAKO) total hip arthroplasty. *Annals of translational medicine, 6.*
- QUAGLIA, C., PETRONI, G., NICCOLINI, M., CACCAVARO, S., DARIO, P. & MENCIASSI, A. 2014. Design of a compact robotic manipulator for single-port laparoscopy. *Journal of Mechanical Design, 136, 105001.*
- RAHMATHULLA, G., NOTTMEIER, E. W., PIRRIS, S. M., DEEN, H. G. & PICHELMANN, M. A. 2014. Intraoperative image-guided spinal navigation: technical pitfalls and their avoidance. *Neurosurgical focus, 36, E3.*
- RASSWEILER, J., HRUZA, M., TEBER, D. & SU, L.-M. 2006. Laparoscopic and robotic assisted radical prostatectomy—critical analysis of the results. *European urology, 49, 612-624.*
- REDDY, V. Y., NEUZIL, P., MALCHANO, Z. J., VIJAYKUMAR, R., CURY, R., ABBARA, S., WEICHET, J., MCPHERSON, C. D. & RUSKIN, J. N. 2007. View-Synchronized Robotic Image-Guided Therapy for Atrial Fibrillation Ablation Experimental Validation and Clinical Feasibility. *Circulation, 115, 2705-2714.*

- REN, J., PATEL, R. V., MCISAAC, K. A., GUIRAUDON, G. & PETERS, T. M. 2008. Dynamic 3-D virtual fixtures for minimally invasive beating heart procedures. *IEEE transactions on medical imaging*, 27, 1061-1070.
- RENKAWITZ, T., HAIMERL, M., DOHMEN, L., GNEITING, S., WEGNER, M., EHRET, N., BUCHELE, C., SCHUBERT, M., LECHLER, P. & WOERNER, M. 2011. Minimally invasive computer-navigated total hip arthroplasty, following the concept of femur first and combined anteversion: design of a blinded randomized controlled trial. *BMC musculoskeletal disorders*, 12, 192.
- REUVEN, A., ALGARNI, A. D., AOUDE, A., KACHANATHU, S. J. & ZUKOR, D. J. 2017. Midterm functional outcomes of imageless navigation-assisted total knee arthroplasty. *Saudi Journal of Sports Medicine*, 17, 135.
- ROBINSON, J. & COLOMBET, P. 2017. Experience with Computer Navigation: Present and Future. *Rotatory Knee Instability*. Springer.
- ROCHE, A. J. & CALDER, J. D. 2015. Arthroscopy of the Ankle: New Approaches. *Sports Injuries: Prevention, Diagnosis, Treatment and Rehabilitation*, 1-20.
- ROCHE, M. 2014. Robotic-assisted unicompartmental knee arthroplasty: the MAKO experience. *Clinics in sports medicine*, 33, 123-132.
- ROCHE, M., O'LOUGHLIN, P. F., KENDOFF, D., MUSAHL, V. & PEARLE, A. D. 2009. Robotic arm-assisted unicompartmental knee arthroplasty: preoperative planning and surgical technique. *American journal of orthopedics (Belle Mead, NJ)*, 38, 10-15.
- ROSENBERG, L. B. Year. Virtual fixtures: Perceptual tools for telerobotic manipulation. *In: Virtual Reality Annual International Symposium, 1993.*, 1993 IEEE, 1993. IEEE, 76-82.
- SCHMIDT, B., KÖKTÜRK, B., TILZ, R., FÜRNKRANZ, A., KONSTANTINIDOU, M., WISSNER, E., METZNER, A., OUYANG, F. & KUCK, K.-H. 2008. Catheter ablation—new developments in robotics. *Herz Kardiovaskuläre Erkrankungen*, 33, 586-589.
- SCHULZ, A. P., SEIDE, K., QUEITSCH, C., HAUGWITZ, A. V., MEINERS, J., KIENAST, B., TARABOLSI, M., KAMMAL, M. & JÜRGENS, C. 2007. Results of total hip replacement using the Robodoc surgical assistant system: clinical outcome and evaluation of complications for 97 procedures. *The International Journal of Medical Robotics and Computer Assisted Surgery*, 3, 301-306.
- SHANER, J., KO, L. M. & LONNER, J. 2016. Handheld Robotics for Unicompartmental Knee Arthroplasty. *Minimally Invasive Surgery in Orthopedics*, 1-11.
- SHANG, J., PAYNE, C. J., CLARK, J., NOONAN, D. P., KWOK, K.-W., DARZI, A. & YANG, G.-Z. Year. Design of a multitasking robotic platform with flexible arms and articulated head for minimally invasive surgery. *In: 2012 IEEE/RSJ International Conference on Intelligent Robots and Systems, 2012.* IEEE, 1988-1993.
- SIDDIQI, A., HARDAKER, W. M., EACHEMPATI, K. K. & SHETH, N. P. 2017. Advances in computer-aided technology for total knee arthroplasty. *Orthopedics*, 40, 338-352.
- SIDHU, R., WEIR-MCCALL, J., COCHENNEC, F., RIGA, C., DIMARCO, A. & BICKNELL, C. 2012. Evaluation of an electromagnetic 3D navigation system to facilitate endovascular tasks: a feasibility study. *European Journal of Vascular and Endovascular Surgery*, 43, 22-29.
- SIEBEL, T. & KÄFER, W. 2005. Clinical outcome following robotic assisted versus conventional total hip arthroplasty: a controlled and prospective study of seventy-one patients. *Zeitschrift für Orthopädie und ihre Grenzgebiete*, 143, 391-398.
- SIEBERT, W., MAI, S., KOBER, R. & HEECKT, P. F. 2002. Technique and first clinical results of robot-assisted total knee replacement. *The Knee*, 9, 173-180.

---

SIKORSKI, J. M. & CHAUHAN, S. 2003. Aspects of current management: Computer-Assisted Orthopaedic Surgery:

Do We Need CAOS? *The Journal of Bone & Joint Surgery (Br)*, 85-B, 319-323.

SIOPACK, J. & JERGESEN, H. 1995. Total hip arthroplasty. *Western journal of medicine*, 162, 243.

SMITH, J. R., RICHES, P. E. & ROWE, P. J. 2014. Accuracy of a freehand sculpting tool for unicondylar knee replacement. *The International Journal of Medical Robotics and Computer Assisted Surgery*, 10, 162-169.

SOFRONIA, R. E., SAVII, G. G. & DAVIDESCU, A. Year. Real-time collision detection for long thin medical instruments in virtual reality-based simulators. *In: Optimization of Electrical and Electronic Equipment (OPTIM)*, 2012 13th International Conference on, 2012. IEEE, 1107-1112.

SOLIS, J., AVIZZANO, C. A. & BERGAMASCO, M. Year. Teaching to write Japanese characters using a haptic interface. *In: Haptic Interfaces for Virtual Environment and Teleoperator Systems, 2002. HAPTICS 2002. Proceedings. 10th Symposium on, 2002. IEEE*, 255-262.

SOLOMON, L., WARWICK, D. & NAYAGAM, S. 2010. *Apley's system of orthopaedics and fractures*, CRC Press.

SONG, S., LI, Z., YU, H. & REN, H. 2015. Shape reconstruction for wire-driven flexible robots based on Bézier curve and electromagnetic positioning. *Mechatronics*, 29, 28-35.

SONG, S., ZHANG, C., LIU, L. & MENG, M. Q.-H. 2018. Preliminary study on magnetic tracking-based planar shape sensing and navigation for flexible surgical robots in transoral surgery: methods and phantom experiments. *International journal of computer assisted radiology and surgery*, 13, 241-251.

STIEHLER, M., GORONZY, J., KIRSCHNER, S., HARTMANN, A., SCHÄFER, T. & GÜNTHER, K.-P. 2015. Effect of surgical experience on imageless computer-assisted femoral component positioning in hip resurfacing—a preclinical study. *European journal of medical research*, 20, 18.

STINDEL, E., BRIARD, J.-L., LAVALLEE, S., DUBRANA, F., PLAWESKI, S., MERLOZ, P., LEFÈVRE, C. & TROCCAZ, J. 2004. Bone morphing: 3D Reconstruction without pre-or intraoperative imaging-concept and applications. *Navigation and Robotics in Total Joint and Spine Surgery*. Springer.

STINDEL, E., BRIARD, J. L., MERLOZ, P., PLAWESKI, S., DUBRANA, F., LEFÈVRE, C. & TROCCAZ, J. 2002. Bone morphing: 3D morphological data for total knee arthroplasty. *Computer Aided Surgery*, 7, 156-168.

STINDEL, É., GÉRARD, R. & LEFÈVRE, C. 2008. Computer-assisted total hip arthroplasty: a global and universal approach using Total Hip Surgetics. *Interactive surgery*, 3, 160-169.

STINDEL, E., GIL, D., BRIARD, J.-L., MERLOZ, P., DUBRANA, F. & LEFÈVRE, C. 2005. Detection of the center of the hip joint in computer-assisted surgery: an evaluation study of the Surgetics algorithm. *Computer Aided Surgery*, 10, 133-139.

SUGANO, N. 2003. Computer-assisted orthopedic surgery. *Journal of Orthopaedic Science*, 8, 442-448.

TAKEBA, J., UMAKOSHI, K., KIKUCHI, S., MATSUMOTO, H., ANNEN, S., MORIYAMA, N., NAKABAYASHI, Y., SATO, N. & AIBIKI, M. 2018. Accuracy of screw fixation using the



- 
- O-arm® and StealthStation® navigation system for unstable pelvic ring fractures. *European Journal of Orthopaedic Surgery & Traumatology*, 28, 431-438.
- TAKEDA, Y., FUKUNISHI, S., NISHIO, S., FUJIHARA, Y. & YOSHIYA, S. 2017. Accuracy of component orientation and leg length adjustment in total hip arthroplasty using image-free navigation. *The open orthopaedics journal*, 11, 1432.
- TANG, A., CAO, Q. & PAN, T. 2014. Spatial motion constraints for a minimally invasive surgical robot using customizable virtual fixtures. *The International Journal of Medical Robotics and Computer Assisted Surgery*, 10, 447-460.
- TARWALA, R. & DORR, L. D. 2011. Robotic assisted total hip arthroplasty using the MAKO platform. *Current reviews in musculoskeletal medicine*, 4, 151.
- TAYLOR, R., JENSEN, P., WHITCOMB, L., BARNES, A., KUMAR, R., STOIANOVICI, D., GUPTA, P., WANG, Z., DEJUAN, E. & KAVOUSSI, L. 1999. A steady-hand robotic system for microsurgical augmentation. *The International Journal of Robotics Research*, 18, 1201-1210.
- TCHING, L., DUMONT, G. & PERRET, J. 2010. Interactive simulation of CAD models assemblies using virtual constraint guidance. *International Journal on Interactive Design and Manufacturing (IJIDeM)*, 4, 95-102.
- THAKKAR, S. C., THAKKAR, R. S., SIRISREETREERUX, N., CARRINO, J. A., SHAFIQ, B. & HASENBOEHLER, E. A. 2017. 2D versus 3D fluoroscopy-based navigation in posterior pelvic fixation: review of the literature on current technology. *International journal of computer assisted radiology and surgery*, 12, 69-76.
- TIAN, W., FAN, M. & LIU, Y. 2017. Pedicle screw insertion in spine: a randomized controlled study for robot-assisted spinal surgery. *EPiC Series in Health Sciences*, 1, 23-27.
- TOSOUNIDIS, T. H., CASTILLO, R., KANAKARIS, N. K. & GIANNOUDIS, P. V. 2015. Common complications in hip fracture surgery: Tips/tricks and solutions to avoid them. *Injury*, 46, S3-S11.
- TSUTSUI, T., GOTO, T., HAMADA, D., WADA, K. & SAIRYO, K. Year. ACCURACY OF ACETABULAR CUP PLACEMENT IN TOTAL HIP ARTHROPLASTY USING COMPUTED TOMOGRAPHY-BASED NAVIGATION SYSTEM. *In: Orthopaedic Proceedings*, 2016. The British Editorial Society of Bone & Joint Surgery, 89-89.
- UEKI, S., KAWASAKI, H., ITO, S., NISHIMOTO, Y., ABE, M., AOKI, T., ISHIGURE, Y., OJIKI, T. & MOURI, T. 2012. Development of a hand-assist robot with multi-degrees-of-freedom for rehabilitation therapy. *Mechatronics, IEEE/ASME Transactions on*, 17, 136-146.
- VAN DE KELFT, E., COSTA, F., VAN DER PLANKEN, D. & SCHILS, F. 2012. A prospective multicenter registry on the accuracy of pedicle screw placement in the thoracic, lumbar, and sacral levels with the use of the O-arm imaging system and StealthStation Navigation. *Spine*, 37, E1580-E1587.
- VERAS, E. J., DE LAURENTIS, K. J. & DUBEY, R. Year. Design and implementation of visual-haptic assistive control system for virtual rehabilitation exercise and teleoperation manipulation. *In: Engineering in Medicine and Biology Society*, 2008. EMBS 2008. 30th Annual International Conference of the IEEE, 2008. IEEE, 4290-4293.
- VICECONTI, M., LATTANZI, R., ANTONIETTI, B., PADERNI, S., OLMI, R., SUDANESE, A. & TONI, A. 2003. CT-based surgical planning software improves the accuracy of total hip replacement preoperative planning. *Medical Engineering & Physics*, 25, 371-377.

- VRESILOVIC, E. J., HOZACK, W. J. & ROTHMAN, R. H. 1994. Radiographic assessment of cementless femoral components: Correlation with intraoperative mechanical stability. *The Journal of Arthroplasty*, 9, 137-141.
- WANG, J., WANG, S., LI, J., REN, X. & BRIGGS, R. M. 2018. Development of a novel robotic platform with controllable stiffness manipulation arms for laparoendoscopic single-site surgery (LESS). *The International Journal of Medical Robotics and Computer Assisted Surgery*, 14, e1838.
- WATANABE, H., KANO, K., KOBAYASHI, Y. & FUJIE, M. G. 2011. Development of a "steerable drill" for ACL reconstruction to create the arbitrary trajectory of a bone tunnel. *IEEE/RSJ International Conference on Intelligent Robots and Systems (IROS), 2011*. IEEE/RSJ.
- WATZINGER, F., BIRKPELLNER, W., WANSCHITZ, F., MILLESI, W., SCHOPPER, C., SINKO, K., HUBER, K., BERGMANN, H. & EWERS, R. 1999. Positioning of dental implants using computer-aided navigation and an optical tracking system: case report and presentation of a new method. *Journal of Cranio-Maxillofacial Surgery*, 27, 77-81.
- WIGGINS, K. & MALKIN, S. 1978. Orthogonal machining of bone. *Journal of Biomechanical Engineering*, 100, 122-130.
- WU, L.-D., HAHNE, H. & HASSENPFUG, J. 2004. The dimensional accuracy of preparation of femoral cavity in cementless total hip arthroplasty. *Journal of Zhejiang University-SCIENCE A*, 5, 1270-1278.
- XIA, Y., BAO, Q. & LIU, Z. 2018. A New Disturbance Feedforward Control Method for Electro-Optical Tracking System Line-Of-Sight Stabilization on Moving Platform. *Sensors*, 18, 4350.
- YAMAMOTO, T., ABOLHASSANI, N., JUNG, S., OKAMURA, A. M. & JUDKINS, T. N. 2012. Augmented reality and haptic interfaces for robot-assisted surgery. *The International Journal of Medical Robotics and Computer Assisted Surgery*, 8, 45-56.
- YAMAMOTO, Y. & ISHIBASHI, Y. 2016. Intraoperative Biomechanical Evaluation Using a Navigation System. *ACL Injury and Its Treatment*. Springer.
- YBINGER, T. & KUMPAN, W. 2007. Enhanced acetabular component positioning through computer-assisted navigation. *International orthopaedics*, 31, 35-38.
- ZHANG, J., WEI, W., DING, J., ROLAND, J. T. J., MANOLIDIS, S. & SIMAAN, N. 2010. Inroads Toward Robot-Assisted Cochlear Implant Surgery Using Steerable Electrode Arrays. *Otology and Neurotology*, 31, 1199-1206.
- ZHENG, G. 2018. Gravity-Assisted Navigation System for Total Hip Arthroplasty. *Intelligent Orthopaedics*. Springer.
- ZHENG, G. & NOLTE, L.-P. 2018. Computer-Aided Orthopaedic Surgery: State-of-the-Art and Future Perspectives. *Intelligent Orthopaedics*. Springer.
- ZHENG, Q., HE, Y., QI, X., ZHANG, P., TAN, S. & LI, B. Year. Automatic Tracking Motion Based on Flexible Forbidden Virtual Fixtures Design in Robot Assisted Nasal Surgery. In: 2018 IEEE 8th Annual International Conference on CYBER Technology in Automation, Control, and Intelligent Systems (CYBER), 2018. IEEE, 271-275.
- ZHOU, K.-H., LUO, C.-F., CHEN, N., HU, C.-F. & PAN, F.-G. 2016. Minimally invasive surgery under fluoro-navigation for anterior pelvic ring fractures. *Indian journal of orthopaedics*, 50, 250.

